USARTL-TR-79-27A

LEVEL II

AD A088474

HELICOPTER DYNAMIC PERFORMANCE PROGRAM VOLUME I - ENGINEER'S MANUAL

R. E. Studwell
SIKORSKY AIRCRAFT DIVISION
United Technologies Corporation
Stratford, Connecticut 06602

July 1980

Final Report for Period November 1976 - November 1978

Approved for public release;
distribution unlimited.

Prepared for

APPLIED TECHNOLOGY LABORATORY
U.S. ARMY RESEARCH AND TECHNOLOGY LABORATORIES (AVRADCOM)
Fort Eustis, Va. 23604

APPLIED TECHNOLOGY LABORATORY POSITION STATEMENT

This report documents the engineering development and implementation procedures of an energy and force balance method of analysis for calculating the space-time-power relationship of a rotorcraft in steady or transient flight. While the current software and associated reports form a good basis from which a comprehensive energy-type rotorcraft analysis tool can be refined, both are in a state of flux. Through continued exercise by qualified users, the code and documents will be progressively refined to a state that they will accomplish the intended purpose. It is therefore fully anticipated that these documents (user's and engineer's manuals) will be subsequently revised and republished or errata sheets issued at an appropriate juncture.

The computer program resulting from this contract will be provided to qualified users, upon request, for use in the design and analysis of rotary-wing aircraft.

The project engineer for this contract was Mr. G. T. White, Aeromechanics Technical Area, Aeronautical Technology Division. Technical review of this report was also provided by Messrs. W. A. Pleasants of Design Integration and Analysis Technical Area, and E. E. Austin of Aeromechanics Technical Area.

Unclassified

SECURITY CLASSIFICATION OF THIS PAGE (When Data Entered)

REPORT DOCUMENTATION PAGE

READ INSTRUCTIONS BEFORE COMPLETING FORM

1 REPORT NUMBER: USARTL-TR-79-27A	2 GOVT ACCESSION NO: AD-A088 474
3 RECIPIENT'S CATALOG NUMBER:	
4 TITLE (and Subtitle): HELICOPTER DYNAMIC PERFORMANCE PROGRAM VOLUME I ENGINEER'S MANUAL	5 TYPE OF REPORT & PERIOD COVERED: Final Report Nov 1976 — Nov 1978
6 PERFORMING ORG. REPORT NUMBER: SER-51011-VOL-1	
7 AUTHOR(s): Robert E. Studwell	8 CONTRACT OR GRANT NUMBER(s): DAAJ02-76-C-0066
9 PERFORMING ORGANIZATION NAME AND ADDRESS: Sikorsky Aircraft Division, United Technologies Corporation, Stratford, Connecticut 06602	10 PROGRAM ELEMENT, PROJECT, TASK AREA & WORK UNIT NUMBERS: 62209A 1F262209AH76 00 174 EK
11 CONTROLLING OFFICE NAME AND ADDRESS: Applied Technology Laboratory, U.S. Army Research and Technology Laboratories (AVRADCOM), Fort Eustis, Virginia 23604	12 REPORT DATE: July 1980
	13 NUMBER OF PAGES: 134
14 MONITORING AGENCY NAME & ADDRESS (if different from Controlling Office): (11) Jul 80	15 SECURITY CLASS. (of this report): Unclassified
	15a DECLASSIFICATION/DOWNGRADING SCHEDULE

16 DISTRIBUTION STATEMENT (of this Report)

Approved for public release; distribution unlimited.

17 DISTRIBUTION STATEMENT (of the abstract entered in Block 20, if different from Report)

18 SUPPLEMENTARY NOTES

Volume I of a two-volume report.

19 KEY WORDS (Continue on reverse side if necessary and identify by block number)

Dynamic Performance
Autorotation
Emergency Flight

20 ABSTRACT (Continue on reverse side if necessary and identify by block number)

A computer program for evaluating helicopter performance in accelerated flight has been developed. The program was designed to permit analysis of any definable single rotor helicopter. Provisions for partial or total power loss at any point along the flight path are included. To accommodate emergency conditions provisions are made for evaluation of auxiliary power devices, tip rockets, JATO, RATO, fly wheels, drag brakes, and dropping of external loads

DD FORM 1 JAN 73 1473 EDITION OF 1 NOV 65 IS OBSOLETE S/N 0102-014-6601

Unclassified

SECURITY CLASSIFICATION OF THIS PAGE (When Data Entered)

322 200

BLOCK 20

Optimization routines for establishing height-velocity envelopes are also included.

The program is linked with a plot package which provides 40 prime output variables to be plotted. A perspective view of the flight path and plots of height-velocity diagrams are also available.

This volume covers the engineering aspects of the program. Volume II presents the User's Manual.

PREFACE

The work reported herein was performed by the Sikorsky Aircraft Division of United Technologies Corporation under Contract DAAJ02-76-C-0066 for the Applied Technology Laboratory, US Army Research and Technology Laboratories (AVRADCOM), Fort Eustis, Virginia. The work was carried out under the technical cognizance of Mr. Tom White of the Applied Technology Laboratory. The program was conducted under the management of Sikorsky Aeromechanics Branch Manager, Mr. Peter Arcidiacono and Aeromechanics Chief of Aerodynamics, Mr. J. Rorke. Aeromechanics personnel involved directly with the analysis and program development was Mr. Robert E. Studwell.

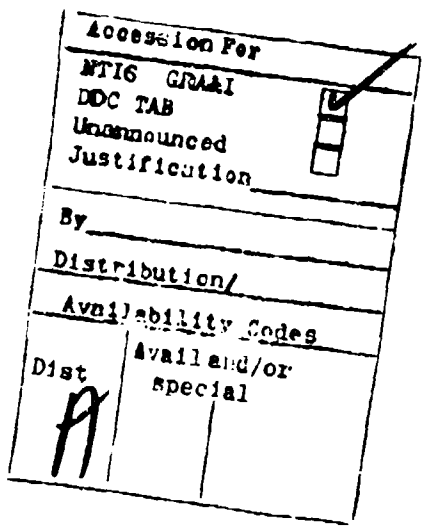

SUMMARY

The computer program developed for this effort is referred to as the Helicopter Dynamic Performance (HDP) Program. It was designed to permit analysis of the capabilities of any definable single rotor helicopter from any heliport location with specified departure or approach procedures. Provisions for partial or total engine malfunction at any point along the flight path are incorporated. The HDP program generates the height-distance-time relationships for any specified vehicle operating weight as functions of horsepower input, tip path plane attitude, and rotor rpm. Provision for collective stick input, in terms of blade pitch at 75% radius (Theta 75), in lieu of rotor rpm, is provided.

To accommodate emergency conditions, provisions were made in the program for evaluation of auxiliary power units, rotor tip rockets, JATO, RATO, fly wheels, drag brakes and dropping of external loads.

Provisions have also been incorporated for calculating the height-velocity envelope for user specified contact velocities and blade structural limit criteria.

The HDP program is coupled to the Sikorsky general plot package to permit interactive capability for rapid flight path evaluation. The program provides an interface between the Engineering routines and the plot package which permits the plotting of 40 pertinent output parameters. The plot interface was designed so that any parameter can be plotted against any other parameter in the list.

In addition to these plots, a perspective view of the flight path can also be obtained. The user has the capability of changing the viewing position to any position in virtual space. A plot of the height-velocity curve for the rotorcraft being evaluated can also be obtained through the graphics interface package.

This volume deals with the engineering aspects and basic rotor performance equations used for obtaining the force and energy balance required during each finite time step of the overall flight path.

A parametric trade-off investigation was conducted to establish the sensitivity of various rotorcraft design parameters. This investigation indicated that the parametric sensitivity is highly dependent on the baseline configuration. It also pointed out that a high interdependence of basic design criteria exists. A means of evaluating the sensitivity and interdependence criteria was established which can be used as a guide for design considerations.

A comparative analysis between program calculated performance and flight test data was conducted to establish program accuracy.

TABLE OF CONTENTS

TABLE OF CONTENTS (continued)

LIST OF ILLUSTRATIONS

LIST OF ILLUSTRATIONS (continued)

HDP PROGRAM OVERVIEW

The HDP Program provides a means of calculating the space-time relationships of a rotorcraft in dynamic (accelerating) flight. The program basically performs a step function integration of rotorcraft unbalanced forces and energy levels to establish incremental space displacement. These displacements are summed for a series of finite time steps to establish the flight path. A basic flow chart depicting program flow is shown in Figure 1. Typical program operation proceeds in the following manner. Given the design parameters of the rotorcraft to be analysed, defined with 23 basic inputs (see Volume 2, Users Manual), and the initial flight conditions, also defined by program input, the program will compute the energy state of the rotorcraft. This energy state assumes the rotorcraft to be in a steady state flight condition at the initial condition input values. Additional program inputs provide a means for the user to specify variations in rotorcraft velocity, tip path plane attitude, rotor RPM and engine power levels. A series of 10 sequences to a maximum of 300 time steps is permitted. A variation of any one or any combination of these inputs will create an unbalanced force on the system. This unbalanced force is computed assuming the rotorcraft to be in steady state flight for the conditions which exist at the mid-point of each time step. Since the rotorcraft acceleration is unknown the following process is used to attain a solution.

Initially the program assumes the acceleration energy to be 0 and computes the unbalanced forces acting on the system due to the perturbation on the input sequence list. Based on these unbalanced forces an acceleration is computed. This acceleration revises the energy state of the system along with the velocity at which the unbalanced forces are generated. The new velocity used is based on that which exists at the mid-point of the time step. This new energy state is then fed back and used to recalculate the rotor forces, unbalanced forces and resulting accelerations. This process is repeated for each time step until the resultant acceleration between two successive iterations is within 0.3 ft/sec^2. To minimize the convergence iterations required, each time step uses the resultant acceleration from the previous step as a starting point.

The flight path is obtained by summing the displacements of each time step.

A discussion of the equations used for computing the rotorcraft energy state, rotor forces, acceleration and displacements are covered in this report.

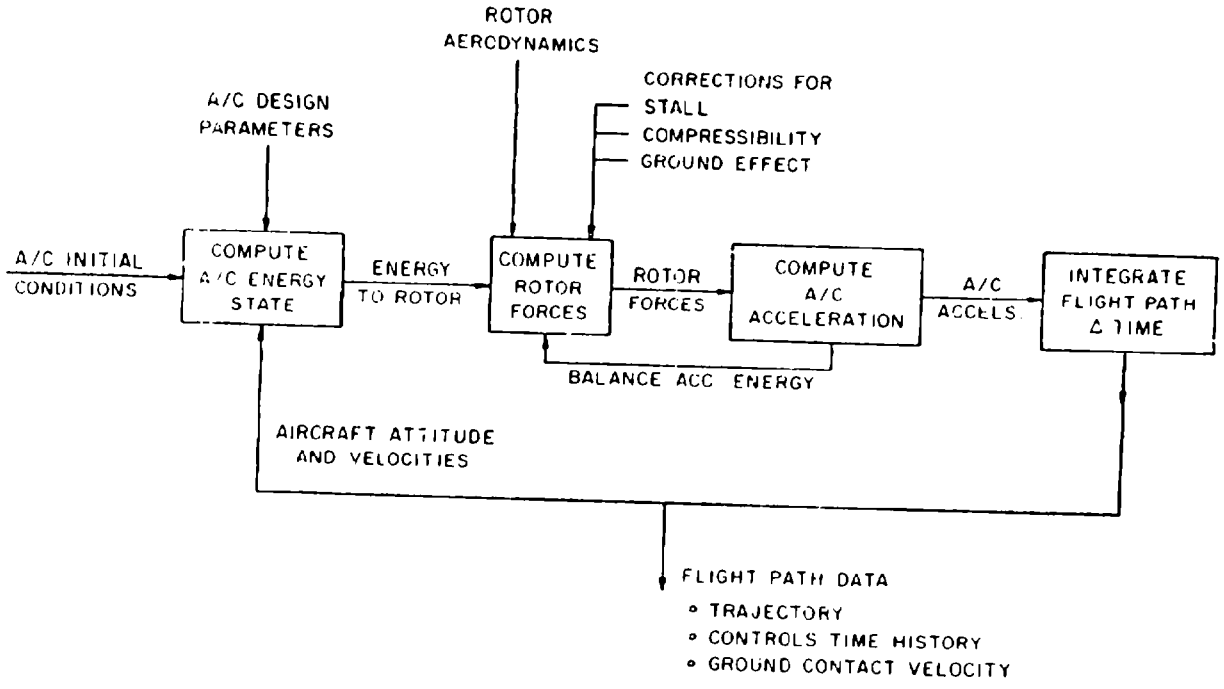

Figure 1. Basic Program Flow Chart

ROTOR PERFORMANCE MODEL

The Helicopter Dynamic Performance Method is a semi-empirical procedure for evaluating rotor and/or rotorcraft performance. The equations derived for this analysis were normalized to permit performance calculations in any flight regime for any predefined rotor system. All equations are continuous between flight regimes.

The analysis was based on an energy method approach modified to account for blade interference effects. The effects of Reynolds Number, Mach Number, and Skewed flow are also accounted for in the analysis.

OUTLINE OF THEORY

Investigation of several means of approach to performance analysis indicated that the energy method was better suited, being more amenable to analysis as flight conditions approach zero speed.

The energy method basically states that the power required for a rotor system to develop a given thrust, in steady-state flight, is equal to the Σ rotor induced power, blade profile power, airframe drag power, climb power, and rotor stall power. The basic rotor system as used for this analysis is shown in Figure 2.

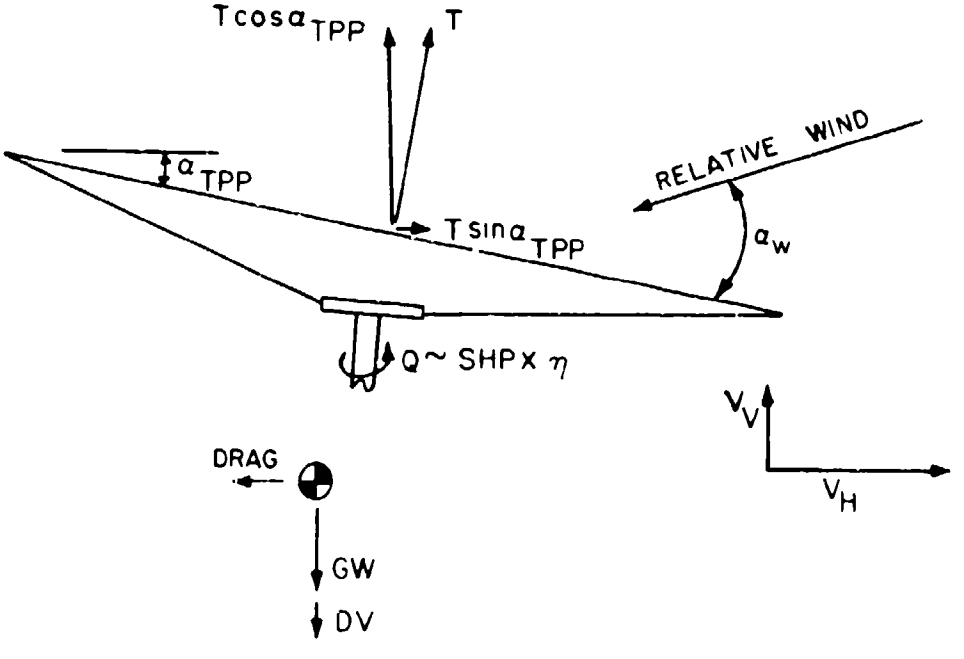

Figure 2. Basic Rotor Force System.

$$hp_a = hp_i + hp_o + hp_p + hp_c + hp_s \qquad (1)$$

It can be seen from the power equation that the use of the energy method reduces itself to the determination of each power component. The analysis used for the determination of each of these components is summarized herein.

INDUCED HORSEPOWER

Impulse-Momentum theory states that the thrust produced by an actuator disc can be mathematically represented by the expression:

$$T = \rho\pi R^2 (V_R + u) 2u \tag{2}$$

When $V_R = 0$, $u = [T/2\pi\rho R^2]^{1/2} = u_o$ (3)

Letting $\bar{u} = u/u_o$ and $\bar{V} = V_R/u_o$,

Wald esbablished that for any flight condition

$$\bar{V} = -\bar{u} \sin \alpha_w \pm (\bar{u}^2 \sin^2 \alpha_w - \bar{u}^2 + 1/\bar{u}^2)^{1/2} \text{(Reference 1)} \tag{4}$$

These equations are based on the following assumptions:

1. The actuator disc consists of an infinite number of blades uniformly accelerating the air through the disc with no loss of thrust at the blade tips.

2. The power required to produce the thrust is represented only by the axial kinetic energy imparted to the air composing the slipstream. A frictionless fluid is assumed so that no blade friction or profile losses exist. Rotational energy imparted to the slipstream is ignored.

3. The disc is infinitely thin so that no discontinuities in velocity occur on the two sides of the disc.

In the actual flow past a rotor with a finite number of blades there is a radial contraction and a rotational motion imparted to the slipstream. This gives a corresponding increase in the axial velocity and a decrease in the tangential velocity components acting on the blade. If it is assumed that the "ideal rotor" (impulse momentum theory) is 100% efficient in generating the induced velocity (u), the increase in the induced velocity due to the contraction of the slipstream in the rotor disc plane can be related with the expression:

$$u_{\text{actual rotor}} = u_{\text{ideal rotor}}/\bar{B}$$

[1]Coleman, R. P., Feingold, A. M., and Stempin, C. W., NACA ARR No. L5E10.

Where $\bar{B}$ represents the efficiency of the actual rotor with respect to the "ideal rotor" (see section on development of the rotor efficiency equation).

Thus it can be stated that

$$u_{o_{\text{actual rotor}}} = [T/2\pi\rho R^2]^{1/2}/\bar{B}$$

or

$$u_{o_{\text{actual rotor}}} = \left[\frac{T}{2\pi\rho(\bar{B}R)^2}\right]^{1/2} \tag{5}$$

This states that the induced velocity generated by an actual rotor of radius R will be the same as that generated by an "ideal rotor" of radius BR.

The horsepower required in generating this induced velocity can be expressed as

$$hp_i = \frac{Tu}{550}$$

Multiplying by u_o/u_o and nondimensionalizing thrust with $\rho\pi R^2(\Omega R)^2$ yields the coefficient of induced power as

$$C_{P_i} = \frac{550\ hp_i}{\rho\pi R^2(\Omega R)^3} = \frac{C_T^{3/2}}{\sqrt{2}\,\bar{B}}\,\bar{u}\,\Lambda \tag{6}$$

This equation establishes a means of computing the induced power requirements for a single rotor. If tandem rotors are assumed, further considerations for rotor interference effects on the induced power must be made.

TANDEM AND COAXIAL ROTOR HOVER PERFORMANCE

Consider two coplanar overlapped rotors as shown in Figure 3.

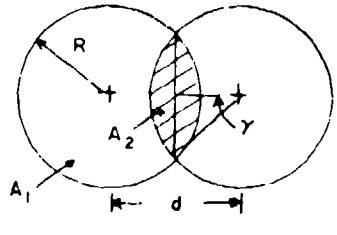

Figure 3. Tandem Rotor Overlap Geometry.

If the profile power is assumed to be independent of the overlap for a given thrust, then for a constant induced power the thrust must vary inversely as the induced velocity for $P_i = Tu_i$. Letting T equal the total thrust of both rotors and $\bar{u}_i$ equal the 'average' induced velocity, the relationship of thrust and induced velocity can be expressed with respect to two similar but non-overlapped rotors as

$$T/T_o = \bar{u}_{i_o}/\bar{u}_i$$

where the subscript o refers to zero overlap

now $\bar{u}_i = [T/2\rho A]^{1/2}$

where $A = 2A_1 + A_2$ (from Figure 3)

and $\bar{u}_{i_o} = [To/2\rho A_o]^{1/2}$

where $A_o = 2\pi R^2$

Therefore $T/T_o = (A/A_o)^{1/3}$ for constant induced power. Similarly, for a constant thrust the ratio of the induced powers with and without overlap is:

$$P_i/P_{i_o} = [A_o/A]^{1/2} \tag{7}$$

If the overlap is defined as d/2R ,the angle γ (shown in Figure 2) is given by

$$\gamma = \cos^{-1} (\text{overlap})$$

and from the geometry of the sketch

$$A/A_o = 1 - \frac{\gamma - \sin\gamma\cos\gamma}{\pi} \tag{8}$$

Considering a zero overlap condition it can be stated that by assuming the thrust of one rotor equal to half the total then $2P_{i_1} = P_{i_2}$.

Where subscript 1 refers to one rotor and 2 to two rotors. Thus for an overlapped condition

$$P_{i_2} = 2P_{i_1}\left[\frac{A_2}{A_{TOT}}\right]^{1/2} \tag{9}$$

where P_{i_1} is based on the thrust and area of one rotor.

Defining df_H as the total rotor interference factor in hover due to overlap then the total induced power for hover can be expressed as

$$P_{i_2} = 2P_{i_1} (1 + df_H/2) \text{ and consequently}$$

$$1 + \frac{df_H}{2} = \left[\frac{A_2}{A_{TOT}}\right]^{1/2} = \left[\frac{A_2}{A_2\left(1 - \frac{\gamma - \sin\gamma\cos\gamma}{\pi}\right)}\right]^{1/2}$$

solving for df_H yields

$$df_H = 2\left[\frac{1}{1 - \frac{\gamma - \sin\gamma\cos\gamma}{\pi}}\right]^{1/2} \tag{10}$$

This analysis was based on the rotors being coplanar and thus assumes that the stream tube contraction for the two rotors is equal. When the rotors do not lie in the same horizontal plane the effects of differential slipstream contraction should be considered. Full scale test data indicated that this effect can be approximated, for hover at least, by multiplying the coplanar interference factor by the expression (1 + 19 VS/R). This term is strictly empirical and justification for its use is only with its apparent agreement with available test data. To maintain conformity with the actuator disc theory, the maximum value of the interference factor (the product of the vertical separation and overlap expressions) is limited to 2.0 where VS refers to the vertical displacement between rotors.

TANDEM AND COAXIAL ROTOR FORWARD FLIGHT PERFORMANCE

A comparison can be made between single rotor and tandem rotor helicopters at the same gross weight by assuming that the thrust is equally divided between the two rotors of the tandem. According to simple momentum relationships, the induced power in forward flight for an isolated rotor is

$$P_i = T^2/2\rho Au$$

for the rear rotor of a longitudinal tandem this becomes

$$P_{i_R} = (T^2/2\rho Au)\ (1 + df_{FR})$$

and for the front rotor

$$P_{i_F} = (T^2/2\rho Au)\ (1 + df_{RF})$$

where subscripts: FR refers to the interference of the front rotor on the rear rotor

RF refers to the interference of the rear rotor on the front rotor.

Thus the total induced power would be

$$P_{i_R} + P_{i_F} = \frac{T^2}{2\rho Au}\ (2 + df_{FR} + df_{RF}) \text{ or } P_{i_{TOTAL}} = 2P_{i_1}\ 1 + \frac{df_{FR} + df_{RF}}{2}$$

Reference 2 derives an expression for coplanar longitudinal tandems where df is defined as

$$df_{FR} = (\ 1 + P^2 + P\sin\zeta)/\ 1 + P^2\ (1 + P^2\cos^2\zeta)$$

and

$$df_{RF} = (\ 1 + P^2 - P\sin\zeta)/\ 1 + P^2\ (1 + P^2\cos^2\zeta)$$

where $\zeta = TAN^{-1}\ 2\rho A_F u^2/1.5T_F$

The factor 1.5 accounts for partial wake contraction at the rear rotor.

Summing the terms yields

$$df_{LF} = df_{FR} + df_{RF} = 2/(1 + P^2\cos^2\zeta) \qquad (11)$$

To account for variations in vertical displacement between rotors test data indicates that this term should be adjusted by the term (1 - 1.35 dv/R). This assumes the rear rotor to be higher than the forward rotor. Where dv is the vertical displacement between rotors.
While this expression appears reasonably valid in high-speed flight, its usage becomes questionable in the low speed regime. To relate the df in forward flight to that derived for hover it was assumed that a linear transition between the hover point and the level flight curve exists. On this basis the df in the low speed regime could be expressed as:

$$df = df_H + \frac{df_{LF} - df_H}{\zeta_{TAN}}\ \zeta \qquad (12)$$

[2]McCormick, B. W., Jr., AERODYNAMICS OF V/STOL FLIGHT, Academic Press, 1967.

where ζ_{TAN} is the wake skew angle at which a line projected from df_H is tangent to the df_{LF} curve for the rotor system in question (see Figure 4).

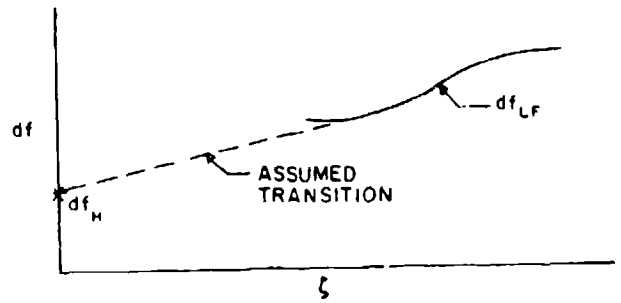

Figure 4. Tandem Rotor Interference (Typical).

The use of these equations yields excellent agreement with test data for tandem rotor helicopters with shaft offset but tend to breakdown as the shaft offset distance (d) approaches zero. (see Figure 5)

Considering a two-rotor system with substantial shaft ... it can be seen that as forward speed is increased the stream tubes ac ...ed by each rotor interfere by an increasing amount.

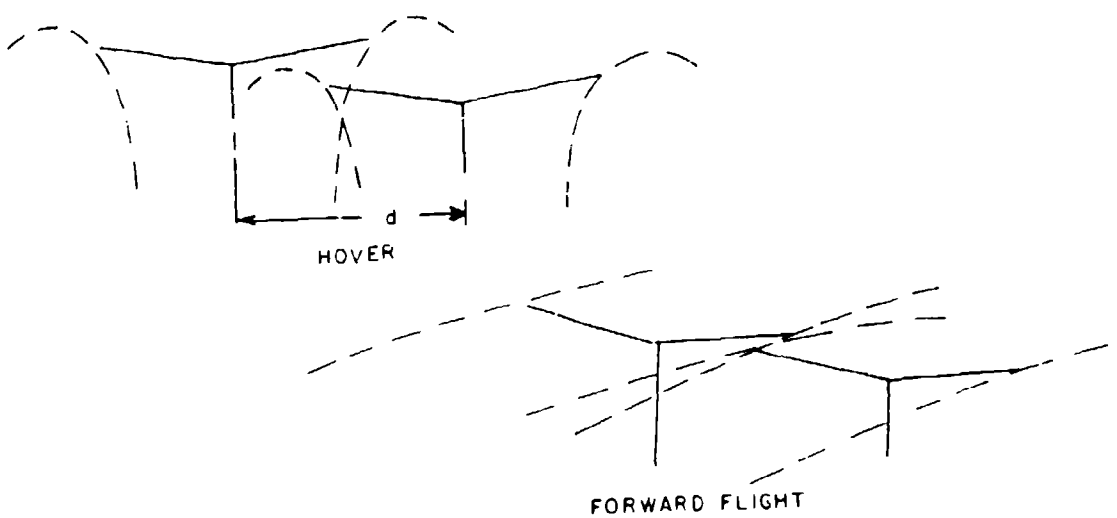

Figure 5. Tandem Rotor Inflow (Typical).

Thus, as stated by the equations above, the interference in hover is low and as V tends to infinity df_{LF} approaches 2, lessening the effective vertical displacement.

Now, as the shaft offset distance is decreased this effect tends to reverse, i.e., the interference is highest in low-speed flight and decreases as speed increases (Figure 6).

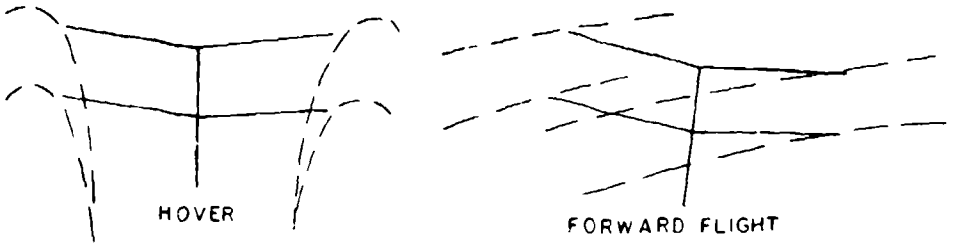

Figure 6. Co-axial Rotor Inflow (Typical).

To properly account for the condition when the offset is zero (coaxial rotors) it is suggested that the interference effects be expressed as

$$df = df_H \cos^2 \zeta \tag{13}$$

and defining the induced power of each rotor as

$$P_{i_{upper}} = [1.1T^2/2\rho A] (1 + d_{f_u})$$

and $$P_{i_{lower}} = [1.4T^2/2\rho Au] (1 + d_{f_l}),$$

thus $$P_{i_{total}} = 2.5T^2/2\rho Au \left[1 + \frac{df_u + df_l}{2}\right] \tag{14}$$

These expressions assume that each rotor is carrying 50% of the lift. The factors 1.1 and 1.4 are purely empirical and are the estimated entrainment effects of one rotor on the other.

It must be stressed again that interference expressions defined above are semi-empirical in nature and exact distributions would require a more rigorous form of computation.

PROFILE HORSEPOWER

The impulse-momentum concept assumes the rotor to be operating in a frictionless fluid and profile drag losses are not accounted for. To account for the profile drag losses, the following relationships were established.

The thrust produced by a rotor system can be expressed on a strip analysis basis as

$$T = \frac{b}{2\pi} \int_0^{2\pi} d\psi \int_0^R \rho/2\ CU^2\ C_{L_{(M)}}\ dr$$

Accounting for the influence of the reversed velocity region on the retreating blade the integral becomes

$$T = \frac{b}{2\pi} \int_0^{2\pi} d\psi \int_0^R \rho/2\ CU^2\ C_{L_{(M)}}\ dr - b/2\pi \int_\pi^{2\pi} d\psi \int_0^{-\mu R \sin\psi} \rho/2\ CU^2 C_{L_{(M)}}\ dr$$

This expression for thrust in terms of $C_{L(M)}$ does not account for slipstream rotation and is therefore representative of an "ideal rotor". Utilizing the analogy that an actual rotor of radius R is equivalent to an "ideal rotor" of radius $\bar{B}R$, the thrust developed by an actual rotor can be computed by integrating along the blade to radius $\bar{B}R$.

Substituting $C_T\ \rho\pi R^2(\Omega R)^2$ for T

and $\Omega r + \mu\Omega R \sin\psi$ for U

Integrating and solving for $C_{L(M)}$ yields

$$C_{L_{(M)}} = 2\ C_T/\sigma_e \left[\frac{1}{\frac{\bar{B}^3}{3} + \frac{\bar{B}\mu^2}{2} - \frac{4\mu^3}{9\pi}}\right] \qquad (15)$$

(Definition of σ_e is discussed later).

The required mean lift coefficient $C_{L(M)}$ can be established in terms of C_T and the resulting mean profile drag coefficient, δ, can be established from the δ-$C_{L_{(M)}}$ relationship of the airfoil in question.

In Glauert's theory of energy loss the expression for profile drag with skewed flow taken into account is

$$D_o/L = \frac{\sigma_e\ \delta}{8\mu\ C_T}\ (1 + n\mu^2)$$

Assuming $L = T \cos\alpha$ and $\cos\alpha = 1$

and substituting $T/\rho\pi R^2(\Omega R)^2$ for C_T

and $V/\Omega R$ for μ

yields $D_o V = [\sigma_e \delta \rho \pi R^2 (\Omega R)^3/8] \quad (1 + n\mu^2)$

expressing in nondimensional terms yields

$$C_{P_0} = \frac{\sigma_e \delta}{8} (1 + n\mu^2) \tag{16}$$

or in terms of horsepower

$$hp_o = \frac{\sigma_e \delta}{8} (1 + n\mu^2) \frac{\rho\pi R^2 (\Omega R)^3}{550} \tag{17}$$

Where n is a function of μ determined by the equation:

$$1 + n\mu^2 = \int_0^{2\pi} \int_0^1 (x^2 + 2x\mu\sin\psi + \mu^2)^{3/2} dx d\psi$$

Where $\mu = V/\Omega R \leq 1$, $x = r/R$

Lacking a simple integral of this equation, Glauert's method (Reference 3) of obtaining approximations by evaluating the inner integrals at the points of $\psi = 0°$, 90°, 180° and 270° and averaging has been adopted. Using this procedure, numerical values of μ and n were evaluated and are given in the following table.

μ	0	.1	.2	.3	.4	.5	.6	.75	1.0
n	4.50	4.53	4.63	4.73	4.87	5.03	5.22	5.53	6.13

The mean profile drag coefficient (δ) is related to the mean lift coefficient ($C_{L_{(M)}}$). This relationship is generally related as a cubic function of $C_{L_{(M)}}$. A typical relationship for an NACA 0012 airfoil is shown in Figure 7.

DEVELOPMENT OF THE ROTOR EFFICIENCY EQUATION

The previous sections show that the calculations of the induced and profile powers are dependent on establishing th otor efficiency. The following analysis is used to establish the rotor efficiency.

[3]Glauert, H., A GENERAL THEORY OF THE AUTOGYRO, ARC R&M No. 111, 1926.

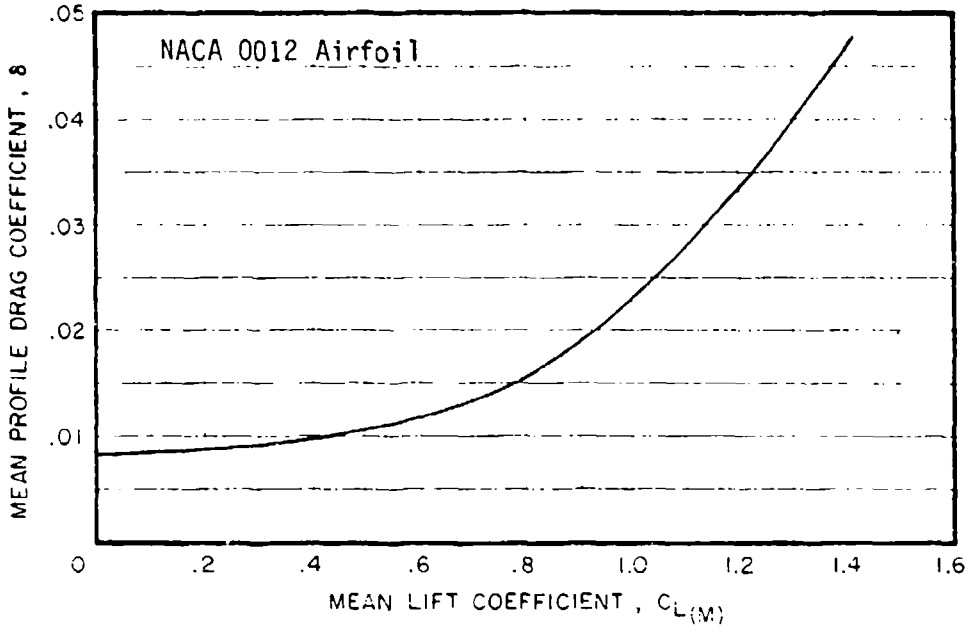

Figure 7. Mean Lift-Mean Drag Coefficient Data 0012 Airfoil.

Simple momentum theory states that the thrust developed from an actuator disc, operating in the normal working state, can be determined from equation 2.

In the actual flow past a rotor there is a radial contraction and a rotational motion imparted to the slipstream. This gives a corresponding increase in the axial velocity and a decrease in the tangential velocity component acting on the blade. Representing a hovering rotor with an infinite series of airfoil sections operating in one plane, the relative velocities acting on each airfoil section can be represented as shown in Figure 8. The distance between consecutive airfoil sections would be $2\pi r/b$ the induced velocity would be u and the whole system would be moving at a velocity Ωr.

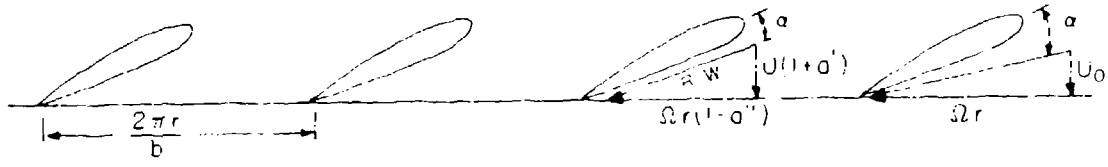

Figure 8. Blade Interference Effects.

Let us consider a' as the axial interference factor and a" as the rotational interference rotor. Then u would become $u(1 + a')$ and Ωr would be $\Omega r(1-a")$. The forces developed by the airfoil section due to these velocities can be represented as shown in Figure 9. The solid lines represent the "Ideal" rotor while the dash lines represent the 'Actual' rotor.

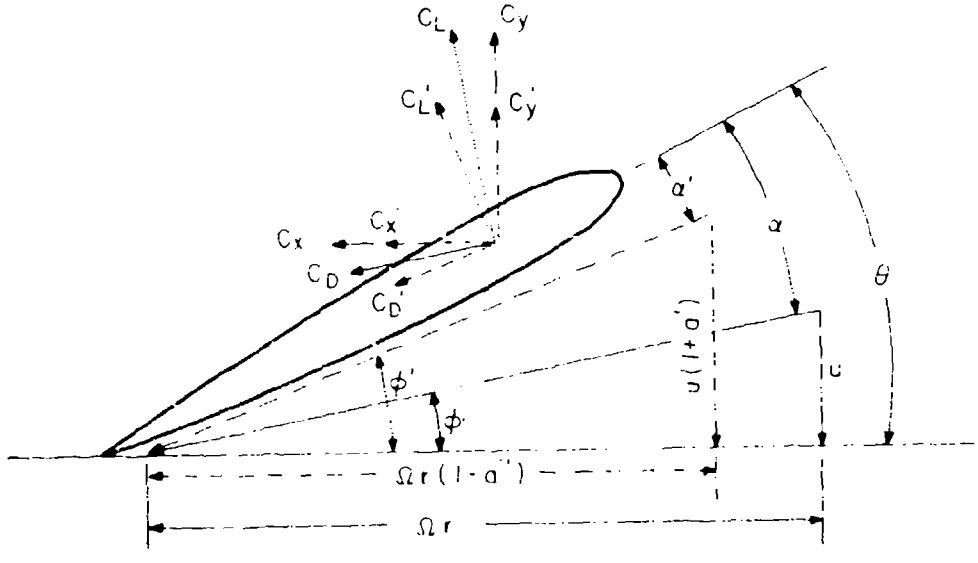

Figure 9. Interference Effects on Blade Forces.

It can be seen from Figure 9 that the vertical and horizontal forces, Cy and Cx, for the Ideal rotor element can be determined from the equations

$$C_y = C_L \cos\phi - C_D \sin\phi$$

$$C_x = C_L \sin\phi + C_D \cos\phi$$

$$\phi = \tan^{-1} u/\Omega r$$

And for the Actual rotor element

$$C_y' = C_L' \cos\phi' - C_D' \sin\phi'$$

$$C_x' = C_L' \sin\phi' + C_D \cos\phi'$$

$$\phi' = \tan^{-1} u/\Omega r \left((1+\alpha')/(1-\alpha'')\right)$$

If the actual blade element is to maintain the same lift coefficient as the ideal blade element the α' must equal α. If α' is to equal α, ϕ must be increased by the amount $\phi' - \phi$. When the ideal and actual blade elements are operating at the same angle of attack, they will both develop the same lift and drag coefficients but the vertical and horizontal components will not be equal as $\phi' > \phi$. In order for the actual rotor to develop the same Cy and Cx values as the ideal rotor the angle of attack must be increased so that $\alpha' > \alpha$. Since the actual rotor must maintain a higher angle of attack to attain the same vertical force, a higher C_L value must be developed which will give a corresponding increase in C_D.

From simple momentum theory the induced velocity (u) can be expressed from equation 2 as

$$u = -\frac{V}{2} \pm \left[\frac{V^2}{4} + \frac{T}{2\rho\pi R^2}\right]^{1/2} \qquad (18)$$

Thus when V = 0 the induced velocity thru an ideal rotor system can be expressed as

$$u_o = \left[\frac{T}{2\rho\pi R^2}\right]^{1/2} \qquad (3)$$

Dividing equation 18 by equation 3 yields

$$u/u_o = -\frac{V}{2u_o} \pm [1/4\ (\frac{V}{u_o})^2 + 1]^{1/2} = \bar{u} \qquad (19)$$

Thus when V = 0, $\bar{u}$ = 1 for an Ideal rotor.

In Figure 8 let's assume that the first blade element represents the ideal rotor and the second element an actual rotor. On this basis it can be seen that the ratio of induced velocity of an actual rotor to an ideal rotor would be greater than 1, since $u(1 + \alpha') > u_o$. This indicates that an actual rotor is less efficient than an ideal rotor.

The efficiency of any real rotor system can be evaluated from the relationship

$$u(1 + \alpha')\bar{B} = u_o = [\frac{T}{2\rho\pi R^2}]^{1/2} \qquad (20)$$

Where $\bar{B}$ represents the rotor efficiency.

This equation can be rewritten as

$$u(1 + \alpha') = [\frac{T}{2\rho\pi(\bar{B}R)^2}]^{1/2} \qquad (21)$$

Which states that the induced velocity through an actual rotor of Radius R can be represented by computing the induced velocity of an ideal rotor of radius $\bar{B}R$. Based on this relationship the rotor efficiency was evaluated from test data in the following manner.

The induced velocity through an actual rotor disc was determined from the equation

$$u(1 + \alpha') = 550\, hp_i / T \qquad (22)$$

Where $hp_i = hp_a - hp_o - hp_p$

hp_i is the induced power

hp_a is the total power measured at the rotor

hp_o is the profile power

hp_p is the parasite power required by the airframe for wind

(equivalent forward speed).

The profile power was determined from the equation

$$hp_o = \frac{\sigma_e \delta}{8} (1 + n_\mu{}^2) \frac{\rho \pi R^2 (\Omega R)^3}{550} \tag{17}$$

where δ is a function of $C_{L_{(M)}}$

and $C_{L_{(M)}} = 2k\, C_T/\sigma_e$

where $k = \dfrac{1}{\frac{\bar{B}^3}{3} + \frac{\bar{B}_u{}^2}{2} - \frac{4\mu^3}{9\pi}}$ (15)

See previous section for the derivation of these equations.

The use of the rotor efficiency $\bar{B}$ in equation 15 accounts for the increased lift (C_{L_M}) requirements and the corresponding increase in profile drag (δ) for the actual rotor.

Total rotor losses $\bar{B}$ were then determined through an iterative solution of these equations. The initial assumption being that $\bar{B} = 1$ in equation (15) and a value of $\bar{B}$ determined from equation 21. This value of $\bar{B}$ was then substituted in equation 15 and the process repeated until convergence.

Utilizing flight test data obtained from hovering flight, values of $\bar{B}$ were determined from equation 21 for various aircraft over a range of thrusts. The mean profile drag coefficient vs. mean lift coefficient polar for the NACA 0012 airfoil was assumed to be substantially correct and used in this analysis. The calculated values of $\bar{B}$ showed variations depending on the number of blades, blade twist and thrust coefficient.

The values of $\bar{B}$ calculated for a five bladed rotor with a blade twist of -14° were approximated by the equation

$$\bar{B} = 1 - \frac{[1.34 C_T]^{1/5}}{5}$$

This was then written in a general form as

$$\bar{B} = 1 - \frac{[1.34 C_T]^{1/b}}{b} \tag{23}$$

It should be noted that this equation form yields $\bar{B} \rightarrow 1$ as $b \rightarrow \infty$ which must be the case as the rotor system approaches the actuator disc form of the ideal rotor. Applying equation 23 to rotors with three and four blades showed that the test data were displaced from the curve predicted by equation 23. It was also noted that this displacement was constant for a given blade twist. This displacement used in conjunction with the corresponding blade twist was approximated with the equation

$$\Delta\bar{B}_{\theta_e} = - [0.14325\theta_e + 0.035]$$

where θ_e is the blade twist expressed algebraically in radians.

A general equation for the total rotor losses in a hovering condition was then written as

$$\bar{B} = 1 - \frac{[1.34C_T]^{1/b}}{b} - [0.14325\theta_e + 0.035] \qquad (24)$$

In translational flight the value of $\bar{V}$ is not zero and the value of $\bar{u}$ is not one. Walds equation, Reference 1, derives a function of $\bar{V}$ vs. $\bar{u}$ for various rotor disc angles. In translational flight an ideal rotor should yield values of $\bar{u}$ obtained from this equation at the proper rotor disc angle and V value. Equation 4 yields values of $\bar{V}$ that would be obtained on an ideal rotor. To obtain values of $\bar{V}$ that are obtained on an actual rotor, equation 19 must be rewritten as

$$V/u_o = V/\left[\frac{T}{2\pi\rho(\bar{B}R)^2}\right]^{1/2} \qquad (25)$$

The total rotor losses in translational flight can then be determined through an iterative solution using equations 21, 22, 17, 15 and 25.

Flight test data were used in determining values of $\bar{B}$ in translational flight. The calculated values of $\bar{B}$ showed variations with the number of blades, blade twist, thrust coefficient and translational speed. When the $\bar{B}$ value as determined from equation 24, hovering flight, was subtracted from the $\bar{B}$ value determined from translational flight tests it was noted that the difference, $\Delta\bar{B}_\mu$, was constant at a given C_T and μ value for all aircraft. It was also noted that $\Delta\bar{B}_\mu$ varied with C_T and μ.

The coning angle of the rotor blades increases as the weight of the aircraft increases. This coning angle is constant for any given weight, temperature, altitude and rpm. Flight tests indicate that for a given set of conditions the coning angle decreased as the translational speed increased, up to the minimum power speed, and then increased with a further increase in speed. This decrease and increase of coning angle in translational flight can be attributed to changes in blade loading, as shown in Figure 10.

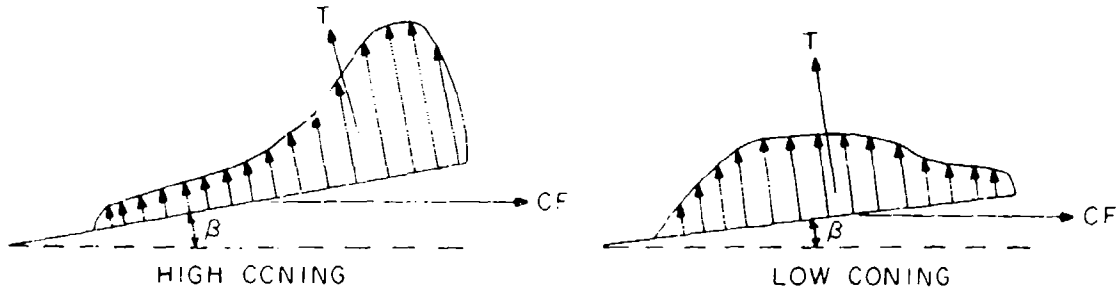

Figure 10. Effect of Thrust Distribution on Blade Coning.

FLIGHT CONDITION	INFLOW	LOAD	CONING
Hovering	Large (Induced)	Toward Tips	High
Minimum Power	Small (small induced small parasite)	More Inboard	Low
High Speed	Large (Parasite)	Toward Tips	High

These variations in blade load distribution indicated that the losses in the system should also vary with speed. Noting that the term V/u_o can be expressed as $\mu(2/C_T)^{1/2}$ and that the blade loading distribution will also vary with azimuth position, a generalized expression for the variation in rotor efficiency with translational speed was written as

$$\Delta\bar{B}_\mu = x\mu(2/C_T)^{1/2} + [\frac{y\mu^2}{C_T} + 1]^{1/2} - [\frac{z\mu^2}{C_T} + 1]^{1/2} \qquad (26)$$

ψ 0° & 180° 90° 270°

where x, y and z are unknown

Values of $\Delta\bar{B}_\mu$ were determined by subtracting the $\bar{B}$ values calculated from equation 24 from the $\bar{B}$ values calculated from translational flight at various test values of μ and C_T. Calculating for several conditions and substituting the results in equation 26 yielded values of x, y and z as

$$x = 0.0905,\ y = 0.5,\ z = 0.6974$$

Equation 14 then becomes

$$\Delta\bar{B}_\mu = 0.0905\mu\ [\frac{2}{C_T}]^{1/2} + [\frac{\mu^2}{2C_T} + 1]^{1/2} - [\frac{0.6974\mu^2}{C_T} + 1]^{1/2} \qquad (26a)$$

The total expression for the rotor losses due to slipstream contraction slipstream rotation and blade tip losses in any flight condition was then written as

$$\bar{B} = 1 - \frac{[1.34C_T]^{1/b}}{b} + 0.0905\mu\,[\frac{2}{C_T}]^{1/2} + [\frac{\mu^2}{2C_T} + 1]^{1/2} - [\frac{0.6974\mu^2}{C_T} + 1]^{1/2} - [0.14325\,\theta_e + 0.035] \quad (27)$$

The equation for $\bar{B}$ having been developed by comparing the induced velocity through an actual rotor to the induced velocity through an ideal rotor is then in effect the efficiency of the actual rotor. The increased profile drag requirements due to the higher lift needed to maintain the same Cy force as the ideal rotor are also accounted for in this analysis.

It should be noted that in the development of $\bar{B}$ the flight path velocity was used in determining values of μ. On this basis the resultant flight path velocity must be used for the determination of μ in the rotor efficiency equation, i.e.,

$$\mu_{\bar{B}} = [V_H^2 + V_V^2]^{1/2}/\Omega R \quad (28)$$

THE INFLOW RATIO IN DESCENT

The power requirements of a rotor system in low-speed flight are largely dependent on the induced power or more specifically the induced velocity through the rotor. In order to fully utilize the equations derived a means of determining the induced velocity during descent must be established. This is necessitated as 'Walds' equation, derived in Reference 1 is deemed not applicable in the negative velocity range between the values of $V/u_o = 0$ and $V/u_o = -2$.

Investigations into the vertical descent range $V/u_o = 0, -2$ have been conducted by Hafner, Glauert and Lock who have proposed various transition curves across this range. Various presentations proposed are summarized in Reference 4. Reference 5 also proposes a transition curve based on test data obtained from Reference 6. It should be noted that the U/u_o, V/u_o relationships for the proposed transition curves are based on "ideal" rotor

[4]Shapiro, J., PRINCIPLES OF HELICOPTER ENGINEERING, McGraw Hill Book Company, Inc., 1955.

[5]Gessow, A., and Myers, G. C., Jr., AERODYNAMICS OF THE HELICOPTER, MacMillian Company, 1952.

[6]NACA MR No. L5D09a.

concepts, i.e., no losses. On this basis

$$u/u_o = \frac{550(hp_a - hp_o)}{T\,[T/2\pi\rho R^2]^{1/2}} \quad \text{and} \quad V/u_o = V_R/[T/2\pi\rho R^2]^{1/2}$$

where hp_a measured from flight test

hp_o computed for flight test conditions

$T = GW$

V_R Resultant Flight Path Velocity

The analysis conducted previously modifies these equations to account for rotor losses and states that for actual rotors the equations would be

$$u/u_o = \frac{550(hp_a - hp_o)}{T\,[T/2\rho\pi(\bar{B}R)^2]^{1/2}} \quad \text{and} \quad V/u_o = \frac{V_R}{[\frac{T}{2\rho\pi(\bar{B}R)^2}]^{1/2}}$$

where $T = f(HP)$; $hp_o = f(\bar{B})$

Reducing the test data for near vertical descent, as given in Reference 6 on this basis, yielded $u/u_o = 1.0$ for all the test points.* This analysis used the rotor efficiency equation for the $\bar{B}$ term in these equations. These results indicate that the transition curve between $V/u_o = 0$ and $V/u_o = -2$ can be expressed on an actual rotor basis, by $u/u_o = 1.0$. The results of this analysis are shown in Figure 11.

Although some scatter is apparent in the results, it is interesting to note that the maximum variation, when converted to power, is only 10 horsepower for the data plotted as squares in Figure 11. The maximum variation for the hover data, plotted as circles is 3.5 horsepower.

These results then define the valid boundaries of 'Walds' equation. These boundaries would be between $\alpha = 0°$ and $\alpha = +90°$ for all positive values of V/u_o including $V/u_o = 0$ and for $\alpha = -90°$ for all V/u_o values less than -2. For the flight regime between $V/u_o = 0$ to -2, $u/u_o = 1$. Utilizing these considerations the relationship of u/u_o to V/u_o, as determined from 'Walds' equation, within the specified limitations, is plotted in Figure 11. These boundaries are used for this analysis.

---

* The four test points shown in Reference 5 for V/u_o values between -0.1 and -0.4 could not be found in Reference 6.

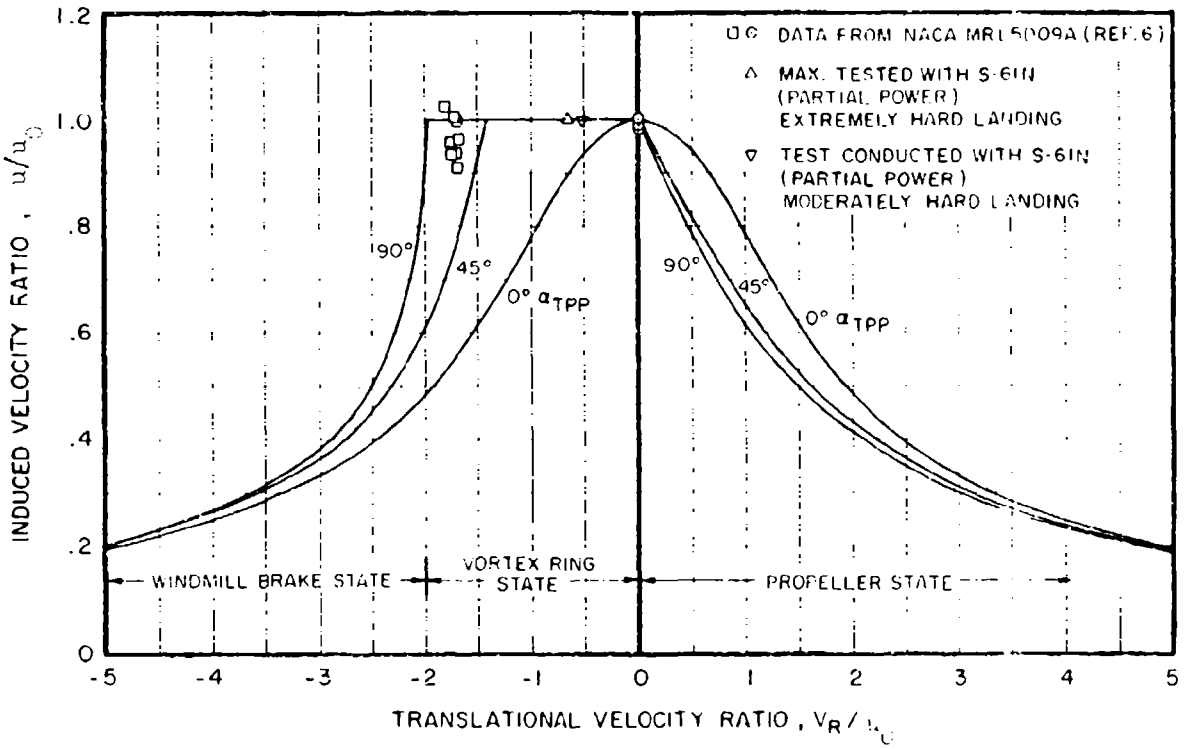

Figure 11. Induced Velocity Ratio as a Function of Translational Velocity Ratio.

While these boundaries establish a means of computing the induced velocity during steep descents, it does not establish the maximum rate of descent for which controllability can be maintained. Assuming that control can be maintained up to the onset of the vortex ring state, then the limit conditions can be determined by defining the vortex ring boundaries. The definition of this boundary is based on the following analogy.

Consider a rotor in a hovering condition with the rotor producing a uniform induced velocity U_o. The stream tube, produced by the rotor, is surrounded by a tube of vorticity generated from the blade tips. For this condition, whirl stand measurements have indicated that the rate at which the centers of the vortex cores move downward is approximately 52.5% of the average induced velocity U_o. Assuming that the onset of the vortex ring occurs when the rate of descent of the rotor increases to the point where the vortex cores no longer move away from the rotor disc, then the critical rate of descent would be

$$ROD_{CRIT.} = -.525\ u_o$$

In order to substantiate the assumptions of this analysis, flight tests were conducted at Sikorsky Aircraft, with an S-61N rotorcraft. These tests were set up to explore this flight regime and to determine the maximum velocity ratio for which positive rotor control can be maintained. The maximum velocity ratio tested, which resulted in an extremely hard landing and landing gear damage ($V/u_o = -.68$), is shown in Figure 11. One other test point which resulted in a moderately hard landing with no rotorcraft damage, $V/u_o = -.528$, is also included in this figure. In all, 623 near vertical descents were conducted in the V/U_o regime ranging from -.05 to -.68. However, only the two extreme points were considered pertinent for the purpose of this section.

The results of these flight tests indicated that positive rotor control could be safely maintained, provided the rate of descent did not exceed 50% of the computed induced velocity. On this basis it was stated that operation within the "Vortex Ring" region of flight ($V/u_o = 0$ to -2) can be safely conducted in close proximity to the ground, provided that the maximum rate of descent at any point along the flight path does not exceed $.5u_o$. These results indicate that, while the rotor airflow is assumed not to breakdown until $V/u_o = -.525$, positive rotor control can only be maintained up to a $V/u_o = -.5$. The positive rotor control limit ($V/u_o = .5$) is used for determining operating capabilities in the Helicopter Dynamic Performance Program.

BLADE TWIST

The blade twist basically establishes the spanwise load distribution which in turn affects the efficiency of the rotor system. The analysis conducted herein has been based on linear twisted blades. To approximate the effects of nonlinear twist on rotor efficiency the twist distribution is converted to a linear twist equivalent in a manner similar to establishing the effective solidity. The expression used for estimating the equivalent linear twist θ_e is

$$\int_0^1 \left| \hat{\theta}_e(x-0.8) \right| x^3 dx = \int_0^1 \left| \hat{\theta}\, x \right| x^3 dx \tag{29}$$

where $x = r/R$

$\hat{}$ denotes reference to 0 twist at $x = 0.8$

PARASITE HORSEPOWER

To determine the power required to overcome the airframe drag, the total drag force was divided into horizontal and vertical components.

Initially dealing with the horizontal component and expressing drag in general terms as

$$D = \frac{F\rho V^2}{2} \tag{30}$$

And nondimensionalizing with the thrust factor $\rho\pi R^2(\Omega R)^2$ yields

$$D/\rho\pi R^2(\Omega R)^2 = \frac{F\rho V^2}{2\rho\pi R^2(\Omega R)^2} = \frac{F}{2\pi R^2}\mu^2 = C_{D_p}$$

Expressing the nondimensional parasite drag in power coefficient terms yields

$$C_{P_p} = \frac{F}{2\pi R^2}\mu^3 \tag{31}$$

or in terms of horsepower

$$hp_p = C_{P_p}\frac{\rho\pi R^2(\Omega R)^3}{550} \tag{32}$$

VERTICAL DRAG

The vertical component of drag is generally added to the operating weight to determine the rotor thrust required. (Steady-state flight.) Utilizing the general expression for drag,

$$D_V = C_{D_\pi} \rho V^2/2 \, S_\pi$$

Determining C_{D_π} in terms of rotor disc area

and V as $u + V_V$

Then, $D_V = C_{D_\pi} \frac{\rho \pi R^2}{2} (U + V_V)^2$

Letting $C_{D_V} = C_{D_\pi}/2$

and nondimensionalizing with $\rho \pi R^2 (\Omega R)^2$ yields

$$D_V/\rho \pi R^2 (\Omega R)^2 = C_{D_V} (u + V_V)^2/(\Omega R)^2$$

Multiplying by u_o/u_o and appropriately expressing u_o as $C_T^{1/2} (\Omega R)/\sqrt{2}\,\bar{B}$, the expression can be nondimensionalized to

$$D_V/\rho \pi R^2 (\Omega R)^2 = C_{D_V} [u/u_o + \frac{2\bar{B}\mu_V}{C_T^{1/2}}]^2 \frac{C_T}{2\bar{B}^2}$$

The expression for the vertical component of thrust in nondimensional terms then becomes

$$C_T \cos \alpha_{TPP} = C_W + C_{D_V} [u/u_o + \frac{\sqrt{2}\bar{B}\mu_V}{C_T^{1/2}}]^2 \frac{C_T}{2\bar{B}^2} \qquad (33)$$

When canted tail rotors are considered the vertical component of the tail rotor thrust must be subtracted from this equation.

The term C_{D_V} can be defined as the vertical drag coefficient.

Defining the vertical drag as a percentage of operating weight with the helicopter in an out-of-ground effect hover, the term C_{D_V} can be defined from the equation

$$D_V = C_{D_V} \rho V^2 S_\pi$$

Using πR^2 for S_π

and u_o for V

Substituting equation (5) for u_o and letting GW + NGW = T where N is equal to the percentage of operating weight for vertical drag then

$$N\,GW = C_{D_V} \rho \left(\frac{GW + NGW}{2\pi\rho\bar{B}^2R^2}\right) \pi R^2$$

Solving for C_{D_V} yields

$$C_{D_V} = 2\bar{B}^2 \left(1 - \frac{1}{1+N}\right) \qquad (33a)$$

CLIMB POWER

The rate of climb (ROC) for any flight condition can be expressed in terms of the excess power from the equation:

$$ROC(FPS) = (HP_{AVAILABLE} - HP_{REQUIRED})(550/T\cos\alpha_{TPP})N_o$$

Where N_o is the rotor aerodynamic efficiency in climb.

The velocity and force vectors in a steady-state climb (Figure 12) indicate that the power required to sustain a climb rate (V_v) must be equal to $(T\cos\alpha_{TPP})V_v$, since $T\cos\alpha_{TPP} = D_C/\sin\gamma$.

The term T (rotor thrust) is used here as the thrust required to sustain the climb condition, and $V_v = V\sin\gamma$ then $(T\cos\alpha_{TPP})\,V_v = D_C V$ or the climb power can be expressed in terms of an equivalent drag force: Climb power required = $D_C V$.

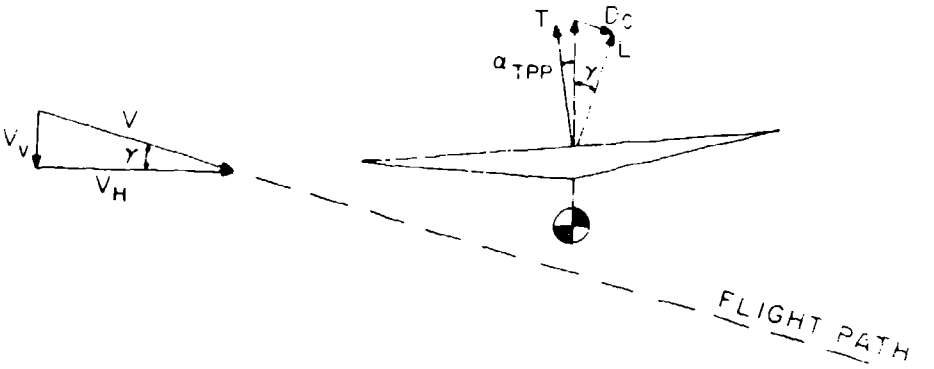

Figure 12. Velocity and Force Vectors in Climbing Flight.

Nondimensionally the additional power required to climb can be expressed as

$$\Delta C_Q/\sigma = (\Delta C_D/\sigma)_{CLIMB}(\mu R/N_o)$$

or $$N_o = (\Delta C_D/\sigma/\Delta C_Q/\sigma)\mu_R$$

It should be noted that the Nondimensional Velocity (u_R) is a function of flight path velocity, thus

$$\mu_R = [V_H 2 + V_V 2]^{1/2}/\Omega R$$

The value of N_o can be approximated by determining the $\Delta C_Q/\sigma$ required by the $\Delta C_D/\sigma = f(T, \frac{Vv}{V})$ at the proper μ, $M_{1,90}$ and δ_e. Evaluation of the rotor aerodynamic efficiency (N_o) indicated that it is dependent on atmospheric conditions and its value can be reasonably approximated by substituting the density ratio (ρ/ρ_o) for N_o. On this basis the climb power requirements are expressed for this analysis as

$$hp_c = (T \cos \alpha_{TPP})V_V \ (\rho_o/\rho)/550 \qquad (34)$$

Multiplying by $550/\rho\pi R^2(\Omega R)^3$ yields

$$C_{P_{CLIMB}} = (C_T \cos \alpha_{TPP})\mu_V(\rho_o/\rho) \qquad (35)$$

ROTOR SOLIDITY

The solidity of a rotor having rectangular blades may generally be expressed as $bC/\pi R$. Since this method of analysis deals with power or torque, the equivalent chord used for determining the solidity should be based on torque to obtain a more accurate determination. This can be expressed for any blade shape and account for various root cutout areas as

$$C_e = \int_0^1 Cx^3dx / \int_0^1 x^3dx \tag{36}$$

Substituting into the general solidity equation $bC/\pi R$ yields

$$\sigma_e = \frac{b}{\pi R} \int_0^1 Cx^3dx / \int_0^1 x^3dx = 4b/\pi \int_0^1 C/R\, x^3dx \tag{37}$$

COMPRESSIBILITY AND STALL

The expression used for determining profile power (δ vs $C_{L_{(M)}}$) does not account for compressibility above drag divergence or retreating blade stall. This procedure, using the mean lift coefficient, does not compute the variations in blade angle of attack or local lift coefficients along the blade or around the disc. To account for the effects of these variations the following analysis was made.

Compressibility Above Drag Divergence

It is assumed that the unaccounted for compressibility effects on profile power starts at $1/2(C_L/\sigma)_{LSL}$. The value of C_L/σ at the start of drag divergence was termed $(C_L/\sigma)_{CRIT}$. The following method is used to calculate $(C_L/\sigma)_{LSL}$.

The major variables which contribute toward compressibility effects were assumed to be μ, C_L/σ, C_D/σ, $M_{(1,90)}$ and θ_e. The condition where $bC_{Qd}/\sigma = .004$ is referred to as the "lower stall limit". Analysis of test data showed that for any given C_D/σ, $M_{(1,90)}$ and θ_e at the lower stall limit the value of $(1-\mu)/C_L/\sigma_{LSL}$ was nominally constant. Utilizing this relationship yielded a means of estimating the onset of blade stall. An expression relating $(1-\mu)/C_L/\sigma)_{LSL}$, C_D/σ. $M_{(1,90)}$ and θ_e was established by a curve fit of these data. (See Figure 13 for typical cross plot.) The resulting curve fit equation relating these variables is

$$(C_L/\sigma)_{LSL} = (1-\mu)/f(C_D/\sigma, M_{1,90}, \theta_e)$$

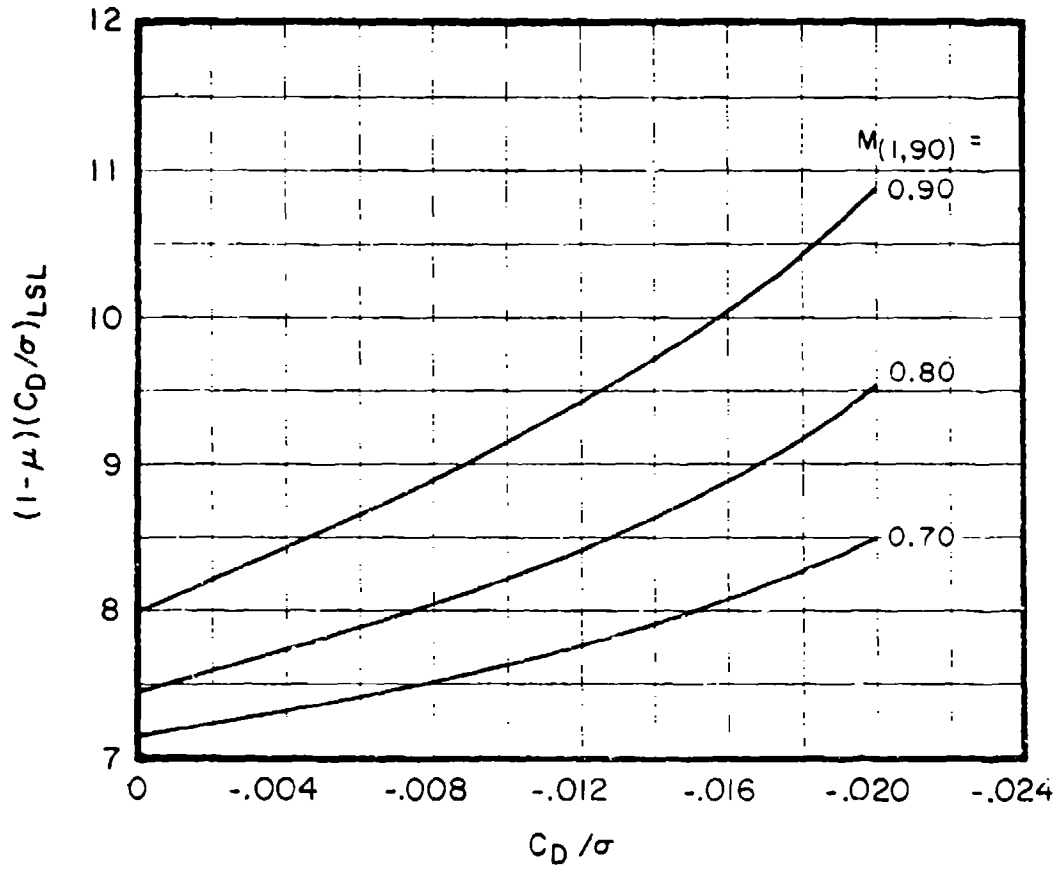

Figure 13. Basic Stall Limit Criteria.

where

$$f(C_D/\sigma, M_{1,90}, \theta_e) = [1750.(C_D/\sigma)^2 - 208.5\ C_D/\sigma(3.6M^2-3.71(M+1))$$

$$+(((C_D/\sigma + .01)^2/.000133)-.752)(M-.7)+38.7M-21M^2-9.9]$$

$$(1.17+1.2175\theta_e) \qquad (38)$$

$(M = M_{1,90})$

Stating that the increases in profile power due to compressibility above drag divergence should be nominally parabolic and a function of the operating and critical C_L/σ, a general expression for the power increase was set up as

$$C_{P_{comp}} = C_T[f(C_L/\sigma-(C_L/\sigma)_{crit})]^2/\text{constant}.$$

The function equation, $f(C_L/\sigma-(C_L/\sigma)_{CRIT})$, relating the operating and critical C_L/σ was set up to determine the difference between the δ at the operating $C_{L_{(M)}}$ and the increased δ due to compressibility. These function equations were evaluated as follows:

for $\mu<.25$

$$f(C_L/\sigma-(C_L/\sigma)_{crit})=(1.-(.33+3.\mu)C_L/\sigma+.133\mu+.036)-(C_L/\sigma)_{crit.} \qquad (39)$$

for $\mu>.25$

$$f(C_L/\sigma-(C_L/\sigma)_{crit})=C_L/\sigma-(C_L/\sigma)_{crit}-(1.08C_L/\sigma-.071) \qquad (40)$$

The parabolic constant in the $C_{P\ COMP}$ equation was evaluated from appropriate flight test data as 0.01.

Retreating Blade Stall

When the operating C_L/σ increases beyond the $(C_L/\sigma)_{LSL}$, retreating blade stall occurs and a further power demand is made that is in addition to the parabolic ($C_{P_{COMP}}$) increase discussed above. Test data indicated that this increase in power was dependent on the differential between the operating C_L/σ and the $(C_L/\sigma)_{LSL}$.

These data also indicated that the additional power increase was linear as the operating C_L/σ increased beyond the $(C_L/\sigma)_{LSL}$>.016→.020. A mean value of .018 was used to establish this stall divergence point. A generalized equation for computing the power increase due to the stall contribution was set up as

$$\Delta C_{P_S} = [f(C_L/\sigma-(C_L/\sigma)_{LSL})]\sigma(C_L/\sigma-(C_L/\sigma)_{LSL})$$

When $C_L/\sigma - (C_L/\sigma)_{LSL} < 0.018$ (41)

$$f(C_L/\sigma-(C_L/\sigma)_{LSL}) = 3.0(C_L/\sigma-(C_L/\sigma)_{LSL})$$

for $C_L/\sigma-(C_L/\sigma)_{LSL} > 0.018$ (42)

$$f(C_L/\sigma-(C_L/\sigma)_{LSL}) = 833.33(C_L/\sigma-(C_L/\sigma)_{LSL})^2 + 30.65(C_L/\sigma-(C_L/\sigma)_{LSL}) + .336$$

Total Horsepower Correction

The total horsepower correction due to compressibility and stall was then expressed as

$$C_{P_S} = [f(C_L/\sigma-(C_L/\sigma)_{crit})^2/.01]\sigma C_T + [f(C_L/\sigma-(C_L/\sigma)_{LSL})]\sigma(C_L/\sigma)_{LSL})\sigma \quad (43)$$

and

$$hp_s = C_{P_S} \rho\pi R^2(\Omega R)^3/550 \quad (44)$$

The coefficients used in the function (f) equations were derived from flight test data conducted in appropriate flight regimes.

GROUND EFFECT

To evaluate rotorcraft performance when operating in close proximity to the ground, a means of accounting for the ground effect had to be established. With the lack of substantiated "classical" methods for this analysis, an extensive flight test program was conducted with an S-56 rotorcraft at Patuxent River, Maryland. A large range of rotor heights and winds were investigated during these tests. These data were nondimensionalized with respect to velocity and rotor height. It was assumed that in ground effect the average rotor induced velocity is reduced, thus reducing rotor induced power and vertical drag. Therefore these data were

incorporated as a reduction factor of the required induced velocity. The resulting curves from this analysis are shown in Figure 14. The symbol used for ground effect, Λ, modifies the induced power term to

$$C_{P_i} = [C_T^{3/2}/\sqrt{2B}](u/u_o)\Lambda \qquad (6)$$

The value of Λ was set equal to 1 when H/D = 1, as power differentials were deemed insignificant above this height. The tests conducted covered lateral airframe protrusions up to 15% R only. The validity of these curves for lateral protrusions in excess of 15% R has not been substantiated.

Using these curves for tandem rotor helicopters the rotor height is assumed to be the average height of the two rotors. The rotor radius assumed for these calculations is based on the radius required to obtain the disc area for a single rotor which is equal to the projected area of the actual system. Reasonable agreement with measured flight test data has been obtained, with these assumptions for tandem rotors.

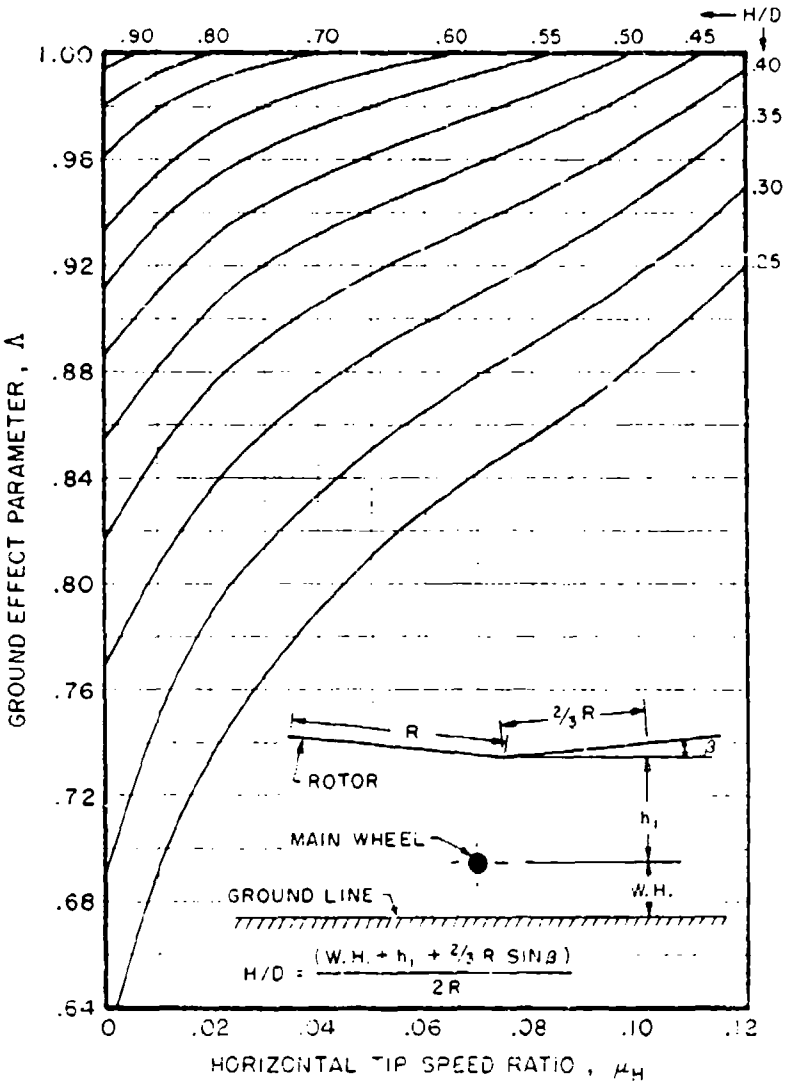

Figure 14. Ground Effect as a Function of Horizontal Tip Speed Ratio and Wheel (SKID) Height.

DYNAMIC FLIGHT

The previous derivations establish a means of calculating the steady-state power requirements for a given rotor system and operating weight. Conversely these equations can also be used to calculate the thrust developed by a given rotor system absorbing a specified power.*

The HDP-method states that the power required by a rotor system can be computed from the equation:

$$hp_a = hp_i + hp_o + hp_p + hp_c + hp_s = f(T)$$

Due to complex involvement of T in these power terms, a direct solution for (T) is impractical. In view of this, an iterative procedure can be used to establish the value of thrust which satisfies the power available. A tolerance of 0.5 horsepower is used to test for convergence.

It should be noted that the tip path plane angle, α_{TPP}, the horsepower available hp_a, and the rotor rpm are required for computing the thrust.

CONTROL INPUTS

The flight path a rotorcraft will follow is a function of the orientation and magnitude of the thrust vector and the power being supplied to the rotor. During take off and landing maneuvers, the manner in which the thrust vector is manipulated, through cyclic and collective input, will define the flight path a rotorcraft will follow. In order to compute the space-time relationship of a rotorcraft during these maneuvers, a means of establishing time histories of the tip path plane angle and power input must be determined. This analysis assumes that the thrust is perpendicular to the tip path plane axis and the tip path plane axis is coincident to the control axis in low speed flight.

TIP PATH PLANE ATTITUDE

Although the pilot has complete freedom of cyclic input control, specified clearance requirements for take off and landing maneuvers demand specific cyclic input rates and limits. Flight tests conducted for confined area operations have indicated that relatively repetitive inputs for a specified procedure are required. The results of these tests are shown in Figure 15. Analysis of these data indicated that the time histories of the tip path plane attitude could be normalized into two equations. These equations can be expressed for the tip path plane transition from its position at the start of an event to the maximum angle used during the event. The

---

* The relationship that T = f(GW) is only applicable to steady state flight conditions.

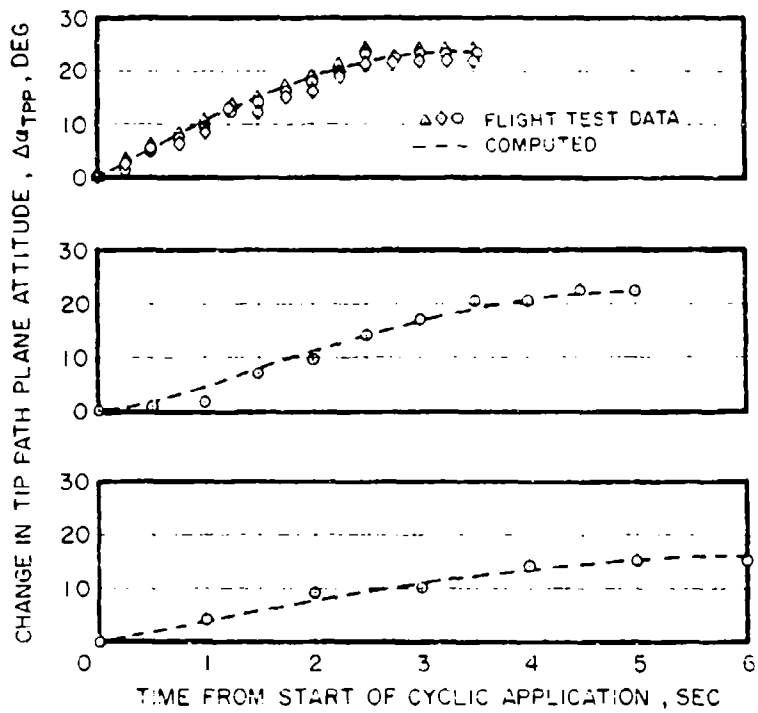

Figure 15. Typical Tip Path Plane Time Histories.

second portion of the equation covers the transition from the maximum angle used to the angle required at the end of an event. These two transitions can be defined as the two segments of an event.

An event is defined as that portion of the maneuver between two specific occurrences, i.e., the variation in tip path plane attitude between lift off and the engine malfunction point (EMP), would be the event between the occurrences of Lift Off and EMP.

These equations were expressed for the two segments of an event as

$$\alpha_{TPP}(K+1) = ANG_0 + (ANG_{MAX}-ANG_0) \sin\left[\pi/2\left(\frac{t(K+1)-t_0}{t_{RATE}}\right)\right] \qquad (45)$$

for the first segment, and for the second segment

$$\alpha_{TPP}(K+1) = \alpha_{TPP_{V_Z}} \sin\left[\pi/2\left(\frac{V_X - V(K)}{V_X}\right)\right] + \tan^{-1}(D/T) \qquad (46)$$

where subscript K is the time index counter
0 is the condition at the start of the event
Max is the maximum value permitted
Rate is the maximum rate permitted
X is the desired limit.
z is the phase out speed.

Equations 45 and 46 yield a means of generating a time history of tip path plane attitude during any event. It should be noted that the transfer from equation 45 to 46 is controlled by:

If $V(K) < zV_X$ use equation 45

If $t(K+1) > t_{RATE}$; $\alpha_{TPP}(K+1) = ANG_{MAX}$

If $V(K) > zV_X$ use equation 46

where z is any desired fraction of V_X.

Thus any tip path plane time history can be generated and controlled by defining, ANG_{MAX}, t_{RATE}, V_X, and z along with the conditions ANG_0, and t_0 at the start of any event. The flight tested rates and limits were applied to equation 45 and the results superimposed on the test data in Figure 15.

These equations of tip path plane attitude yield a good representative time history of control input capability. Since this normalization of tip path plane attitude permits an infinite number of combinations, caution should be used so that the time history generated are within reasonable pilot work load limits when establishing trends and/or takeoff procedures.

POWER INPUT

Aside from the tip path plane attitude, the power applied to the rotor and the rate at which this power is applied also directly affects the flight path the rotorcraft will follow:

Power (energy per unit time) can be supplied to the rotor in three ways: from the engines, from a change in rotor rpm, and from a change in kinetic energy. In the Helicopter Dynamic Performance program the power input from the engine is generally assumed to be a linear function with time. Exceptions to this linear function are made for power application during landings and controlled flight path takeoff procedures.

For the general case the horsepower available at any time point can be expressed as

$$SHP(K+1) = SHP(K) + HP_{MAX}/(t_{RATE}) \tag{47}$$

up to the specified power available or transmission rating, whichever is lower.

Power application rates during landings are determined by the power required to maintain the desired approach rate of descent. This power required is determined for the average conditions occurring during a specified power available or the transmission rating, whichever is lower.

ROTOR ENERGY

Rotorcraft are designed to prevent wide excursions in rotor RPM. This is accomplished by coupling the collective stick with the fuel control or throttle so that the selected RPM is maintained with collective stick inputs. When the maximum engine power level is reached, the rotor RPM will change with further increases in collective settings. Similar to the Tip Path Plane variations, the pilot has full control of these changes. There are some exceptions to this which will be discussed later. In order to evaluate rotorcraft capabilities in dynamic flight, the effect of these RPM variations must be evaluated. This evaluation considered the following relationships.

The power that is released or absorbed by a rotating system can be evaluated by considering the rotating mass of the system.

The stored energy in any rotating system can be expressed from the general equation:

$$\text{ROTATING ENERGY} = [J_M/2](\Omega^2)$$

where J_M is the mass moment of inertia of the rotating system.

If a change in the rotational speed occurs, the change in energy level can be expressed as:

$$\Delta \text{ROTATING ENERGY} = [J_M/2](\Omega_1^2 - \Omega_2^2)$$

By specifying the time interval for which this change in RPM occurs the horsepower being released or absorbed by the system can be expressed as

$$HP_{\dot{\Omega}} = [J_M/1100](\Omega_1^2 - \Omega_2^2)/\Delta t \qquad (48)$$

To utilize these relationships a means of establishing rotor RPM variations with time must be established. Since the pilot can control the RPM excursions through collective adjustment, the basic aerodynamic drag-inertia relationships are inappropriate for this analysis. To determine typical variations of rotor RPM with time, flight tests were conducted under saturated (maximum power) engine conditions. These tests were conducted for specified collective application rates and RPM excursion limits. The results of these tests are shown in Figure 16. These test results indicate that for the specified conditions, variations in rotor RPM with time are reasonably repetitive. Analysis of these data further indicated that the change in RPM over a specified time period can be generally expressed from the equation

$$dN_R = \Delta N_R \sin\left[\pi/2\left(\frac{t(K+1) - t_o}{t_{RATE}}\right)\right]$$

where dN_R is the RPM change

ΔN_R is the total RPM excursion

t_{RATE} is the total excursion time

t_o is the time of collective application

$t(K+1)$ is the time at any interval between t_o and t_{RATE}

The results of this equation, computed for the test conditions, were superimposed on the test data in Figure 16.

On this basis the RPM at any point during any given time period can be expressed as

$$N_R = N_{R_0} + \Delta N_R \sin\left[\pi/2\left(\frac{t(K+1)-t_o}{t_{RATE}}\right)\right] \qquad (49)$$

when $t(K+1) - t_o \geq t_{RATE}$; $N_R = N_{R_0} + \Delta N_R$

where N_{R_0} is the RPM at the start of the event.

Further flight tests were conducted to establish the effects of random rates of collective application between a specified RPM excursion. These

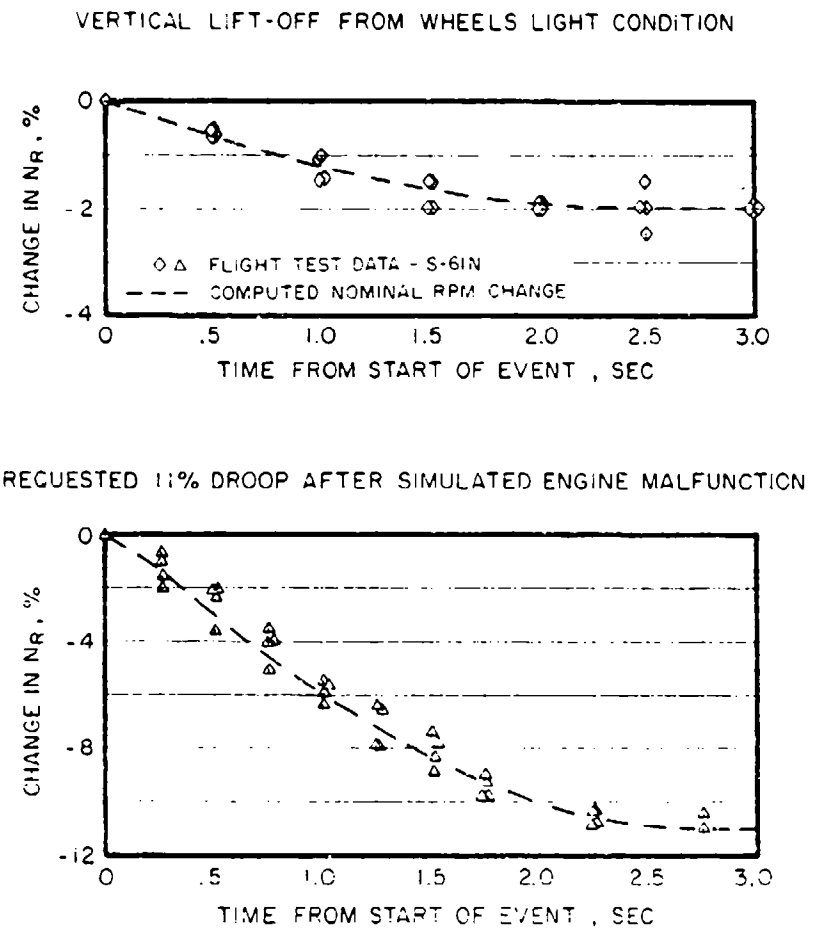

Figure 16. Typical Rotor RPM Change Time Histories.

tests were also conducted under saturated engine conditions. The results of these tests are shown in Figure 17. The generalized equation, calculated for the overall RPM excursion, was superimposed on these test data for reference. These data show that large variations in the rates of change in RPM occur when large variations in collective application rates are used. To further evaluate these data, the rate of change in RPM with time were plotted. These results are shown in Figure 18. Analysis of these curves showed that independent of the manner in which the RPM varied across the time period, the total energy change during the total time period is the same. This can be seen from the equations

$$\Delta N_R = \int_o^t \frac{d\Delta N_R}{dt} dt$$

and $$\Delta KE_{o \to t} = [J_M/2](\Omega_0^2 - \Omega_t^2)$$

On this basis it was stated that the energy transferred by the rotor system can be established between any specified end points during an event using equation 49 to establish the time history of the RPM during the event.

It should be noted that while this equation might not yield the exact time history of the RPM variation, as can be seen in Figure 17, the overall effects on the flight path will be insignificant as the total energy transferred is accounted for. This assumes that reasonable collective application rates are used and the period of RPM change consitutes a small portion of the overall flight path being evaluated.

There are some areas where the pilot does not have full control of the RPM variations. These include rapid collective application during take off and during a specified collective application time delay at the point of engine malfunction.

The RPM droop or decay during power application will vary with different engine models or control unit designs. The amount and rate of droop is best established from flight tests conducted with the particular engine configuration and allowable control system rates being used. The amount of rotor droop during a specified collective delay at the engine malfunction point is a function of the rotor inertia and collective setting at the time of malfunction.

The collective setting required by the rotor system is a function of the power being absorbed by the rotor, which is in turn related to the thrust or C_T being produced. A relationship between collective setting, θ_{75}, and rotor thrust, C_T, for any given flight condition can be established from blade element theory as

$$\alpha = \frac{(1+1.5\mu^2)\frac{6C_T}{\sigma a} + 1.5\lambda\,(1-0.5\mu^2)}{(1-\mu^2+2.25\mu^4)} \qquad (50)$$

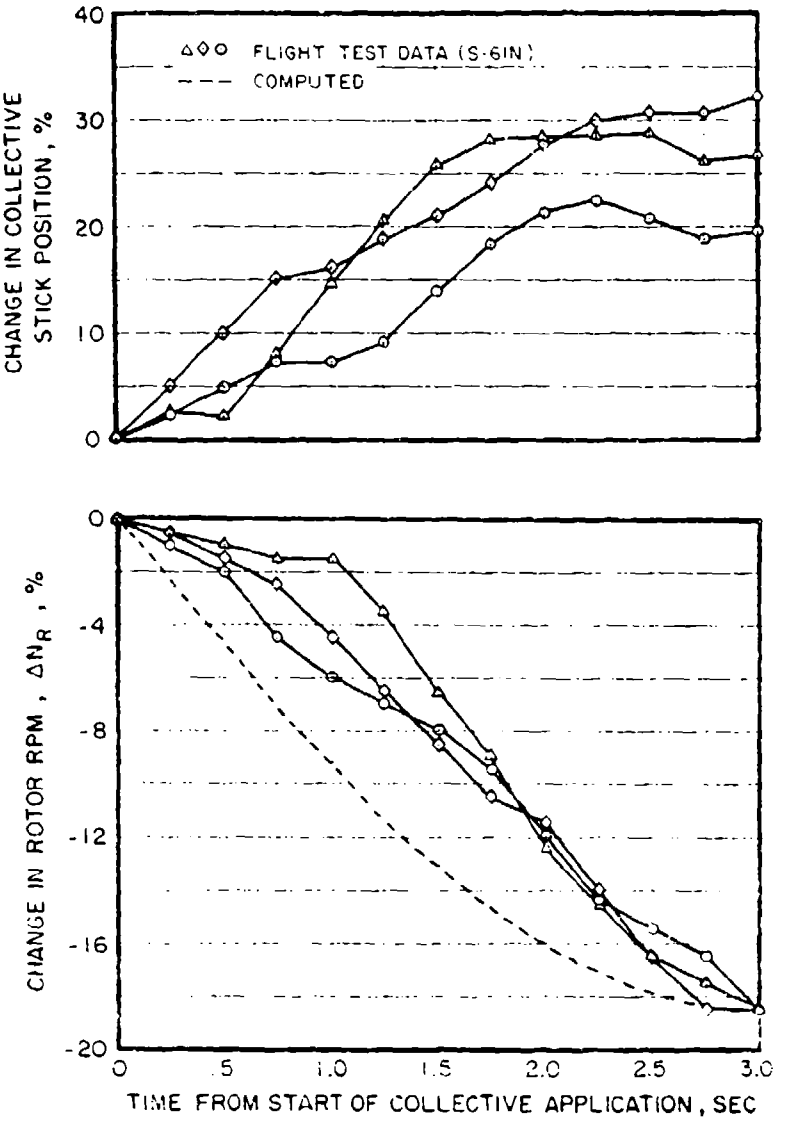

Figure 17. Effect of Collective Application Rates.

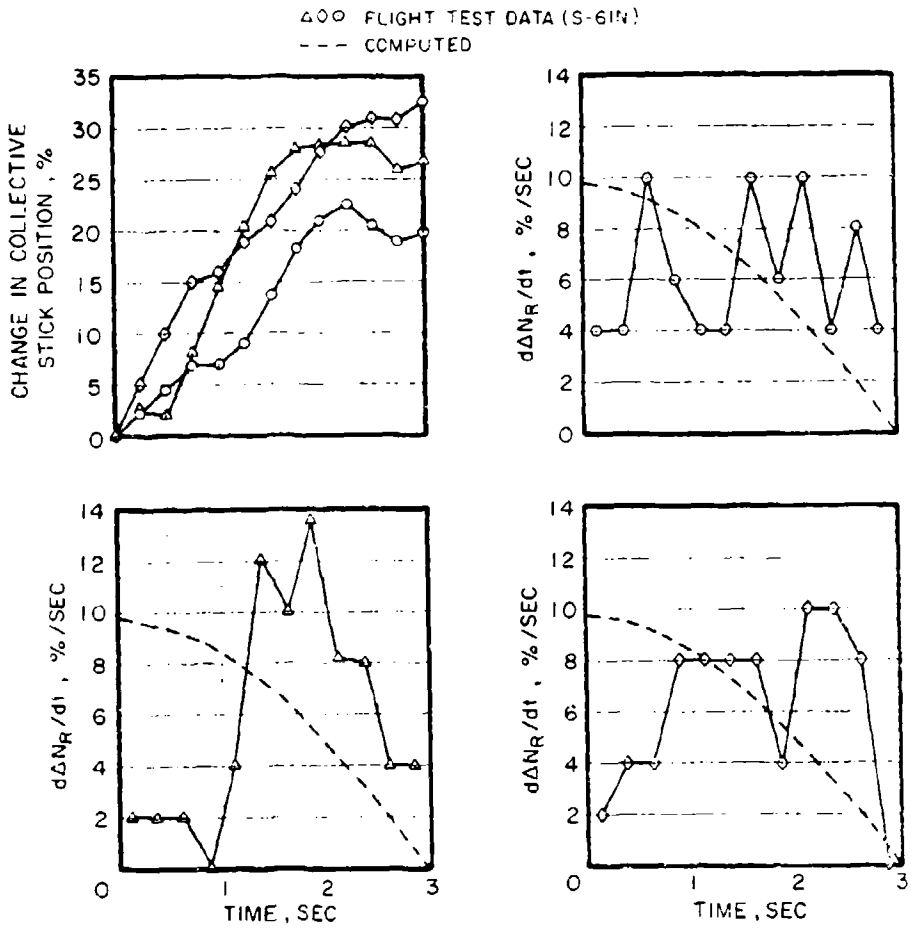

Figure 18. Energy Transfer With Collective Application Rates.

α can be referenced to θ_{75} as

$$\alpha = \theta_{75} - \Phi \tag{51}$$

Defining μ as $\frac{V}{\mu R} \sin\alpha_s$ and α_w as the tip path plane angle relative to the airstream, then the inflow ratio λ can be defined as

$$\lambda = \frac{V\sin\alpha_w - u}{\Omega R}$$

Where the value of μ can be established from Wald's equation using the relationship

$$u = u/u_o \; u_o = \bar{u}u_o$$

substituting

$$\lambda = -\mu_H \sin_{\perp s} - \frac{\bar{u}\sqrt{.5C_T}}{\bar{B}} \tag{52}$$

Assuming constant induced velocity it can be stated that

$$\Phi = \tan^{-1}(\quad) \tag{53}$$

These equations are then used to calculate the change in rotor RPM for a specified change in collective stick position, as follows:

For a specified θ_{75} and flight condition the rotor thrust coefficient (C_T) can be calculated from the equation

$$C_T = \frac{(1-\mu^2+2.25\mu^4)a - 1.5\lambda(1-0.5\mu^2)}{(1+1.5\mu^2)} \quad (\tfrac{\sigma a}{6}) \tag{54}$$

With C_T known the power required for the flight condition can be calculated from the basic energy equations. The difference in the power required and the power available must be accounted for by an increase in power level or a change in rotor RPM when the maximum power available is reached. Relating this power differential to the rotating energy equation yields

$$HP_{REQ} - HP_{AV} = HP_{\Omega} = \frac{J_M}{1100}(\Omega_1^2 - \Omega_2^2)/\Delta t$$

Solving for the RPM at point 2 yields

$$\Omega_2 = \left[\Omega_1^2 - \frac{1100\, HP_{\Omega}\,\Delta t}{J_M}\right]^{1/2} \tag{55}$$

The term (a) in equation 54 is the lift curve slope. In fixed wing and blade element theories this term takes on values of 5.73 with variations that depend on airfoil section and element Mach numbers. This term in rotorcraft momentum theory corresponds to the mean lift coefficient ($C_{L_{(M)}}$) slope of the total rotor disc. Values of (a) can be established by solving equation 54 for (a) substituting in known values for C_T and θ_{75} required for the initial conditions and the program will compute the lift curve slope. If the θ_{75} at the initial point is not input, the program will use the value of 2.66 as typical.

DETERMINATION OF SPACE-TIME RELATIONSHIPS

The previous sections established a means of determining the thrust a rotor is capable of developing for any given power input. A means of establishing rotor RPM levels, tip path plane orientation and horsepower levels during any given event were also defined. Considering that take-off and landing performance is nothing more than a specified series of events, then the flight path a rotorcraft will follow can be established by specifying the occurrences during each event of the maneuver.

This analysis establishes the flight path using a step function integral approach. This approach assumes that the RPM, tip path plane, horsepower, and velocities are constant during any given time period. These values are based on the computed level for the mid-point of the time interval used. With these values established, for the time interval in question, the thrust the rotor is producing can be determined.

With the rotor thrust established, the unbalanced forces acting on the rotorcraft during the time interval can be determined from the equations

$$F_x = T\cos\alpha_{TPP_{LONG}} \sin\alpha_{TPP_{LAT}} - D_x \tag{56}$$

$$F_y = T\sin\alpha_{TPP_{LONG}} \cos\alpha_{TPP_{LAT}} - D_y \tag{57}$$

$$F_z = T\cos\alpha_{TPP_{LONG}} \cos\alpha_{TPP_{LAT}} - (GW + D_V) \tag{58}$$

The displacement of the rotorcraft can then be determined from the equations

$$a = F/M \tag{59}$$

$$V_{NEW} = V_{OLD} + a\,dt \tag{60}$$

$$\Delta S = V_{OLD}\,dt + 1/2\,a\,dt^2 \tag{61}$$

$$S_{TOTAL} = \Sigma_{o}^{t} \Delta S \tag{62}$$

These basic equations of motion are applied for the unbalanced forces in the X (longitudinal), Y (lateral), and Z (vertical) directions to establish the flight path. The velocity terms in these equations are referenced to ground speed using the relationship $V_{GRND} = V_{AIR} - W_{(\ )}$.

The subscript ( ) refers to the wind components in the X, Y and Z directions and can be computed from the equations:

$$W_{(X)} = V_W \cos(DIR_X - HDG) \cos(DIR_Z) \tag{63}$$

$$W_{(Y)} = V_W \sin(DIR_X - HDG) \cos(DIR_Z) \tag{64}$$

$$W_{(Z)} = V_W \sin(DIR_X) \tag{65}$$

Where DIR is the wind direction
HDG is the A/C heading
V_W is the resultant wind velocity

When accelerations are imposed on an object, a change in kinetic energy occurs. The energy expended to effect this change can be expressed in terms of horsepower as:

$$HP_{ACC} = \Delta KE/550\ \Delta t \tag{66}$$

Where $\Delta KE = KE_2 - KE_1$

The kinetic energy of a body is computed from the equation

$$KE = 1/2M\bar{V}a^2$$

Where M is the mass of the body, $\bar{V}a$ is the absolute scalar velocity.

This acceleration power is included in the horsepower available term (hp_a)

for the determination of rotor thrust. Since the accelerations are a result of the time step calculation, the following process is used for evaluating each time step. Initially the acceleration from the previous time step is assumed. For the first time step, zero acceleration is used. Based on this assumption the unbalanced forces and resulting accelerations are computed. The initial and resulting accelerations are then compared. If the initial and resulting accelerations are within 0.3 ft/sec^2 (.0093 G's) in the horizontal, lateral and vertical directions the time step is considered to be converged. If these tolerances are not met the initial accelerations are set equal to the resulting accelerations and the time step is repeated until the tolerances are met.

CONTROLLED FLIGHT PATHS

It has been stated previously that the flight path a rotorcraft will take is entirely dependent on the tip path plane attitude, the rate of power application, and the maximum power used during the maneuver. If the flight path a rotorcraft is to follow is controlled, as would be required if a height-velocity envelope existed, then the rate of power input or tip path plane attitude must be controlled.

Evaluations of height-velocity diagrams, Reference 7 resulted in a means of normalizing the boundaries of the low speed height velocity envelope. This normalized diagram is shown in Figure 19. Only the lower portion of this curve is shown herein.

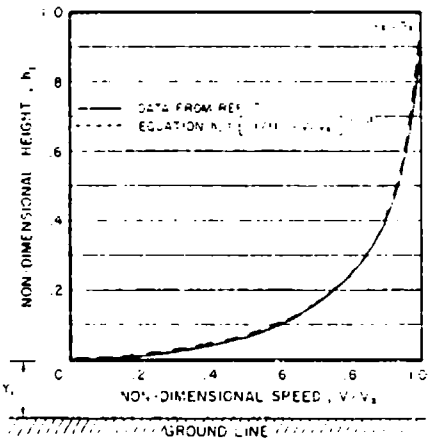

Figure 19. Nominal HV Lower Limb.

Using these data the actual height and speed at any point along the curve can be determined by specifying V_x, h_x and y_1 from the equations.

$$V = (V/V_x)V_x$$

and $$Y = h_1(h_x - y_1) + y_1$$

Reference 7 specifies the coordinates of this curve in tabular form. Analysis of this data showed that this curve could be reasonably approximated by the equation

$$h_1 = \left[\frac{.11}{1.1 - V/V_x}\right] - .11 \qquad (67)$$

[7] Pegg, R. J., AN INVESTIGATION OF THE HELICOPTER HEIGHT-VELOCITY DIAGRAM SHOWING EFFECTS OF DENSITY ALTITUDE AND GROSS WEIGHT, NASA TN D-4536, May 1968.

A comparison of the tabulated data from Reference 7 and this equation is also shown in Figure 19.

This equation then yields a means of defining any flight path by specifying the end point of the curve, V_x, h_x and the initial height y_1.

In order to establish the power input rate, required to follow this flight path, the following manipulations of the h_1 equation were conducted.

The slope of the curve at any point can be defined by taking the first differential of h with respect to V, thus

$$h = y - y_1 = \left\{\left[\frac{.11}{(1.1 - V/V_x)}\right] - .11\right\}(h_x - y_1)$$

$$dh/dv = \frac{.11V_x(h_x - y_1)}{(1.1V_x - V)^2}$$

Multiplying the left side of the equation by dt/dt yields

$$[dh/dv](dt/dt) = (dh/dt)/(dv/dt) = V_v/a_H$$

therefore, the permitted vertical velocity at any point along the flight path can be established from

$$V_v = \left[\frac{.11V_x(h_x - y_1)}{(1.1V_x - V)^2}\right]a_H \qquad (68)$$

Thus, the power required to sustain the permitted vertical velocity can be established for the time interval in question. It is assumed that the tip path plane attitude, α_{TPP}, is specified for the time intervals. It should be noted that if the computed rate of power application is greater than the maximum allowable rate, the maximum allowable rate will be used, also, if the power requirements exceed the maximum allowable power, the maximum allowable power will be used.

Flight paths can be controlled in this manner (within the imposed limits of tip path plane attitude, power application rates and power limits) for any predefined flight path. The flight path can be predefined by specifying the three coordinate points y_1, h_x, and V_x.

Another form of a controlled flight path would be to specify a level acceleration at maximum power up to a given speed or distance. In this case the power is allowed to vary as a linear function up to the maximum available, or transmission limit, and the tip path plane attitude required to maintain level flight is computed. The tip path plane attitude is computed on the basis that if level flight is to be maintained then $T\cos \alpha_{TPP} = GW + D_V$ or

$$\alpha_{TPP} = \cos^{-1}\left(\frac{GW+D_V}{T}\right) \tag{69}$$

where $T = f(SHP \ \& \ \alpha_{TPP})$

This requires an iterative solution. Caution should be used when using this type of controlled path to insure that sufficient ground clearance is maintained as high tip path plane attitude requirements could result from high power available to power required ratios.

AUXILIARY POWER DEVICES

The HDP program was designed to accommodate various program options to provide investigation of various auxiliary power devices, dropping of external loads or activating drag brakes. The various available devices and the equations used for their derivation are listed below.

1. Auxiliary Power Units. These units are assumed to deliver a specified horsepower to the main rotor gearbox for some finite time period. This power is added to the horsepower available (if any) for the determination of the thrust during the time span for which it is applied.

2. Rotor Tip Rockets. Tip rockets are handled by converting the rocket thrust to horsepower for inclusion into the power available term. This rocket thrust is converted using the equation $hp_{a_R} = T_R R \Omega b/550$.

   The HDP program assumes that if tip rockets are being used, there is one mounted on each rotor blade. Here again the point in the flight path at which the rockets are to be ignited and the time duration for which they are to be used are specified

3. Flywheels. The use of flywheels in the drive train is handled in the same manner as the rotor energy. The horsepower contribution to the system is computed using equation 48, where J_M is the mass moment of inertia of the flywheel and the angular velocity is computed from the relationship Ω_{MR} RPM flywheel/RPM rotor.

   If flywheels are being used the program assumes them to be on line during the entire flight.

4. External Propulsion Units. These units are considered as JATO or RATO units attached to the airframe. The program assumes that these units are mounted so that the resultant thrust vector passes through the airframe center of gravity. The program handles these thrust units by applying the horizontal, lateral and vertical components of thrust to the summation for determining the unbalanced forces. The basic inputs required are the portion of the flight that units are to be applied, the thrust per unit, the number of units being used, the mount angle of the unit, and the time duration that the thrust is available.

5. Dropping of External Load. Provisions have been made in the HDP Program for dropping an external load, if applicable, in case of emergency. The program also allows for a change in airframe drag if this option is used. The program considers this delta weight change when summing forces to obtain the unbalanced forces. The change in 'F' is considered in the evaluation of the power-thrust relationship.

6. Drag Brakes. To minimize the program code the use of drag brakes is handled using the same program logic block as used for dropping an external load.

In this case the load dropped would weigh 0.0 pounds and the change in 'F' would be $+\Delta F$ ft^2. This effectively provides evaluation of the drag brakes. In both cases, items 5 and 6, the portion of the flight during which the load is to be dropped or the drag brakes applied can be specified. Once this option has been turned on the program assumes that it applies until the end of the flight.

The auxiliary power devices discussed in this section can be accessed in the HDP program through input locations 207-218. Refer to Volume II for the explicit input requirements for their activation.

AIRFRAME ATTITUDE

The treatment of airframe pitch and roll attitudes in the HDP program is based on a summation of moments about the rotorcraft center of gravity. Referring to Figure 20 it can be seen that a summation of moments about the CG would yield

$$\Sigma M = -T_{TR}D_{TR} + H_M \sin(\text{SHAFT TILT}) + T_{MR}D_R \cos\alpha_{TPP}\sin\beta$$

If the rotorcraft is in a steady-state condition

$$\Sigma M = 0$$

and $$\beta = \sin^{-1}(-T_{TR}D_{TR} + H_M \sin(\text{SHAFT TILT})/(T_{MR}D_R\cos\alpha_{TPP})$$

and $$\text{AIRFRAME PITCH ANGLE} = \beta - \gamma$$

Considering the rotorcraft in a dynamic state with a time variant tip path plane attitude, the airframe attitude can be related to the tip path plane attitude by considering the airframe as a pendulum with a pivot point at the main rotor centroid.

On this basis the unbalanced moment acting on the airframe can be expressed as

$$P_M = T_{TR}D_{TR} - (2\,D_R\,T_{MR} + H_M)\sin(.5\beta) \tag{70}$$

Where $$\beta = \alpha_{TPP_t} + \beta_{t-1} - \beta_o \tag{71}$$

Transferring the airframe inertia to the main rotor centroid

$$I_{yy_{MR}} = I_{yy_{CG}} + w/gD_R^2 \tag{72}$$

and the pitching acceleration would be

$$P_A = P_M/I_{yy_{MR}} = \ddot{\beta} \tag{73}$$

The airframe pitch velocity during the time interval in question can be expressed as

$$\dot{\beta}_t = \dot{\beta}_{t-1} + \ddot{\beta}_t\Delta t \tag{74}$$

and $$\beta_t = \dot{\beta}_t \Delta t + .5\ddot{\beta}_t \Delta t^2 + \beta_{t-1} \quad (75)$$

It should be noted that the HDP program does not evaluate airframe aerodynamics beyond the parasite power. Thus airframe lift forces and pitching moments are not included in the above analysis. To account for these items a damping term was applied to the pitch velocity evaluation. Thus the pitch velocity equation was written

$$\dot{\beta}_t = (\dot{\beta}_{t-1} + \ddot{\beta}_t \Delta t)\text{PDAMP} \quad (74m)$$

On this basis PDAMP (pitch damper) takes on the definition that infinite damping is attained when PDAMP = 0 and no damping occurs when PDAMP = 1. Thus various values of damping can be evaluated by specifying values of PDAMP between 0 and 1.

The use of this term does require the user to establish the value of PDAMP for the rotorcraft being evaluated by correlation of body attitude vs time with flight test measured time histories of dynamic flight. Once this value has been established, trade-offs can be conducted to evaluate the effects of changes in static stability by using variations of PDAMP from the base value and ratio the PDAMP values with the base static stability to find the new static stability.

The evaluation of airframe roll attitude is conducted in the same manner as the airframe pitch analysis. When dealing with the roll axis the airframe inertia is based on the XX or longitudinal airframe axis. The basic sketch showing the dimensions and forces for the roll analysis is shown in Figure 21.

Yaw attitude is not considered in the HDP Analysis.

A dynamic body attitude analysis for tandem rotors has not been conducted.

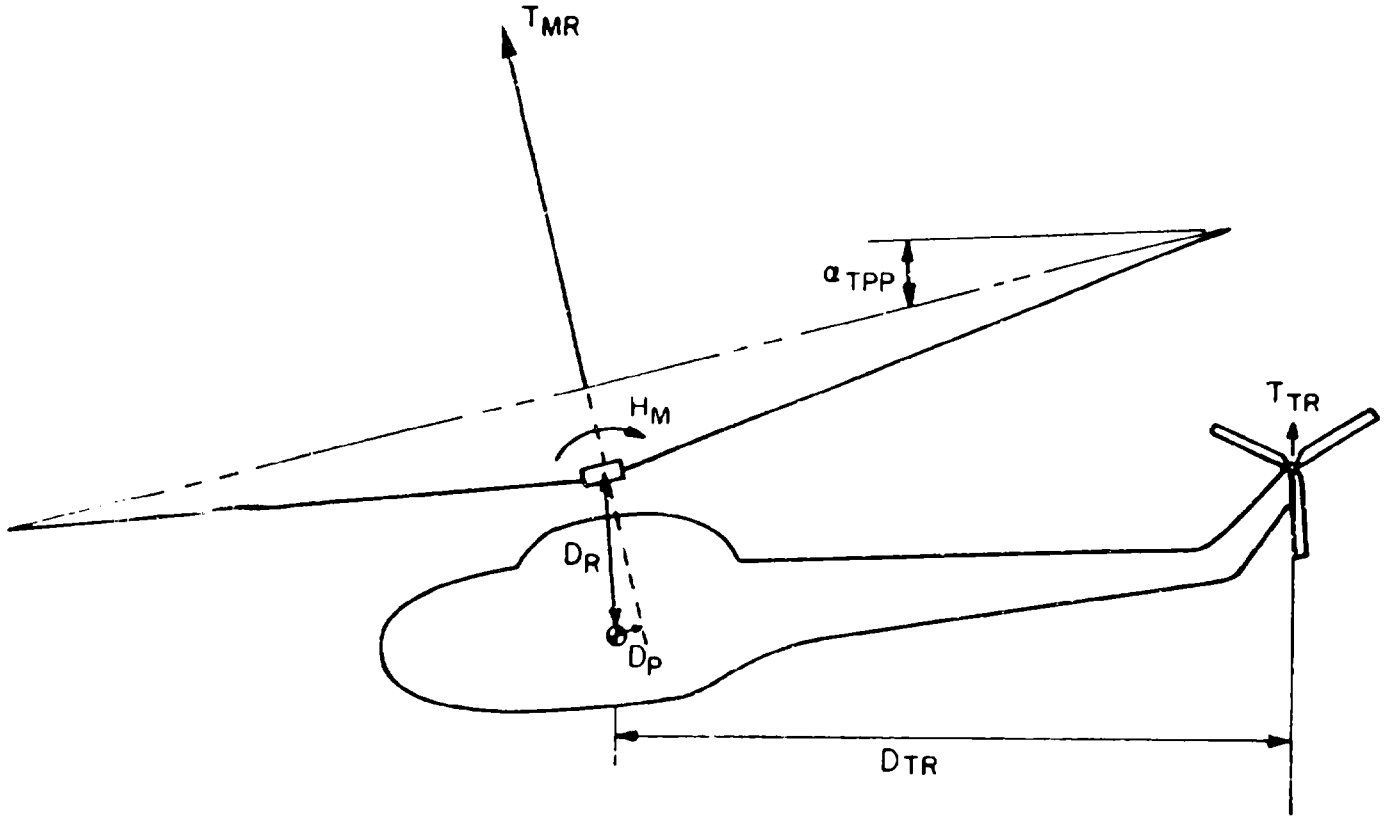

Figure 20. Airframe Force-Moment Diagram for Establishing Airframe Pitch Attitude.

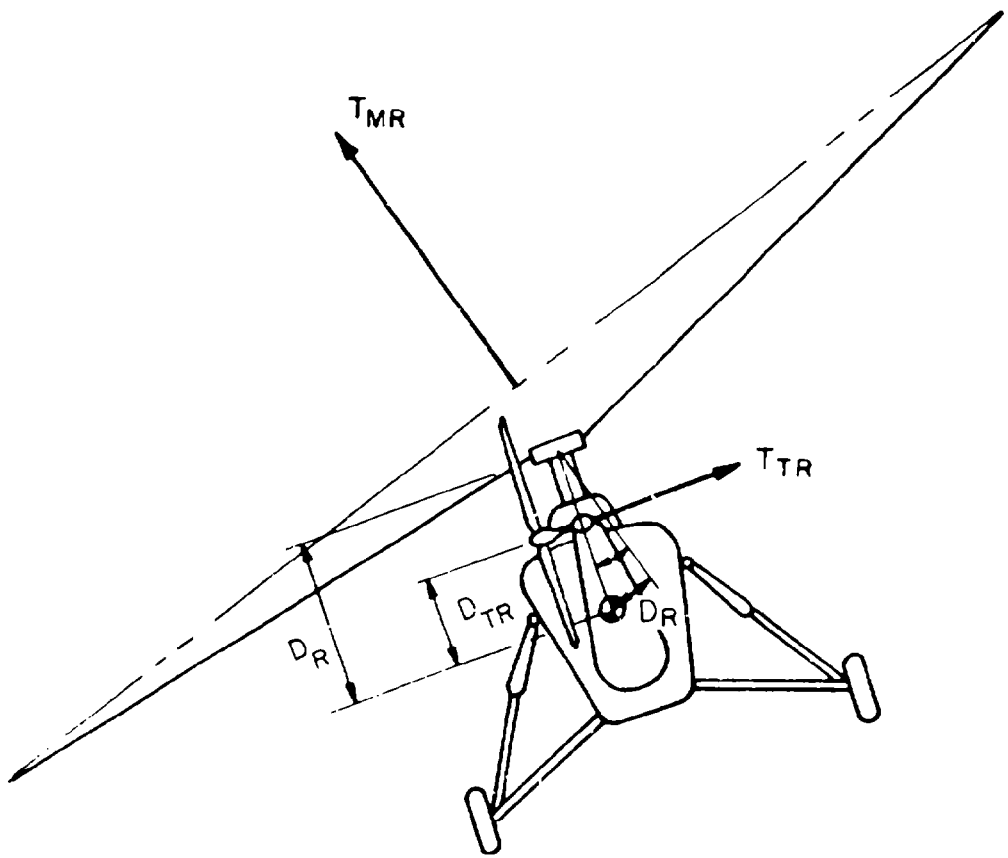

Figure 21. Airframe Force-Moment Diagram for Establishing Airframe Roll Attitude.

H-V ENVELOPES

The HDP program has incorporated the capability of computing the low-speed HEIGHT-VELOCITY (H-V) diagram. When the program is operated in this mode the user need not be concerned with the control input requirements for program operation. The program is designed to establish the best, 'optimum' flight procedures to use for minimizing the avoid area of the H-V envelope. The basic input requirements for this program mode is summarized in section 6.3 of the User's Manual (Volume II).

The construction of the H-V envelope is based on the following procedures. Reference 7 outlines a procedure and normalized equations for estimating HEIGHT-VELOCITY envelopes. Using this as a basis, the three key points of the H-V curve can be calculated.

These three key points being low hover height, nose point, and the high hover height. Based on Reference 7, the low hover height (h_{lo}) can be estimated using the equation:

$$h_{lo} = - \frac{J_M \Omega_d V_v}{1100\ HP_{\infty A}} (1-2.24\sqrt{C_T/\sigma})$$

To account for partial power conditions (multi-engine rotorcraft) the $HP_{\infty A}$ term was modified to an unsupported power loading term. Thus, to account for any partial power condition, the $HP_{\infty A}$ terms can be expressed as

$$HP_{UNS} = HP_{\infty A}(1-HP_{AV}/HP_{\infty A}) \tag{76}$$

and

$$h_{lo} = - \frac{J_M \Omega_d^2 V_v}{1100\ HP_{UNS}} (1-2.24\sqrt{C_T/\sigma}) \tag{77}$$

It should be noted that if the horsepower available is equal to or greater than that required to hover i.e., $(HP_{AV}/HP_{\infty A} \geq 1)$, then no HEIGHT-VELOCITY diagram exists and further evaluation is unnecessary.

Using this estimated h_{lo} point as a starting point, the program cycles through a double iteration scheme, adjusting the h_{lo} height so as to satisfy a user specified vertical touchdown velocity and C_T/σ limit. The results of this iteration yields the flight procedures required and the maximum low hover height from which these imposed conditions can be met. (For further optimization discussion refer in text to the Appendix.)

The estimate for the nose point critical speed is outlined in Reference 7 in graphical form. This figure is shown as a function of velocity for minimum power and C_L/σ. The term C_L/σ is in turn defined in terms of the minimum power speed as

$$C_L/\sigma = 2/\mu_{MIN}\ C_T/\sigma \tag{78}$$

Expressing the family of curves given in Reference 7 in equation form, yields

$$V_{CR} = 2.809V_{MIN} + 5.618C_L/\sigma - 169.776$$

The minimum power speed (V_{MIN}) can be obtained by setting the first differential of the basic power equation to zero. Expressing the basic speed-power curve as

$$C_Q = \frac{C_T^2}{2\mu\bar{B}^2} + \frac{F}{2\pi R^2}\mu^2 + \frac{\sigma\delta}{8}(1+n\mu^2) + C_T\mu\gamma$$

Assuming $n\mu^2$ and $C_T\mu\gamma$ (CLIMB POWER) small at minimum power speed then

$$\partial C_Q/\partial\mu = -1/2\left(\frac{C_T}{\bar{B}}\right)^2 \frac{1}{\mu^2} + 3/2\ F/\pi R^2\ \mu^2$$

at minimum power $\partial C_Q/\partial\mu = 0$

Solving for μ yields

$$\mu_{MIN} = \left(\left(C_T/\bar{B}\right)^2 \frac{2\pi R^2}{6F}\right)^{1/4}$$

To better approximate the minimum power speed because of the terms dropped a factor of 0.95 was used, thus

$$\mu_{MIN} = 0.95\left[\left(C_T/\bar{B}\right)^2 \frac{2\pi R^2}{6F}\right]^{1/4} \tag{79}$$

To account for partial power conditions the critical speed (V_{CR}) was modified by the unsupported power loading. For this condition the power required to hover was reduced by the climb power differential for the desired impact speed, or

$$V_{CR} = (2.809V_{MIN} + 5.618\ C_L/\sigma - 169.776)\left(1 - \frac{HP_{AV}}{\left(HP_{\infty A} + \frac{GW\ V_{V_D}}{550}\right)}\right) \quad (80)$$

Here again if the horsepower available is equal to or exceeds that required at touchdown no HEIGHT-VELOCITY diagram exists.

Based on the results given in Reference 7, the height for the nose point is used as 95 feet. For partial power conditions available test data indicate that 50 feet is more appropriate for use as a starting estimate.

The high hover height as given in Reference 7 can be estimated from the equation

$$h_{hi} = 0.18V_{CR}^2 + 199.0 \quad (81)$$

for total engine malfunction.

When considering partial power conditions available test data indicate that the relationship

$$h_{hi} = \frac{GW}{\pi R^2}\left(1 - \frac{HP_{AV}}{\left(HP_{\infty A} + \frac{GW\ V_{V_D}}{550}\right)}\right) + 111.0 \quad (82)$$

Yields a closer approximation to actual test conditions.

Evaluation of the non dimensional shape of the HEIGHT VELOCITY envelope as given in Reference 7 indicates that the following relationships can be used. For the lower limb (from h_{lo} to nose point),

$$h_x = h_{lo} + (0.11/(1.1-V_x/V_{CR}) - .11)(h_{CR} - h_{lo}) \quad (83)$$

and for the upper limb (h_{hi} to nose point),

$$h_x = h_{hi} - (1-(1-V_x/V_{CR})^{1/2})\ (h_{hi} - h_{CR}) \quad (84)$$

The equations outlined in this section are used in the HDP program for estimating the starting points for the optimization of the flight procedures and iterating the three critical points to attain user specified ground contact conditions. The HEIGHT-VELOCITY curve is then formed by using the

nondimensional shaping equations with the three critical points for the extremities.

PROGRAM LOGIC FLOW CHARTS

The equations contained in this report were assembled into a series of subroutines to form the Helicopter Dynamic Performance program. A brief summary for each of these subroutines is given in Table 1. The subroutines summarized in Tables 2 and 3 pertain to the plotting interface routines provided for linking with the TEKTRONIX Plot 10 and AG II plot package and the Houston Plot Package supplied by the Government, respectively.

Program logic flow charts for the Engineering analysis, that is, all routines contained in Table 1 have been provided. Due to the size of the logic flow charts, these charts are contained in a separate reference compendium. A copy of this compendium, in microfisch form, may be obtained from ATL, Aeromechanics technical area by contacting Mr. T. White, phone (804) 878-3874--2062 or autovon 927-3874/2062.

While computer plots, both interactive with the GT-40 scope, TEKTRONIX 4010, 4012 and 4014 and Houston plot bed capability are a contractural requirement, the details of each of the subroutines are beyond the scope of this contract. The basic plot package consists of 188 subroutines. It will suffice to say that the interface between the Engineering Branch of the program and the plot package interface routines provides all parametric plotting capabilities required by contract.

Table 1. Helicopter Dynamic Performance-Engineering Subroutine Description

ROUTINE NAME	PURPOSE	ARGUMENT LIST	COMMON BLOCKS	EXTERNAL REFERENCES	LIBRARIAN NAME
Y239TL	MAIN CONTROL PROGRAM	--	EVCD, INPT, SVU, OTPT, ISW, CONTR, CHK, NRG, TERM, ATT, WIND, PWR, KTCIP, OPTIT, PROBS, TITA	PREPRO, START, CLECT, FINITT SWSET1	AA
PREPRO	INITIALIZES COMMON BLOCKS	ISTP, ICASE	INPT, OTPT, CONTR, PWR, CHK, EVCD, TITA	LOAD, TYPE, SOLID, SWSET	AB
LOAD	PROCESSES INPUT DATA	ISTP, ICASE	INPT	LOADS (IBM), LOADER (UNIVAC) SEEDAT	AE
SEEDAT	ALLOWS REVIEW OF LOADER DATA (INTERACTIVE)	--	---	---	DZ
LOADS	READS IN INPUT DATA	U	ACONVR, ACONVI	FREFLD	BL
TYPE	SETS UP ROTOR TYPE AND CONFIGURATION CONSTANTS	--	INPT, CONTR	ARCOS, (ACOS-UNIVAC)	AF
SOLID	COMPUTES TORQUE WEIGHTED SOLIDITY (M/R)	--	INPT, CONTR	---	AG
SWSET	INITIALIZES INTERNAL CONTROL SWITCHES	FMODE	ISW	---	AH
START	INITIALIZES AND SEQUENCES FLIGHT	K, J	INPT, SVU, OTPT, CONTR, CURVEV, PWR, ISW, ATT, LNDLNK, CHK, KTCIP, OPTIT, LIMRNG, PROBS, EVCD	CRVDA, RNGL, RGLIM, TSTDAT, OPTSET, HPCDP, STDY, THET75, TRAP, PREPR, ALAND, HVA, CNTL, CYCL, CKPT, BDYAT, HVOPT, ITERM, EVCK	AC
CRVDA	LOADS CURVLV COMMON BLOCK	--	CURVEV	---	EA
RNGL	COMPUTES REYNOLDS NO. AND GLAUERT CORRECTIONS	VAL, N	CONTR, CURVEV	AFCIP	AZ
RGLIM	SETS MIN-MAX LIMITS FOR FLIGHT	K, J	INPT, LIMRNG, ISW, CONTR, WIND	---	ET
TSTDAT	ALLOWS TEST DATA INPUT	--	NOT AVAILABLE	---	BV

Table 1. Continued

ROUTINE NAME	PURPOSE	ARGUMENT LIST	COMMON BLOCKS	EXTERNAL REFERENCES	LIBRARIAN NAME
OPTSET	SETS UP ESTIMATED HGT-VEL CURVE	K, J	INPT, SVU, CONTR, OTPT, ISW, EVCD, OPTIT, LIMRNG	STDY	EF
HPCDP	COMPUTES PWR REQUIRED AT EMP	K, J	INPT, CONTR, OTPT, ISW	STDY	EP
STDY	COMPUTES STDY STATE POWER REQUIRED	SHPR, ANGI, K	INPT, CONTR, PWR, ISW, CHK, WIND EVCD, OTPT	PREPR, GRNEF, ROTE, PERF1, MEFF	AK
THET75	COMPUTES THETA 75 FOR INFLOW CONDITIONS	K, J	INPT, CONTR, ATT, T75K	TH75K	EV
TH75K	COMPUTES INFLOW CONSTANTS FOR THETA 75	--	CONTR, T75K	---	EW
TRAP	SETS THE STARTING AND FINAL CONTROL VALUES FOR EACH EVENT ALONG THE FLIGHT PATH	J	INPT, OTPT, CONTL, EVCD, ISW	---	AW
PREPR	SETS TIME DEPENDENT VARIABLES	K	INPT, OTPT, CONTR, NRG, WIND	---	BG
ALAND	CONTROLS LANDING FLIGHT PATH	K, J, IRE	INPT, OTPT, CONTR, LNDLNK, PWR, ISW, CHK, WIND, EVCD, LIMRNG	ENTRY, CNTL, PREPR, STDY	BB
HVA	PERMITS PRESCRIBED FLIGHT PATH CALCULATION	K, J	INPT, OTPT, CONTR, ISW, PWR, CONTL, WIND, EVCD, PROBS	CNTL, STDY, CYCL, PREPR, GRNEF, PERF, CYCL1, WING, ARCOS	AJ
CNTL	COMPUTES INCREMENTAL CONTROL INPUTS FOR EACH TIME STEP	K, J	INPT, OTPT, CONTR, CONTL, ISW, WIND	---	AX
CYCL	CONTROLS ROTOR THRUST ITERATION LANDING AND BALK LANDING	IRE, K, J, CTSG	INPT, OTPT, CONTR, PWR, ISW, WIND, LIMRNG	GRNEF, PERF, TDVV, DEL75, CYCL1, ROTE, PERF1, ACDIS, ALAND, PREPR CYCL2	AU
CYCL1	CONTROLS ROTOR THRUST ITERATION TAKE-OFF AND REJECTED TAKE-OFF	IRE, K, J, CTSG	INPT, OTPT, CONTR, PWR, ISW, WIND	ROTE, PERF1	EU
CKPT	CHECKS FOR KEY POINTS ON FLT. PATH	K	INPT, OTPT, CONTR, ISW, CHK	---	BE
BDYAT	COMPUTES BODY PITCH AND ROLL ATTITUDE	K, J	INPT, OTPT, CONTR, ATT, EVCD, ISW, PWR	CTTR, WING, TDMAT, ARSIN	BT

Table 1. Continued

ROUTINE NAME	PURPOSE	ARGUMENT LIST	COMMON BLOCKS	EXTERNAL REFERENCES	LIBRARIAN NAME
HVOPT	SEQUENCES HGT-VEL OPTIMIZATION	K, J, IRE	INPT, OPTIT	LOHVR, SWSET1, NOSEPT, HIHVR, FLYIT	EG
LOHVR	OPTIMIZES LOW HOVER HGT ON HGT-VEL ENVELOPE	K, J, IRE, NOPT	INPT, OTPT, CONTR, EVCD, ISW, LIMRNG, OPTIT, CHK, PROBS, ATT	---	EI
NOSEPT	OPTIMIZES HGT-VEL NOSE POINT	K, J, IRE, NOPT	INPT, OTPT, CONTR, EVCD, ISW, LIMRNG, OPTIT, CHK, PROBS, ATT, SVU	---	EJ
HIHVR	OPTIMIZES HIGH HOVER HGT ON HGT-VEL ENVELOPE	K, J, IRE, NOPT	INPT, OTPT, CONTR, EVCD, ISW, LIMRNG, OPTIT, CHK, PROBS, ATT, SVU	---	EK
SWSET1	RESETS INTERNAL CONTROL SWITCHES	K, J	ISW, CHK, INPT, PROBS, OTPT	---	EH
FLYIT	OPTIMIZES MAX. RANGE IN AUTOROTATION	K, J, IRE, NOPT	INPT, CONTR, EVCD, ISW, LIMRNG, OPTIT, CHK, PROBS, SVU	---	EL
ITERM	CHECKS FOR FLIGHT TERMINATION	IGO, K, J, TLMT	INPT, OTPT, ISW, CONTR	EVCK	BD
EVCK	CHECKS FOR END POINT OF EACH EVENT	K, J, V6	INPT, OTPT, EVCD, ATT, CONTR, ISW	TRAP	AV
AFCIP	INTERPOLATES CURVE DATA (LINEAR)	ID, NC, LOC, X, Y, Z, XB, YB, A, B, C, 2	COCIP, KTCIP	---	EZ
GRNEF	COMPUTES GROUND EFFECT	K	INPT, OTPT, ISW, CURVEV, CONTR, EVCD, CHK	AFCIP	BA
RGTE	COMPUTES ROTOR EFFICIENCY	--	INPT, CONTR	---	AP
PERF1	COMPUTES INSTANTANIOUS POWER REQUIRED	--	INPT, CONTR, PWR, CURVEV, WIND	UUOCT, TANDIN, DFAULT, RNGL, HPM	AL
MEFF	COMPUTES MECHANICAL EFFICIENCY	VAL, ETA	INPT	---	AS

Table 1. Continued

ROUTINE NAME	PURPOSE	ARGUMENT LIST	COMMON BLOCKS	EXTERNAL REFERENCES	LIBRARIAN NAME
ENTRY	COMPUTES AUTOROTATION ENTRY	K, J, IRE	INPT, OTPT, CONTR, CONTL, EVCD, PWR, ISW, ATT, WIND	CNTL, PREPR, PERF1, PERF, ACDIS	AI
PERF	COMPUTES INSTANTANIOUS PWR AVAILABLE	K, J	INPT, OTPT, CONTR, PWR, EVCD	MEFF	AY
WING	COMPUTES WING LIFT AND DRAG FORCES	WLX, WLY, WLZ	NOT AVAILABLE	---	BW
TDMAT	COMPUTES BODY ATTITUDE (TANDEM ROTORS)	K, J	NOT AVAILABLE	---	BU
CTTR	COMPUTES TAIL ROTOR THRUST	---	INPT, CONTR, PWR	---	AO
UUOCT	COMPUTES ROTOR INDUCED VELOCITIES AND ROTOR THRUST	--	INPT, CONTR	WING, CTTR, ROTE	AM
TANDIN	COMPUTES ROTOR INTERFERENCE FOR TANDEM ROTOR HELICOPTERS	--	INPT, CONTR	---	AN
DFAULT	SETS PROGRAM WITH 0012 AIRFOIL DATA IF NOT USER SPECIFIED	--	CONTR	---	AQ
HPM	COMPUTES ROTOR MACH NO. EFFECTS	--	CONTR, PWR	---	AR
ACDIS	COMPUTES ACCELERATIONS AND DISPLACEMENTS	K, J, IRET	INPT, CONTR, LNDLNK, PWR, ISW, OTPT, CONTL, WIND, CHK, EVCD, NRG, ATT	WING, THET75, OUTF	BC
DEL75	COMPUTES THRUST FOR SPECIFIED ΔC 75 INPUTS	K, J	INPT, CONTR, PWR, CONTL, ISW, EVCD, OTPT, T75K, ATT, LIMRNG	STDY, TH75K, PREPR	EX
TDVV	CONTROLS TOUCHDOWN VERTICAL VELOCITY	K, J	INPT, CONTR, OTPT, ISW, LIMRNG	TAKEIT	EQ
TAKEIT	ADJUSTS COLLECTIVE CONTROL TO TOUCHDOWN AT SPECIFIED VERTICAL SPEED	K, J	INPT, CONTR, PWR, CONTL, ISW, OTPT, EVCD, LIMRNG	STDY, PREPR, PERF	ER
OUTF	WRITES INTERMEDIATE DATA TO SCRATCH FILE FOR LATER RETRIEVAL.	FX, FY, FZ, PTOT	INPT, CONTR, PWR	---	BX

Table 1. Continued

ROUTINE NAME	PURPOSE	ARGUMENT LIST	COMMON BLOCKS	EXTERNAL REFERENCES	LIBRARIAN NAME
CLECT	CONTROL ROUTINE FOR BRANCHING BETWEEN HARD COPY OUTPUT AND PLOTTING ROUTINES	K, J, NU	INPT, OTPT, NRG, TERM, ISW, ATT, CHK, PROBS, OPTIT, TITA	OUTPT, EXOUT, PLOTA	AD
EXOUT	PRINTS OUT SECOND ORDER TIME HISTORY OUTPUT DATA	NU	INPT, OTPT	DUMP	GO
DUMP	RETRIEVES SECOND ORDER OUTPUT FROM SCRATCH FILE	K, VAL, N	INPT, OTPT, ATT, CONTR, WIND	---	GP
OUTPT	PRINTS OUT FLIGHT SUMMARY AND PRIMARY TIME HISTORY DATA	J, NU, NUPL	INPT, OTPT, ISW, CONTR, EVCD, CHK, NRG, KTCIP, ATT, TITA, PROBS	INPRNT, DIAGS	BF
DIAGS	PRINTS OUT PERTINENT DIAGNOSTICS OF FLIGHT PATH OR DATA INPUT PROBLEMS	--	PROBS	---	EY
INPRNT	PRINTS OUT INPUT REQUIREMENTS FOR OPTIMIZED FLIGHT PATH	NU	INPT, OPTIT	---	ES
CYCL2	CONTROLS ROTOR THRUST ITERATION. ALL MODES	K, J, TSV	OTPT, CONTR, PWR, INPT, ISW, WIND	ROTE, PERF1, PREPR	AT
FREFLD	PERMITS FREE FIELD LOADER INPUT	N	ACONVR, ACONVI, NCONVR	NCONV	BY

Table 1. Concluded

ROUTINE NAME	PURPOSE	ARGUMENT LIST	COMMON BLOCKS	EXTERNAL REFERENCES	LIBRARIAN NAME
PLOTA	SETS UP OUTPUT DATA FOR PLOTTING	NUPL	TERM, LSCODE, PLTYPE, TLOC, LOKAT, WINDL, IGRID, NRG, OTPT, CONTR, ATT, BLSMBL, INPT, OVER37, OVER01, INDX, ISW, OPTIT, PLTCGC, TITA, TCS10	CGCOM, NULL, ZSET, DMENU, LABL, AUXPLT, SETIT, TUBPLT, GETIT, PIXON, HDPLT, PERPLT, HVPLT, PIXOFF, ANMODE[1], NEW PAG[1], MOVABS[1]	BM
DMENU	PRINTS PLOT SELECTION LIST TO SCREEN. INTER-ACTIVE MODE ONLY.	---	---	---	BN
LABL	SETS UP CURVE LABLES	JX, IY, Z	CONTR, TITA	ACON	BO
AUXPLT	SETS UP CURVE SELECTIONS 21-40 FOR PLOTTING	I, A, ASV, IX, IY	INPT, OTPT, LSCODE, INDX, BLSMBL	DUMP	GN
SETIT	SETS UP CURVE FRAME FOR OVERWRITE MODE	X, Y, Z, XMI, XMA, YMI, YMA	LSCODE, BLSMBL, TCS10	---	EC
GETIT	PASSES SERIES OF UNIVARIATE CURVES IN OVERWRITE PLOT MODE	J, X, Y, Z, IS, IY, NPT, NU1	INDX, LSCODE, BLSMBL, TCS1)	---	ED
HVPLOT	PLOTS HGT-VEL DIAGRAM	XP, YP, ZP	TITA, CONTR, OPTIT, LSCODE, TCS10	ACON	EO
PERPLT	PROVIDES PERSPECTIVE VIEW OF FLIGHT PATH	XP, YP, ZP, NUPL, DROP, RTO	LSCODE, TERM, TCS10, SRFACE, VIRTUL, LOKAT, WINDL, CONTR, OTPT, TITA	ZNORM1, SPACE, PVIEW, ACON	BP

(1) TEKTRONIX PLOT 10 ROUTINES TO BE SUPPLIED BY GOVERNMENT.

Table 2. Sikorsky General Plot Package-Tektronix Interface Subroutine Description

ROUTINE NAME	PURPOSE	ARGUMENT LIST	COMMON BLOCKS	EXTERNAL REFERENCES	LIBRARIAN NAME
TUBPLT	INITIALIZES TEKTRONIX PLOT PACKAGE AND CONTROLS CURVE PLOTTING	X, Y, Z	TERM, LSCODE, PLTYPE, TLOC, LOKAT, WINDL, IGRID	ULOC, EQRES, EQRES1,[1] LIMITS BIVAR, KONPLT,[1] INITT[1], BINITT[1], PLACE[1], ANMODE[1], DLIMX[1], DUMY[1], NEWPAG[1], TSEND[1], MOVABS[1]	BQ
ULOC	ALLOWS USER TO CONTROL FRAME LOCATION AND SIZE	---	WINDL	SLIMX[1], SLIMY[1]	GD
EQRES EGRES1	ADJUSTS DATA AND FRAME SIZE TO PROVIDE EQUAL RESOLUTION	X, Y, Z	PLTYPE	ZNORM[1]	GH
LIMITS	SETS UP DEFAULT SCALING FOR TEK. PLOTS	X, Y, Z	PLTYPE	MNMX[1]	EE
KONPLT	SETS UP CONTOUR PLOTS PROVIDING LINES OF CONSTANT VALUES	---	NOT SUPPLIED. NOT APPLICABLE TO CONTRACT	DUMMY ROUTINE PROVIDED TO SATISFY REFERENCES	DF
BARGRA	PROVIDES BAR CHART PLOTS	---	NOT SUPPLIED. NOT APPLICABLE TO CONTRACT	DUMMY ROUTINE PROVIDED TO SATISFY REFERENCES	DE
BIVAR	SETS UP BI-VARIATE PLOTS	X, Y, Z	PLTYPE, LSCODE, INDX	LIMITS, BARGRA, UNIPLT, DLIMX[1], LINE[1], SYMBL[1]	GA
UNIPLT	SETS UP X, Y DATA FOR PLOTTING	X, Y, Z	TLOC, INDX, LSCODE, IGRID, PLTYPE	EPLT,[1] MORLIN,[1] TITL, ALABEL,[1] XMFRM[1], YMFRM[1], XFRM[1], YFRM[1], XTYPE[1], YTYPE[1], SYMBL[1], LINE[1], STEPS[1], CHECK[1], XLAB[1], YLAB[1], DSPLAY[1], CPLOT[1]	GB
EPLT	SETS UP EQUAL RESOLUTION FRAME SIZE	Z	WINDL	SLIMX[1], SLIMY[1]	GE
MORLIN	PERMITS INCREASE OF GRID DENSITY ON PLOT OUTPUT	---	IGRID	COMGET[1], COMSET[1], IBASEX[1], IBASEY[1]	GC
TITL	SHIFTS CURVE TITLES AND LABELS TO FRAME	Z	TLOC, LOKAT, WINDL	---	GF

(1) TEKTRONIX PLOT 10 ROUTINES TO BE SUPPLIED BY THE GOVERNMENT.

Table 2. Concluded

ROUTINE NAME	PURPOSE	ARGUMENT LIST	COMMON BLOCKS	EXTERNAL REFERENCES	LIBRARIAN NAME
ALABEL	CONVERTS TITLE AND LABEL DATA FROM ALPHA-NUMERIC STRINGS TO ASCII FOR SCREEN WRITE	ALPHA, ICHAR IDIR, LOCX, LOCY	---	KAM2AS[1], MOVABS[1], HLABEL[1], VLABEL[1]	GG
SPACE	PERMITS USER TO CHANGE VIEWING POSITION FOR PERSPECTIVE PLOTS	---	VIRTUL, SRFACE, PLTYPE	---	GK
PVIEW	PROVIDES PERSPECTIVE TRANSFORMATION	X, Y, Z, N1, XP, YP	VIRTUL, SRFACE	ARSIN, (ASIN-UNIVAC)	GJ
ZSET	REFRESHES PLOT PACKAGE Z-VECTOR	Z, IDIM	---	---	EN
NULL	REFRESHES PLOT PACKAGE COMMON BLOCKS	---	PLTYPE, LOKAT, LSCODE, IGRID, TLOC, INDX, WINDL, OVER01, BLSMBL, OVER37	---	EM
MIN	FUNCTION ROUTINE FOR INTEGER MIN VALUE	K, J	---	---	GL
MAX	FUNCTION ROUTINE FOR INTEGER MAX VALUE	K, J	---	---	GM
ZNORM1	DEFINES DATA NORMALIZATION RANGE	ZVEX, ZMAX, ZMIN	---	---	GI

(1) Tektronix Plot 10 Routines to be Supplied by the Government.

Table 3. Sikorsky General Plot Package- Houston Plotter Interface-Subroutine Description

ROUTINE NAME	PURPOSE	ARGUMENT LIST	COMMON BLOCKS	EXTERNAL REFERENCES	LIBRARIAN NAME
HDPLT	CONTROLS SETUP FOR HOUSTON PLOT PACKAGE	X, Y, Z, N	BLSMBL, OVER37, OVER01, PLTYPE, TERM	EQRES, SCALIT, PREVU, BLPLT2, NEWPAG[1], ANMODE[1]	BR
SCALIT	CONTROLS CURVE SCALING	X, Y, Z	---	DATSCL, SCLIT	CB
PREVU	ALLOWS PREVIEW OF HOUSTON PLOTS ON TEKTRONIX SCREEN	X, Y, Z	TERM, BLSMBL, GT40	SCALIT, PLTTEX, BLPLT2, NEWPAG[1], MOVABS[1], ANMODE[1]	BS
BLPLT2	CONTROLS HOUSTON PLOTS	X, Y, Z	BOUNDS, OVER01, BLSMBL, GRIDCM, OVER37, CALCOM, ISYM, BONOMO, BENSON, DELAX, SCLBDS, TERM	CBLANK, PLOT[2], USRSCL, FMTFDR, ACON, RANGE, AXISCL, EQUSCL, MVCHAR, NCMEN, LABELS, PLPLTB, PNTSBL	CF
DATSCL	SETS UP DATA SCALES FOR HOUSTON PLOTS	X, Y, Z	---	ZNORM1, AXISCL	CD
PLTTEX	SETS UP PREVIEW OF HOUSTON PLOTS	VALN, VALO, IPC	---	PLOT[2], INITT[1], ANMODE[1], NEWPAG[1]	DI
CGCOM	INITIALIZES HOUSTON PLOT PREVIEW COMMON	---	PLTCGC	---	EB
PIXON	INITIALIZES HOUSTON PLOT OUTPUT TAPE	---	---	PLOTS[2]	CA
PIXOFF	END FILES HOUSTON PLOT OUTPUT TAPE	---	---	PLOT[2]	DD
PLOTCG	PROVIDES PREVIEW OF HOUSTON PLOTS	X, Y, IP, ICON	PLTCGC	SNIPLT, MOVABS[1], ANMODE[1], NEWPAG[1], TSEND[1], DRWABS[1]	DG
SCLIT	SETS UP AXIS LENGTH FOR FIXED SCALE LENGTH	AMIN, AMAX, DEL, SCL	---	---	CC
SNIPLT	CLIPS LINE AT FRAME EDGE	X1, Y1, X2, Y2, XV, IC	---	---	DC

(1) TEKTRONIX PLOT 10 ROUTINES TO BE SUPPLIED BY GOVERNMENT
(2) HOUSTON PLOT ROUTINES TO BE SUPPLIED BY GOVERNMENT AND MODIFIED BY SIKORSKY AIRCRAFT

Table 3. Continued

ROUTINE NAME	PURPOSE	ARGUMENT LIST	COMMON BLOCKS	EXTERNAL REFERENCES	LIBRARIAN NAME
ACON	CONVERTS NUMERIC STRING TO ALPH-NUMERIC STRING	N, R, FMT	---	CORE	FA
CORE	ASSEMBLY ROUTINE FOR READING FROM CORE	---	---	---	FB
ZMID	FINDS MIDPOINT OF ALPHA-NUMERIC STRING	FIELD, LENGTH	---	MVCHAR	CT
PLTSYM	SETS PLOT MARGINS	X, Y, XB, YB	BOUNDS	---	CM
AXSPLT	SETS UP CURVE LAYOUT	IZA, IZL, IGRID, IZMIN, IZMAX, IZDLT, IZEXP	CALCOM, DELAX	GRIDSK, SCLCHR, ZMID, PLTSYM, SYMBOL[2], AXIS	CV
CLIPLT	SETS VALUES IN COMMON FOR CLIPPING	VALN, VALD, IPC	PLTCGC	PLOT[2]	DH
OPNSBL	PLOTS SPECIAL SYMBOLS	X, Y, ISBL	---	PLOT[2]	CU
GRIDSK	PROVIDES A 1-INCH GRID OVERLAY	IORIEN, IAXIS, IXDIM, IYDIM	BENSON	PLOT[2]	CW
SCLCHR	SCALES CHARACTER SIZE	IMAX, IMIN, IDLT, IXPT, NCH, CHSCAL CHXPNT	---	ACON, MVCHAR	CX
AXIS	SETS UP CURVE AXIS	IORIEN, LINE, NUMZVL, ZSEPN,NZ	BENSON	PLOT[2]	CY
CBLANK	CONVERTS NUMERIC SERIES TO BLANKS	STRING, NWDS	---	---	CG
PLOT[2]	TRANSFORMS DATA TO PLOTTER COORDINATES	X, Y, IPEN	---	PLOTCG	CZA
USRSCL	SETS UP USER SUPPLIED SCALES	ZMIN, ZMAX, ZDLT, IMIN, IMAX, IDLT, IEXP	---	---	CH

(2) HOUSTON PLOT ROUTINES TO BE SUPPLIED BY GOVERNMENT AND MODIFIED BY SIKORSKY AIRCRAFT

Table 3. Concluded

ROUTINE NAME	PURPOSE	ARGUMENT LIST	COMMON BLOCKS	EXTERNAL REFERENCES	LIBRARIAN NAME
FMTFOR	FIND FORMAT FOR NUMERIC STRING	BAL, NAL, ISB	---	---	CI
RANGE	ESTABLISHES DATA RANGE	X, Y, K, XMIN, XMAX	---	---	CJ
AXISCL	SETS UP DATA SCALES	ICEN, ZMIN,ZMAX, IFST, ILST, IDLT, ISCL	---	---	CK
EQUSCL	SETS UP EQUAL SCALES	LEN, ZMIN,JDLT, JEXP, IMIN,IMAX, IDLT, IEXP	---	---	CL
MVCHAR	ASSEMBLY ROUTINE FOR MANIPULATING CHARACTER STRINGS IN CORE	SO. LO, SI, LI, N	---	---	FD
NOMEN	SETS UP NOMENCLATURE BLOCK	NMH, Z40, Z41, CHARS	BOUNDS, CALCOM	ZMID, PLTSYM, SYMBOL[2]	CP
LABELS	PRINTS OUT CURVE LABELS	XL, YL, TITLE, NMH, Z41, YMIN, YMAY	CALCOM, GRIDCM, SCLBDS	ZMID, PLTSYM, SYMBOL, AXSPLT	CQ
PLPLTB	PLOTS POINTS AND LINES	X, Y, N, NUMCUR, ICNO, ISYMBL	CALCOM, ISYM, BENSON	CLIPLT, PLOT[2], SYMBOL[2], OPNSBL	CR
PNTSBL	PLOTS POINTS FOR SCATTER PLOTS	X, Y, N, NUMCUR, ICNO, ISYMBL	CALCOM, BENSON	CLIPLT, SYMBOL[2], OPNSBL, PLOT[2]	CS

(2) HOUSTON PLOT ROUTINES TO BE SUPPLIED BY GOVERNMENT AND MODIFIED BY SIKORSKY AIRCRAFT.

REFERENCES

1. Coleman, R. P., Feingold, A. M., and Stempin, C. W., NACA ARR No. L5E10.

2. McCormick, B. W., Jr., AERODYNAMICS OF V/STOL FLIGHT, Academic Press, 1967.

3. Glauert, H., A GENERAL THEORY OF THE AUTOGYRO, ARC R&M No. 111, 1926.

4. Shapiro, J., PRINCIPLES OF HELICOPTER ENGINEERING, McGraw Hill Book Company, Inc., 1955.

5. Gessow, A., and Myers, G. C., Jr., AERODYNAMICS OF THE HELICOPTER, MacMillian Company, 1952.

6. NACA MR No. L5D09a.

7. Pegg, R. J., AN INVESTIGATION OF THE HELICOPTER HEIGHT-VELOCITY DIAGRAM SHOWING EFFECTS OF DENSITY ALTITUDE AND GROSS WEIGHT, NASA TN D-4536, May 1968.

8. ENGINEERING FLIGHT TEST OF THE OH-6A HELICOPTER (CAYUSE) PHASE D, Final Report, USATECOM Project No. 4-6-0250-01, USAASTA Project No. 65-37, April 1969.

9. ENGINEERING FLIGHT TEST AH-1G HELICOPTER (HUEY COBRA) PHASE D, PART 2 PERFORMANCE, Final Report, USATECOM Project No. 4-6-0500-01, USAASTA Project No. 66-06, April 1970.

10. ENGINEERING FLIGHT TEST AH-1G HELICOPTER (HUEY COBRA) PHASE B, PART 6, Final Report, USATECOM Project No. 4-6-0500-01, USAASTA Project No. 66-06, November 1969.

11. HEIGHT VELOCITY TEST AH-1G HELICOPTER AT HEAVY GROSS WEIGHT (LOW ELEVATION), Final Report, USAASTA Project No. 74-19, June 1974.

BIBLIOGRAPHY

1. Jacobs, E.N., Sherman, A. NACA TR586, "Airfoil Section Characteristics as Affected by Variations of the Reynolds Number:.

2. Durand, W.F., "Aerodynamic Theory" Vol IV

3. Rouse, H., "Elementary Mechanics of Fluids". John Wiley & Sons Inc., 1950.

4. Autry, C.P., "Helicopter Power Requirements" Aircraft Engineering, October 1946.

5. Shapiro, J.S., "Reflections on the Interrelation of Helicopter and Heliport Design". Aircraft Engineering, November 1955.

6. Toms, C.F., "The Performance of Rotary Wing Aircraft Rotors". Aircraft Engineering May 1947.

7. Stepniewski, W.Z., "Introduction to Helicopter Aerodynamics". Rotorcraft Publishing Committee.

8. Wood, K.D., "Technical Aerodynamics". McGraw-Hill Book Co, Inc., 1947.

9. Turskis, J., Griswold, P., Leonoff, G., "Methods for Calculating Performance of a Single Main Rotor Type Helicopter" Sikorsky Engineering Report SER-2578. February 1956.

10. Hanley, W.J., DeVore, G., "An Analysis of the Height-Velocity Diagram Including a Practical Method for Its Determination". Tech. Report ADS67-23 FAA October 1967,

11. Sikorsky, I.A. "Correlation of Helicopter Performance Equations". (Unpublished).

12. Studwell, R.E., "Preliminary Investigation of Main Rotor Test Stand and Flight Test Data for the Effects of Blade Twist and Number of Blades on the Rotor Performance of a Constant Chord Blade Having an NACA 0012 Airfoil Section". Sikorsky Engineering Report SER-50097, December 1959.

13. Studwell, R.E., "Investigation of the Flow Effects on Rotor Performance in a Partial Power Vertical Descent with Application to and S-61 Model Rotorcraft". Sikorsky Engineering Report SER-611102. May 1965 (Unpublished).

14. Studwell, R.E., "A Method for Calculating Rotor and Rotorcraft Performance Using a Semi-Emperical Approach". Sikorsky Engineering Report SER-50730, October 1971.

15. Studwell, R.E., "A Method for Calcualting Take-Off and Landing Flight Paths for Rotary will Aircraft". Sikorsky Engineering Report SER-50740. April, 1972.

16. Studwell, R.E., "A Method for Calculating Co-Axial and Tandem Rotor Performance Using a Semi-Emperical Approach". Sikorsky Engineering Report SER-50849, September 1973.

17. Charts for Estimating Rotary Wing Performance in Hover and High Forward Speeds. Sikorsky Engineering Report SER-50379, Tanner.

18. SER-65254, CH-53A Helicopter Demonstration Report, December 1964.

APPENDIX A

A METHOD FOR EVALUATING AUTOROTATION

To the engineer and designer a "good" autorotation will always result in a "safe" power off landing, and efforts are directed toward obtaining the highest possible hover height for the lower limb of the height-velocity (H-V) curve, the lowest possible hover height for the upper limb, and the minimum possible critical speed for the "nose" of the curve. Practical factors, such as the ability to accurately measure airspeed, or concern for control input and field size requirements are generally not considered.

Pilots' comments and "feelings" on autorotation capabilities can be related to rotor and rotorcraft parameters which should be considered in the design. A selection of some of these comments and the related tangible parameters are listed below.

Pilot Comment: "Engine malfunction can occur at any time. I don't want restrictions placed on my flight envelope."

Tangible Parameter: Design consideration for minimizing the avoid area of the height-velocity diagram.

Pilot Comment: "After engine malfunction, there's not much time until I'm on the ground."

Tangible Parameter: Provide low, controllable rates of descent. Design considerations for disc loading, rotor RPM and airfoil type.

Pilot Comment: "It wouldn't be bad if I were over Kansas but all I can find is a small rough clearing."

Tangible Parameter: Design for reasonable roll on velocities, landing gear design, tail wheel or structurally and psychologically safe tail rotor protection.

Pilot Comment: "When I get into a high cyclic flare I loose all ground reference."

Tangible Parameter: Cockpit visibility, minimize attitude change requirements.

While these are not all of the pilot reactions to emergency autorotation, they are pertinent and provide a starting point for an approach to a meaningful analysis of autorotative characteristics

In order to evaluate the effect of design or parametric changes on the autorotative capabilities, a means of extracting the maximum capabilities for a given parametric set must be established. The Helicopter Dynamic Performance (HDP) program provides a means of evaluating rotorcraft take-off and landing performance with power on, and with partial or total engine malfunction. The transition phase between power on and power off, autorotative entry, is also included in the HDP program. Using this program as a base, several subroutines were written and inter-faced with the base HDP program. These subroutines were designed to generate the program inputs required to minimize the height-velocity (H-V) envelope for a given configuration description and specified end point constraints. Based on pilot comments, the most pertinent end point constraints were selected as:

1. vertical velocity at touchdown
2. blade loading, C_T/σ, at touchdown
3. body attitude at touchdown
4. horizontal roll-on speed.

Based on these end point constraints, subroutines were written to determine the point in space where the rotorcraft would have to be and the flight procedures to be used to best satisfy the imposed end point limits. Three routines were written for this purpose. One for the low hover height, one for a forward speed approach, and the third for the high hover height.

Low Hover Height

The low hover height routine establishes the maximum hover height from which, if a total engine malfunction occurred, the rotor craft could land without exceeding an imposed vertical touchdown speed or the imposed blade loading (C_T/σ). This routine assumes a pure vertical descent so that the roll on speed and the body attitude criteria are not pertinent. Program output for this condition provides the maximum low hover height and the collective control application procedures required to effect the landing. All time history data provided by the main program is also available.

Minimum Speed

The second routine deals with a total engine malfunction occurring during forward flight. The purpose of the routine is to establish the minimum forward speed and altitude from which a landing can be effected within the imposed end point constraints. The flight procedures required to effect this landing are also a program output requirement.

Initially it would appear that the only requirement is to adjust the controls from the point of engine malfunction to touchdown at the specified vertical impact speed while bringing the C_T/σ and body attitude to the stated limit and bringing the horizontal roll on speed to the lower specified limit. A more detailed review of the stated end point con-

straints shows that certain combinations of input criteria could result in conflicting conditions. For example, if a 10-foot-per-second vertical impact speed is requested and a maximum C_T/σ of 0.20 is used, analysis for some disc loading conditions could show that the rotorcraft would have a brief positive rate of climb. Another conflicting situation could occur if a low body attitude at touchdown was requested along with a low horizontal roll on speed. In this case the body attitude restriction could preclude the deacceleration required to reach the imposed roll-on speed requirement.

In view of these potential conflicts, the end point constraint criteria were set up on a priority basis with the following interpretations.

1. Vertical touchdown criteria.
   This parameter has first priority and must be met within $\pm$0.5 foot per second of the requested value.

2. Blade loading, C_T/σ.
   This input has second priority and is interpreted as the maximum allowable value. The program will accept a lower value if the specified limit is not consistant with the other constraints.

3. Touchdown body attitude.
   This input retains a high priority status provided the tip path plane attitude required to attain the permitted touchdown angle does not cause the rotorcraft to accelerate during the final phase of the maneuver. If acceleration is required to meet the criteria, the tip path plane angle is set to -1 degree and the touchdown body attitude limits are ignored. The program will print out a diagnostic message if this condition exists.

4. Horizontal roll-on speed.
   This input limitation carries the lowest priority of the four. Since the main purpose of these subroutines is to minimize the height-velocity envelope and the other three criteria carry a higher pilot concern, the program will establish the flight procedures which maximize the other criteria while minimizing the horizontal approach speed and roll-on speed independent of the roll-on speed requirement. It should be noted that the program will work toward getting the rotorcraft within the specified criteria so that the inputs for these values should not be ignored. The program will print out a message if the input requirements cannot be met.

High Hover Height

A third routine has been set up for determining the high hover height of a height-velocity envelope. This high hover height can be defined as the minimum height at which a rotorcraft can hover and effect a safe landing after total engine malfunction. It differs from the low hover height in that acceleration to some forward speed is required to safely effect the landing. The same end point constraint criteria and priority order and definition are used for this routine as for the minimum speed point.

Other Constraints

Aside from the end point constraints as discussed above, the program user can also specify the maximum range of cyclic (tip path plane), collective (THETA 75), and minimum and maximum rotor RPM within which the program can operate. These inputs are interpreted as the maximum limits and the program will work within the range imposed, but not necessarily use them if a lower value produces a "better" flight path. The "better" flight path is defined as that path which best satisfies the end point constraints.

Design Criteria Evaluation

These height-velocity routines, coupled with the HDP program, provide a means of evaluating various rotorcraft design criteria. The premise for this is based on the ability of these routines to compute the minimum boundaries of the H-V envelope for a given rotorcraft configuration, control limits, and end point constraints. Then, by the perturbation of any one pertinent parameter, the resultant change in the H-V envelope is a measure of how the safety of the base rotorcraft is improved or compromised. A systematic parametric evaluation can then highlight the design parameters which have significant effects on autorotative capability.

Note that these routines generate the control input requirements to maximize rotorcraft capabilities without regard to pilot work load. The H-V envelope predicted could therefore be beyond realistic pilot-rotorcraft capability. See Section 4, Volume II.

PARAMETRIC EVALUATION OF AUTOROTATIVE CAPABILITIES

The HDP program was used to evaluate two helicopters in autorotative flight. The purpose of this study was to determine what effect, if any, various design parameters have on the autorotative capability of these rotorcraft. The rotorcraft used for this study were specified by contract as the Hughes OH-6A and the Bell AH-1G. The parameters to be varied are listed below:

1. Disc Loading
2. Altitude
3. Center-of-Gravity Location
4. Rotor Inertia
5. Maximum Flare Attitude
6. Rotor Profile Drag
7. Pilot Control Initiation Delay Time
8. Initial Rotor RPM
9. Aircraft Parasite Drag
10. Airframe Static Stability
11. Vertical Touchdown Velocity
12. Touchdown Body Attitude
13. Maximum C_T/σ

Three additional parameters were deemed as not appropriate for the following reasons:

1. Airspeed - The airspeed required at the nose point of the H-V envelope is a result of the calculations for minimizing the H-V envelope and cannot be a program input.
2. Initial steady-state rate of climb and descent. The use of approach conditions other than hover and steady-state level flight for H-V determination is not pertinent.
3. Horizontal touchdown speed. This is a program input. Due to touchdown criterion priorities, the use of this criterion for explicit variations in capabilities might not be meaningful.

The evaluation of each rotorcraft was conducted by first establishing a baseline condition for the given helicopter. Aside from the basic aircraft configuration data, baseline conditions of sea level standard atmosphere and neutral CG were used.

Initial calculations were conducted to establish the H-V envelope for each rotorcraft at a disc loading of 4. The results of these calculations, shown in Figure A-1(a), show that significant differences exist for these aircraft, in autorotative capability, at these baseline conditions.

To obtain a more meaningful evaluation of parametric variations, the perturbations were conducted from a baseline H-V curve which would provide a common H-V speed range for both aircraft. While an exact commonality could not be found, a reasonable common base was determined with the OH-6A at a disc loading of 3.5 and the AH-1G at a disc loading of 5. A comparison of the baseline H-V curves is shown in Figure A-1(b) parametric listing of baseline conditions is in Table A-1 for the OH-6A and Table A-2 for the AH-1G. The parametric variations used are shown in the diagonal or staggered boxes in Tables A-1 and A-2. The effect of each parametric change was then established by computing the minimum H-V envelope for the imposed conditions and comparing the differences from the baseline curve. The differences between the H-V curves can be defined as the change in low hover height, approach speed at the "nose" point, high hover height, and the horizontal roll-on speed from the "nose" point and high hover height. The resulting H-V curve and variations from the baseline are tabularized on the lower portion of Tables A-1 and A-2. These variations from the baseline are also shown in bar graph form in Figure A-2 for the OH-6A and in Figure A-3 for the AH-1G. (Sea Level standard conditions apply except as otherwise noted.)

A review of these figures shows that while the sensitivity of each parametric variation differs between aircraft, the trend of increasing or decreasing the H-V envelope is nominally the same. A generalized overview of the effect of each parametric change is presented in Table A-3.

DISCUSSION OF PARAMETRIC TRADE-OFFS

An analysis has been conducted to establish the effect of basic design parametric changes on the autorotative capabilities of the representative rotorcraft. While this study points out the trends of each parametric change, it also points out that the magnitude of the change was dependent on the aircraft in question. Based on this, it cannot be said that a certain parametric change is going to have a given effect on all rotorcraft. An example of this can be seen with the effects of increasing rotor inertia. Analysis of the OH-6A shows that a 50% increase in the rotor inertia decreases the overall H-V envelope and permits a lower roll-on speed from both the "nose" point and high hover height condition. On the other hand, the same percent increase in rotor inertia for the AH-1G raises the low hover height, shows no change in the "nose" point speed and requires a slight increase in the high hover height. The resulting H-V envelopes for this evaluation is shown in Figure A-4. Review of the roll-on speeds, Table A-2 shows a slight decrease from the "nose" point and an increase from the high hover height.

From these results it appears that the sensitivity of the rotor inertia parameter is dependent on the baseline rotorcraft. While this is partially the case, one must keep in mind the priority of the end point constraints imposed on the analysis. The analysis stated that the vertical impact speed and touchdown body attitude have top priority and blade loading, C_T/σ, and horizontal roll-on speed have second priority. Based on this, a review of the maximum C_T/σ levels used in affecting the landing would provide further insight as to potential effects. A comparison of the maximum C_T/σ levels required to effect the landing with the base aircraft and rotor inertia changes is shown below.

A/C	OH-6A		AH-1G	
	C_T/σ	C_T/σ	C_T/σ	C_T/σ
Cond.	BASE	50% Jm Inc.	BASE	50% Jm Inc.
Low Hvr. Hgt.	.137	.146	.145	.146
"Nose" Pt.	.128	.134	.130	.121
High Hvr. Hgt.	.122	.122	.142	.105

It can be seen that for the OH-6A the maximum C_T/σ reached is nominally the same for both the baseline and increased inertia case. The resulting H-V envelopes show significant improvement with the increased inertia. For the AH-1G the low hover height shows the same maximum C_T/σ was used and an increase in the low hover height, comparable with the OH-6A, was also shown. On the other hand, while the "nose" point and high hover height maximum C_T/σ was near maximum for the baseline AH-1G (a maximum value of 0.15 was imposed), the C_T/σ level, used with increased inertia, had to be reduced to meet the end point constraints. From this, it can be seen that if the AH-1G pulled the same C_T/σ with the increased rotor inertia, the vertical impact speed and/or the horizontal roll-on speed could be reduced. It should be noted that while this roll-on

speed reduction appears possible, the touchdown body attitude limit might be the constraining factor which precludes the use of the tip path plane angle required for effecting the speed reduction.

Conversely, it can be stated that by maintaining the baseline H-V envelope, increasing the rotor inertia will increase the level of safety for specified end point constraints.

This leads to the conclusion that one cannot always point to a singular parameter and state "this is the one that will make things better." As in the case discussed here, a 50% increase in rotor inertia for the OH-6A shows a significant reduction in the H-V envelope while using initially the same blade loading, C_T/σ potential. On the other hand the same inertia increases for the AH-1G shows no significant change in the H-V envelope (except the low hover height) primarily because the permitted body attitude at touchdown does not allow the rotor to use the available blade loading potential.

To obtain a more meaningful comparison of parametric effects of autorotation, a rating factor, based on the ratio of blade loading potential and blade loading used for attaining a given H-V envelops is introduced, i.e., C_T/σ allowed/ C_T/σ used. This rating factor has a baseline value of 1.0. The effect of any given parametric change is basically reflected in the change in the H-V envelope. In conjunction with this H-V change, variations of the rating factor from 1.0 indicates that this parametric change could be more effective provided it was changed in conjunction with another parameter.

As an example, a 50% increase in rotor inertia makes a significant change in the H-V envelope for the OH-6A and negligible change in the rating factors. See Table A4 and Figure A-4(a). On the other hand the same inertia increase for the AH-1G yields a negligible change in the H-V "nose" point and high hover height out a significant change in the rating factors occurs, See Table 4 and Figure A-4(b). This indicates that minimal benefits can be attained by increasing the AH-1G rotor inertia unless a change in touchdown body attitude is permitted so as to utilize the benefits of the inertia change.

One might argue that the rating factor could also be interpreted as a safety margin. This safety margin could serve as an indicator of the margin of error or skill level for the pilot in conducting the autorotational landing. This is a valid argument, and the significance of increased inertia would be based on the magnitude of the rating factor

In either case, the combination of H-V envelope change and rating factors provide a useful guide for determining the effect of parametric changes on the autorotative capabilities of the subject helicopter.

A table showing the effect of singular parametric changes from a baseline configuration of the OH-6A and AH-1G is provided in Table A-4. The interpretation of this table would be as follows.

Based on the "optimum" H-V envelope having a rating factor of 1.0, the baseline OH-6A at a disc loading of 3.5 could be improved. Review of the various parameters shows that, using a 009.5 airfoil section, a 5% increase in the low hover height could be attained with slightly improved error margins. This airfoil change would also provide a 14% reduction in the "nose" point speed and the high hover height and bring the rating closer to an "optimum" design point. Obviously, other design considerations must be weighed prior to making such a change.

Review of the AH-1G baseline data (Table A-4) shows that at a disc loading of 5 no one parametric change could significantly improve the baseline H-V envelope but rather a combination of parametric changes would be required.

The parametric trends shown in Table A-4 are only valid for the disc loadings for which they were generated. This disc loading basically specifies the speed range for rotorcraft evaluation. The effect of parametric changes in other speed ranges could be significantly different. An example of this is shown in Figure A-5. This figure shows the effect of disc loading of the two baseline rotorcraft. It can be seen from these data that as disc loading increases the H-V envelope boundaries increase. The sensitivity of airframe drag in different velocity ranges could be significantly different. Other major parameters are similarily affected. The effect of increasing altitude has a similar effect on increasing the H-V envelope as shown in Figure A-6. In view of this, any analysis conducted for the purpose of improving or designing rotorcraft, for minimizing H-V envelope boundaries must be conducted for the intended operational disc loading and altitude for the rotorcraft in question. A parametric trade-off can then be conducted, for the design point, and a listing of the sensitivities compiled in a similar manner as Table A-4.

The parameter sensitivity list, as presented, is only intended for use as a guide of design considerations for improving autorotational characteristics of helicopters and is only applicable for the disc loadings for which it was developed.

HDP CORRELATION WITH FLIGHT TEST DATA

To establish the confidence level of the Helicopter Dynamic Performance (HDP) Program, a comparative analysis between calculated and flight test performance was conducted. This comparative analysis was categorized to cover the major assumptions used in the analysis. The rotorcraft used for this study were the Hughes OH-6A and the Bell AH-1G.

Initially, the HDP Program was used to evaluate steady-state hover performance for the subject rotorcraft at various wheel heights. The results of this evaluation are shown in Figure A-7. The fairings used for the test data were obtained from Reference 8 for the OH-6A and from Reference 9 for the AH-1G. The results of this comparison show excellent agreement between theory and flight test at all wheel heights tested. It should be noted that although an apparent discrepancy exists for the OH-6A at high C_W levels, these values are only attainable at high altitudes. The maximum power levels for sea level standard and 10,000 ft. standard are shown on this curve for reference. Based on the power limitations, the maximum deviation between calculated and flight test is 10 SHP. This is regarded as being within measuring accuracy and test scatter in the basic hover data.

The apparent deviation between the calculated and faired curves at the low C_W values for the AH-1G can be accounted for by referring to the actual measured test data used in establishing the comparison. The measured data for the low C_W range is included on Figure A-7 for reference. Also shown for reference is a ΔC_p band of 2×10^{-5} which equates to 55 SHP at sea level standard conditions.

Program verification for forward speed performance was conducted with the HDP program set in a steady-state mode for the speed range of the rotorcraft in question. The comparison between calculated and measured test data for the OH-6A at sea level, 5000 and 10,000 ft. density altitudes is shown in Figure A-8. The test data used for this comparison were obtained from Figures 32, 33, and 40 of Reference 8.

Comparisons of level flight performance for the AH-1G in the clean and heavy hog configuration are shown in Figure A-9. The test data for these figures were obtained from Figures 9 and 4 (respectively) of Reference 10. The calculated level flight performance shows excellent agreement with the measured test data, thus verifying the analytical rotor performance model

---

[8] ENGINEERING FLIGHT TEST OF THE OH-6A HELICOPTER (CAYUSE) PHASE D, Final Report, USATECOM Project No. 4-6-0250-01, USAASTA Project No. 65-37, April 1969.

[9] ENGINEERING FLIGHT TEST AH-1G HELICOPTER (HUEY COBRA) Phase D, Part 2 Performance, Final Report, USATECOM Project No. 4-6-0500-01, USAASTA Project No. 66-06, April 1970.

[10] ENGINEERING FLIGHT TEST AH-1G HELICOPTER (HUEY COBRA) Phase B, Part 6 Final Report, USATECOM Project No. 4-6-0500-01, USAASTA Project No. 66-06, November 1969.

in level flight. It is interesting to note that a 7 sq. ft. ΔF was required above the AH-1G clean configuration to obtain the Heavy Hog configuration performance. This is in agreement with the flight test findings as reported in Reference 10.

With the rotor performance model verified in powered flight, a further analysis was conducted to establish its validity in power-off (autorotative) steady-state flight. The results of these calculations are shown in Figure A-10. The measured test data, obtained from Figure 55, Reference 8, for the OH-6A and Figure 15, Reference 10, for the AH-1G were superimposed on the calculated curves.

Review of the OH-6A comparison indicates a high degree of test scatter in the data. In an attempt to account for this scatter, several computer runs were conducted to establish the sensitivity of the descent rate with variations in trimmed tip path plane angle. The results of this study, superimposed on this figure, show a 100-FPM variation in rate of descent per 1 degree variation in tip path plane angle from the trimmed condition (OH-6A). In view of this, along with the variation in the test data at a given speed, a 550-FPM variation at 35 knots 850-FPM variation at 45 knots, and 220-FPM variation at 55 knots, it was judged that the program output was well within the measuring accuracy of the test data. The tests conducted with the AH-1G demonstrated a higher degree of repeatability and the calculated results are within ± 1.5 ft./sec. of the measured data. The sensitivity of the AH-1G rate of descent with tip path plane angle variations from trim was calculated to be 100 FPM/0.75 deg. Δ tip path plane angle from steady-state trim.

This portion of the comparative analysis covered the major aspects of the rotor performance model. The agreement shown between theory and flight test basically verified the assumptions made in regard to ground effect, number of blades, blade compressibility and stall, and the distribution of power measurements in regard to induced, profile, parasite and climb. The ability to represent the airfoil data as a cubic equation in a mean lift coefficient/mean drag coefficient relationship was also verified. It should be noted that the OH-6A has a four-bladed rotor system using a 0015 airfoil section while the AH-1G uses a two-bladed rotor with a 9.33 percent symmetric airfoil section.

To verify the dynamic portion of the program, three autorotative flight test landings conducted with the AH-1G were simulated with the HDP. These landings were initiated from a steady-state flight condition with a simulated engine malfunction followed by a 1 to 2 sec. collective delay and full autorotative touchdown.

The first condition evaluated was a power cut from a 15-foot hover, (representative of the height-velocity low hover height). The results of the calculated flight were superimposed on the test data traces in Figure A-11(a). The calculated results show excellent agreement with

---

[11]HEIGHT VELOCITY TEST AH-1G HELICOPTER AT HEAVY GROSS WEIGHT (LOW ELEVATION), Final Report, USAASTA Project No. 74-19, June 1974.

rotor RPM droop. A 2-second time delay was used for this flight. The vertical accelerations and displacements along with the collective stick position also show excellent agreement with the flight test test time history. The flight test data was obtained from Figure 6 of Reference 11. The summary sheet of the completed flight path is shown in Figure A-11(b).

A forward flight entry condition, 72 knot approach at 195 feet, (nominally representing the H-V nose point) was evaluated and the results are shown in Figure A-12(a). The summary sheet for the calculated flight is presented in Figure A-12A(b). Evaluation of a throttle chop flight from 670 ft. AGL (indicative of AH-1G H-V high hover height) is shown in Figure A-13(a) with the computed flight summary sheet shown in Figure A-13(b). These data were obtained from Figures 3 and 1 of Reference 10.

Review of these data shows excellent agreement between theory and flight test The program shows some variation, however, in vertical acceleration and airframe pitch attitude during the mid-portion of the maneuver i.e., after the time delay and prior to the cyclic flare. The program also indicates that the rotor RPM starts to drop off slightly sooner and at a slightly higher rate during the final collective flare than the test data indicates. The reason for this is not readily apparent as the calculated vertical accelerations and airframe pitch attitudes are in nominal agreement with measured data.

It should be noted that the true airspeed trace shown for the flight test data refers to flight path speed. Although some discrepancy exists between calculated and measured velocities, excellent agreement between the calculated and measured horizontal distances was obtained.

Detailed time history data for autorotative landings with the OH-6A rotorcraft was not available for this study. In view of this, two autorotative landings conducted with the Sikorsky CH-54B were used for this comparative analysis. While these flights do not include the entry into autorotation they do pick up the flight during the steady-state descent and final flare maneuver. Flights at a nominal sea level standard density altitude and 10,000 feet density altitude were used for this analysis. These data are shown in Figure A-14.

In the HDP analysis, θ_{75} refers to the mean blade angle required over the total rotor disc for generating the desired thrust. This blade angle is referenced to the tip path plane axis system. The relationship between θ_{75} and the collective stick position requires the transformation from the tip path plane axis system to the airframe axis system along with the collective rigging of the rotorcraft in question. The HDP analysis presently does not incorporate the capability to conduct this angle transformation or provide for rotorcraft rigging inputs.

However, a evaluation of the transformation equations required was conducted externally from the program for an axial flight condition with the AH-1G. This condition was selected since the tip path plane and body attitude were constant throughout the flight. Based on the rigging

assumption that full collective stick travel will produce a 21-degree change in mean blade angle for a neutral CG, the transformation of θ_{75} (average blade angle) to collective stick position shows excellent agreement. (Figure A-11). In conducting this evaluation, the HDP program was set up to use the $\Delta\theta_{75}$ input option. This option provides the capability of specifying the mean blade angle and computing the resulting flight path and rotor RPM changes with time. As can be seen in Figure A-11, the time history of rotor RPM and flight path shows excellent agreement with flight test, thereby verifying, at least from hover, the energy concept for calculating the rotor mean blade angle. The transformation of the mean blade angle to collective stick position in translational flight would require the details of the control rigging relationships for the rotorcraft in question.

SPECIFICATION COMPLIANCE

The OH-6A and AH-1G autorotative capabilities with regard to their compliance with MIL Spec. MIL-H-8501A, General Requirements for Helicopter Flying and Ground Handling Qualities, were reviewed. The pertinent paragraphs of the MIL Spec. for this evaluation were 3.5.4.4, 3.5.5., 3.5.5.1 and 3.5.7. The HDP evaluation for this specification compliance check was established using HDP time history output. The results of 96 autorotative landings are summarized in Tables A-1 and A-2. Presentation of the detailed time histories is beyond the scope of this effort.

Paragraph 3.5.4.4 - from a 35-knot autorotational touchdown, bring the helicopter to a stop within 200 feet.

HDP calculations indicate that this criterion cannot be met with a skid type gear when a level asphalt surface is used.

Paragraph 3.5.5 - Enter into autorotation at all speeds from hover to maximum forward speed--Collective pitch control motion has been delayed for at least 2 seconds following loss of power.

HDP analysis indicates that a 2-second time delay can be tolerated for AH-1G normal operating weights up to 75% maximum forward speed. This 2-second collective delay cannot be safely tolerated at overload operating weights or at forward speeds in excess of 75% maximum, but must be reduced to 1 second. This is based on the AH-1G test data (Reference 13) and the HDP analysis for these data shown in Figures A-12 and A-13. Again, no OH-6A autorotation time history data was available at the time this report was written.

Paragraph 3.5.5.1 - Sudden loss of power with collective control fixed, shall not produce pitch, roll, or yaw attitude changes in excess of 10 degrees in 2 seconds, except that at speeds below that for best climb, a 20-degree yaw in 2 seconds will be accepted.

HDP analysis indicates that both aircraft can meet the intent of 3.5.5.1 for the pitch and roll attitude rates within the limitations of permissible collective delay. See 3.5.5 above. The HDP program does not evaluate yaw attitudes.

Paragraph 3.5.7 - It shall be possible--to make repeatedly safe, power-off autorotative landings (touchdown) at speeds of 15 knots or less.

HDP analysis indicates that neither the OH-6A nor the AH-1G can comply with this specification at normal operating gross weights.

CONCLUSIONS

This study was conducted to establish the sensitivity of various design parameters on the autorotational characteristics of helicopters. The Helicopter Dynamic Performance (HDP) program was used for the study. Based on the results of this effort, it is concluded that:

The sensitivity of any given design parameter is highly dependent on the baseline conditions from which the sensitivity is desired.

The sensitivity of a given parameter on a given rotorcraft cannot be directly used as typical for all rotorcraft even when the same baseline H-V capability exists.

A highly generalized effect of various parameters can be categorized, as shown in Table A-3. In using this table the designer must keep in mind that these parameters are highly interdependent and the changing of one might not be effective without the modification of others which would permit attaining the desired change.

The benefits of parametric changes on autorotational capabilities must be evaluated on an aircraft by aircraft basis.

The designer must also consider the effects these parametric changes might have on the overall power-on flight envelope for the intended design.

The sensitivity of parametric changes as predicted by the HDP program is based on control input requirements which maximize the aircraft capabilities. Pilot capabilities for duplicating this maneuver are not considered. The resulting calculated H-V envelope must then be considered as the minimum possible.

The results of the comparative analysis between program calculated performance and flight test data show excellent agreement in all areas investigated. In view of this, the Helicopter Dynamic Performance program can be used with a high degree of confidence for estimating rotorcraft capabilties in power-on and emergency flight conditions.

RECOMMENDATIONS

The Helicopter Dynamic Performance (HDP) program developed under this contract provides a useful tool for evaluating rotorcraft takeoff and landing procedures and capabilities. Its use is intended to be a guide for evaluating rotorcraft designs and/or flight procedures. Its use does not, however, suggest the elimination of flight tests to verify "real life" aircraft and pilot workload capabilities.

It is recommended that this program be used prior to actual flight testing to provide some insight as to basic aircraft capabilities and possibly dangerous conditions. This preliminary effort will minimize the time and cost of required buildup flight test as well as minimize the risk in conducting them.

Its use as a tool for evaluating various design concepts is also recommended. Analysis of parametric sensitivities should be conducted in a manner similar to that used herein. The change in H-V envelope from the baseline, variations in rating factors, and overall effect on the intended flight envelope should be fully evaluated prior to committing to final design or configuration changes.

To improve the versatility of this program, it is recommended that additions to the program be made for evaluation of wings and/or tail planes, and co-axial rotors. Further development for coupling the HDP program with an acoustic analysis to provide acoustic foot prints or detectability criteria during powered takeoff, landing and nap-of-the-earth maneuvers should be considered.

Further analysis should be conducted to better establish the relationship of the mean blade angle ($\theta_{.75}$), as defined for the energy method, and the collective stick position during translational flight.

The program should also be modified to permit the input of known flight test control input time histories for correlation with flight test data.

Additional correlation over a wider range of helicopter types is recommended. This correlation could lead to the development of a validated and calibrated autorotative index for "rule-of-thumb" evaluation of helicopter autorotative capabilities.

The HDP program can also be used for effectively optimizing power-on takeoff and landing procedures for small field operation studies.

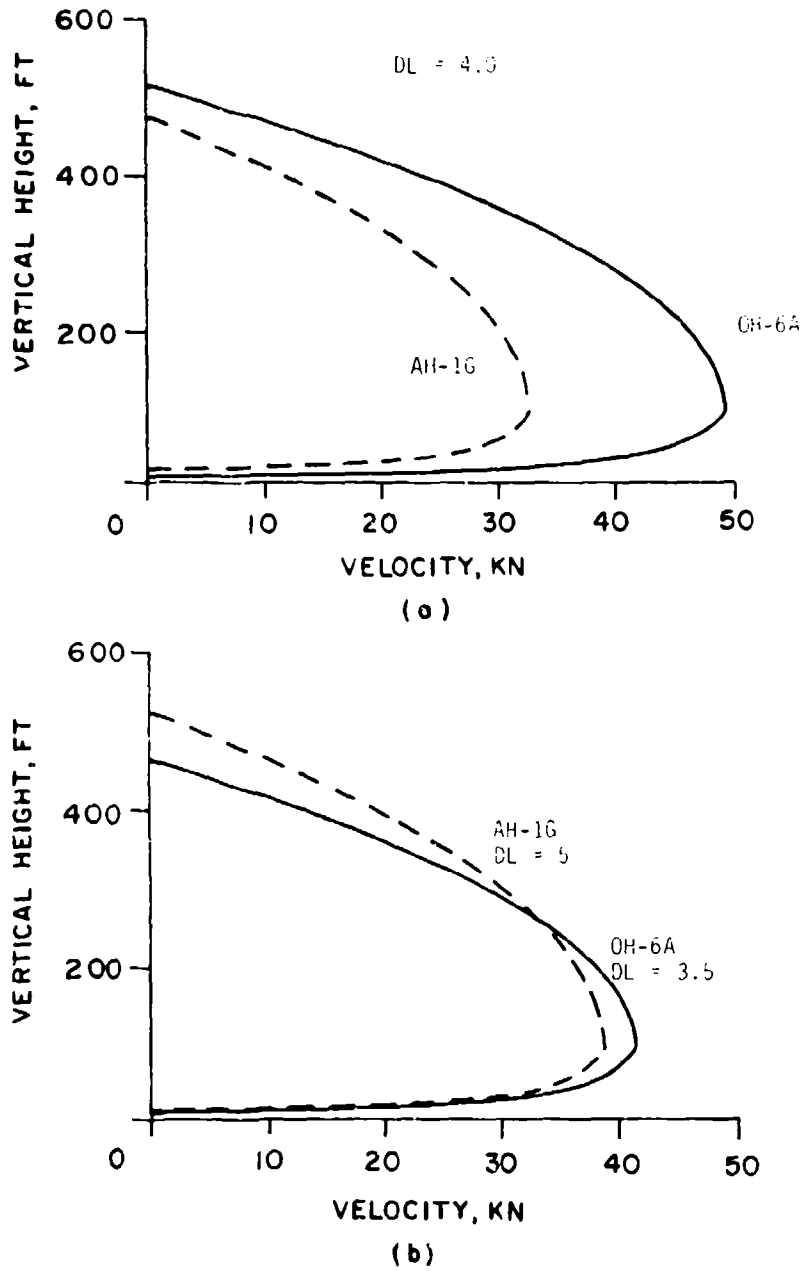

Figure A-1. Height Velocity Comparison of Baseline Configuration.

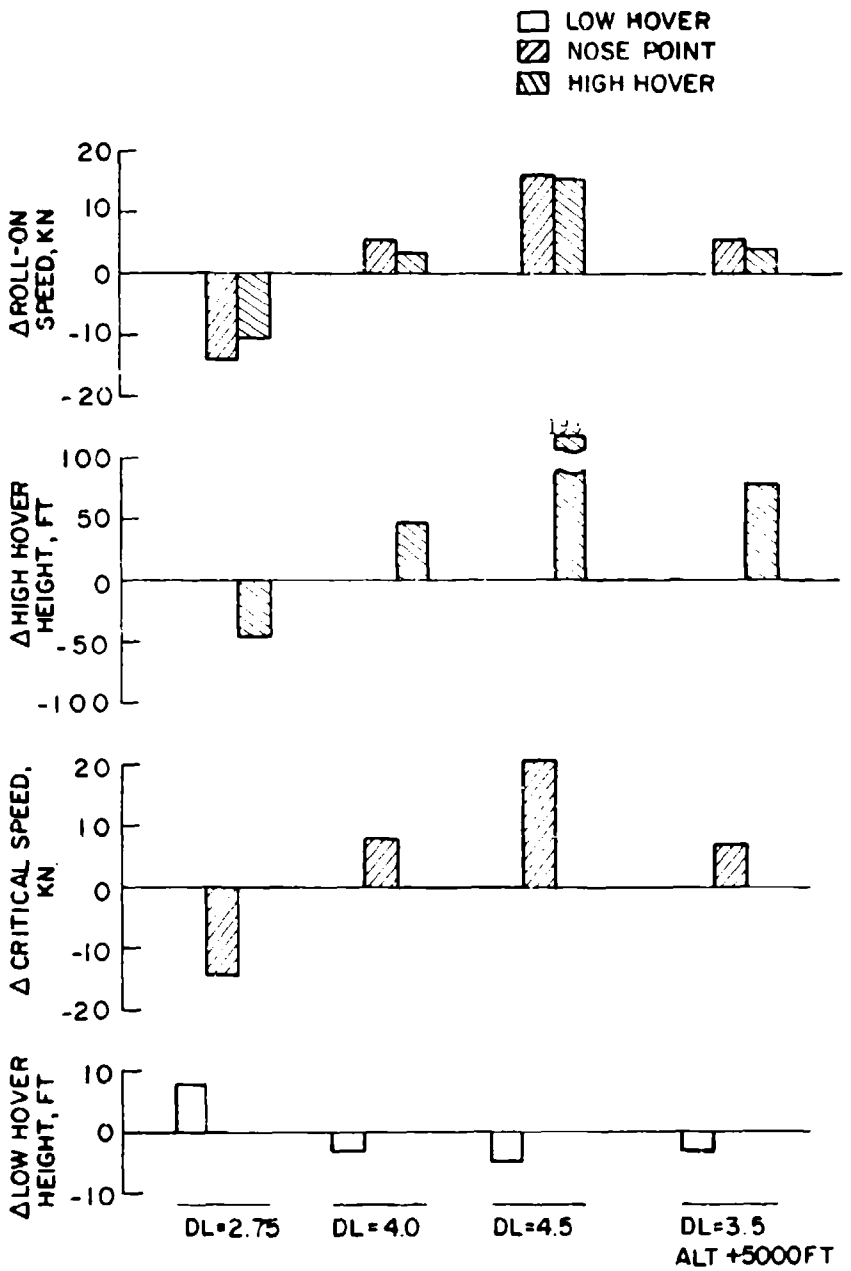

(a) EFFECT OF DISC LOADING AND ALTITUDE

Figure A-2. OH-6A Height-Velocity Envelope Sensitivity, Baseline Disc Loading-3.5.

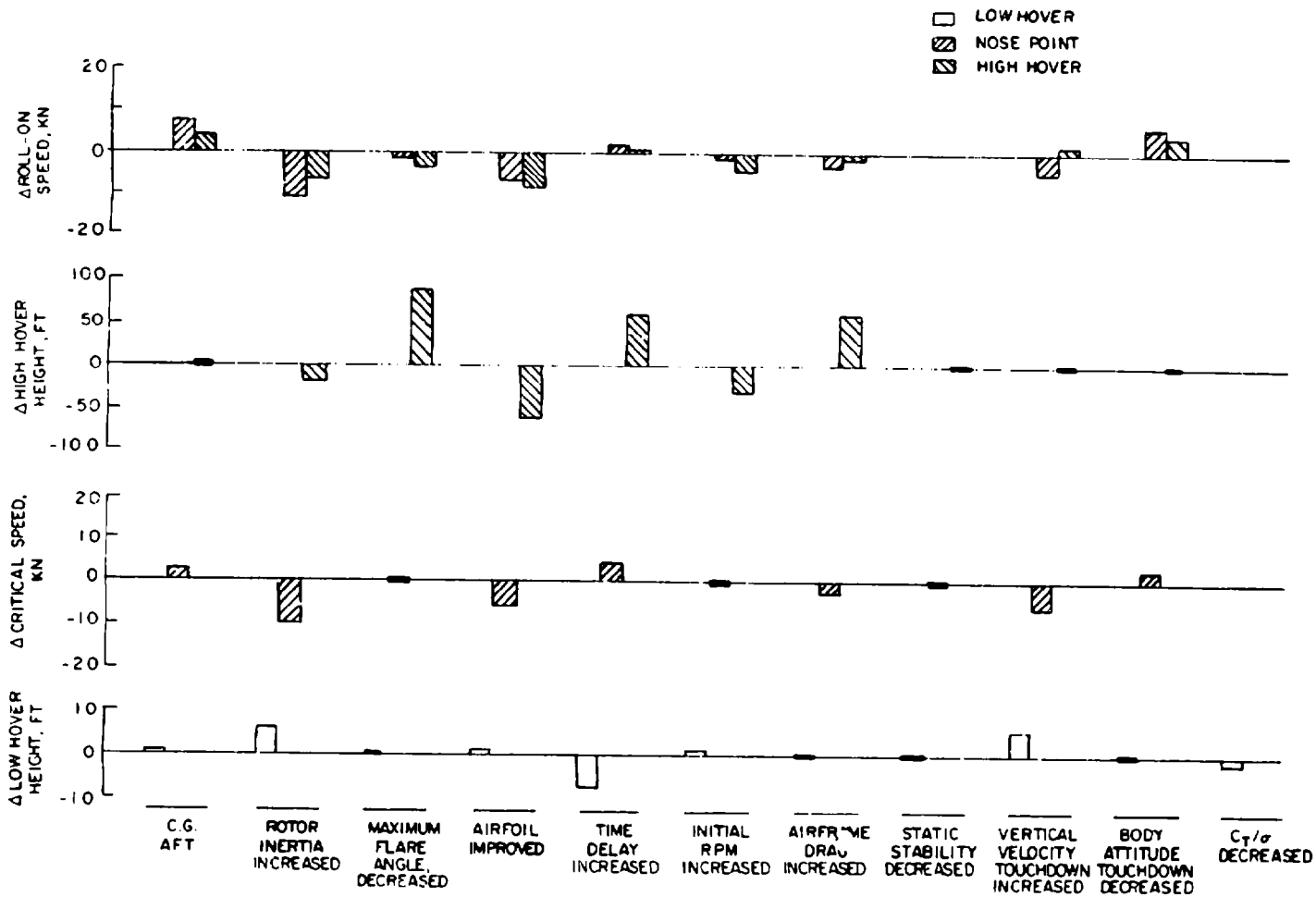

(b) EFFECT OF PARAMETRIC VARIATIONS

Figure A-2. Concluded.

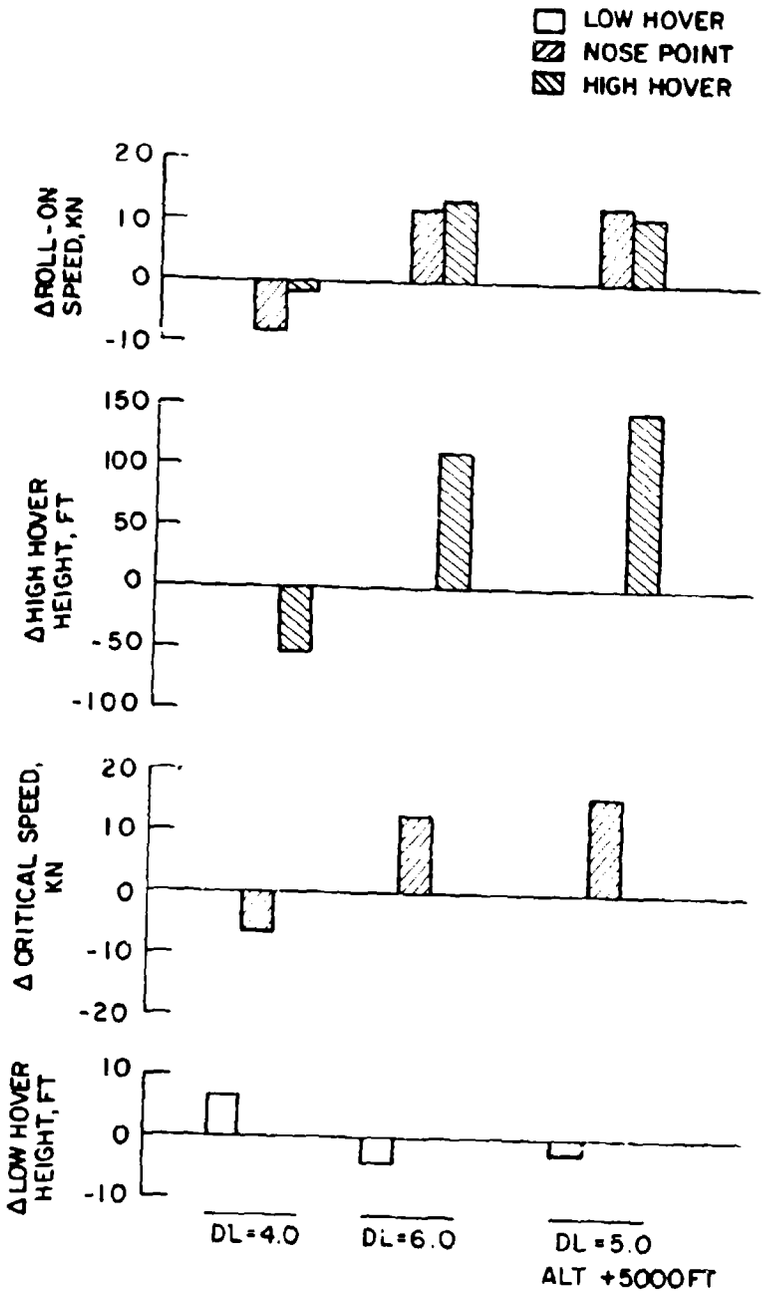

(a) EFFECT OF DISC LOADING AND ALTITUDE

Figure A-3. AH-1G Height Velocity Envelope Sensitivity, Baseline Disc Loading - 5.0.

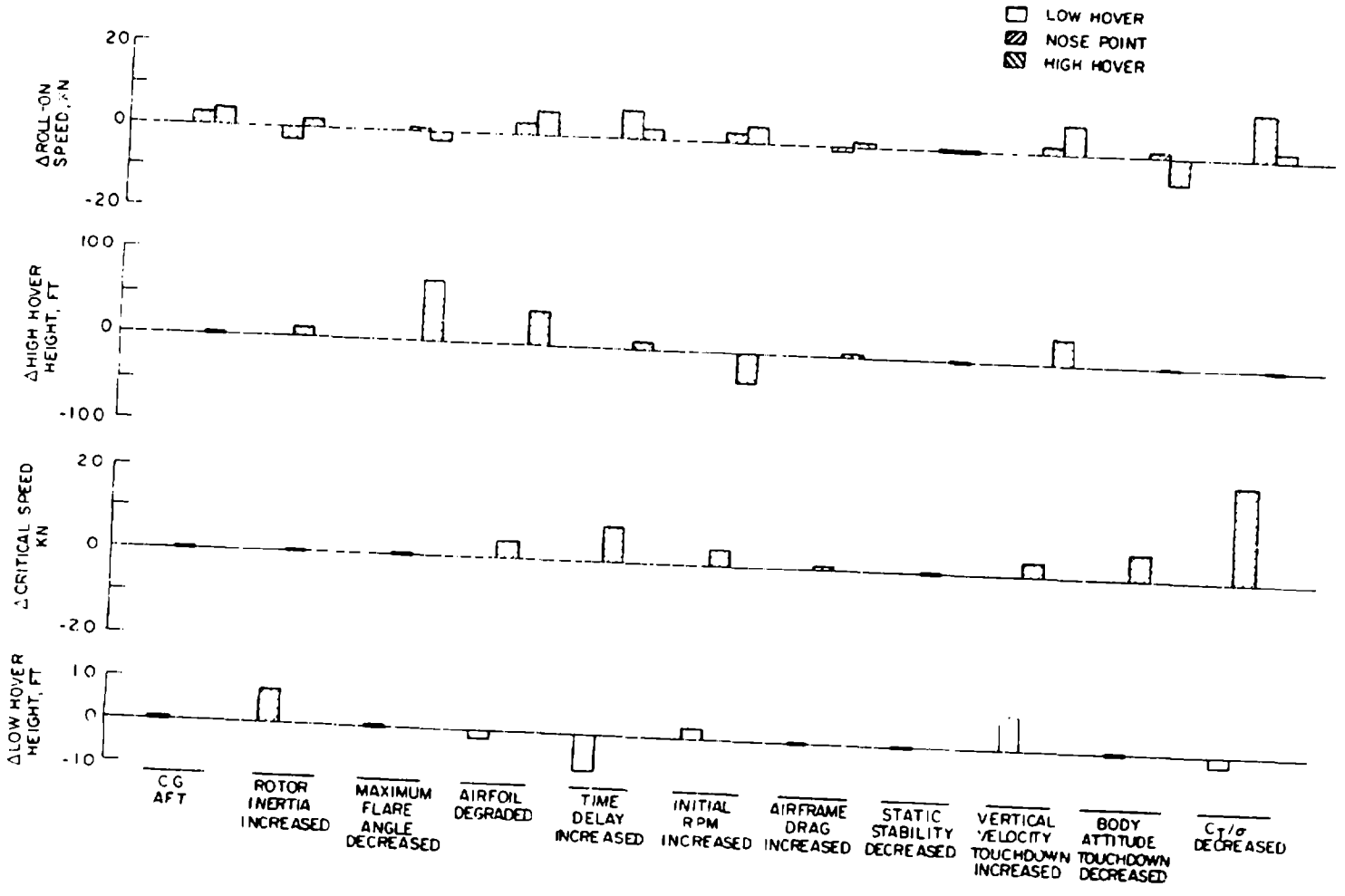

(b) EFFECT OF PARAMETRIC VARIATIONS

Figure A-3. Concluded.

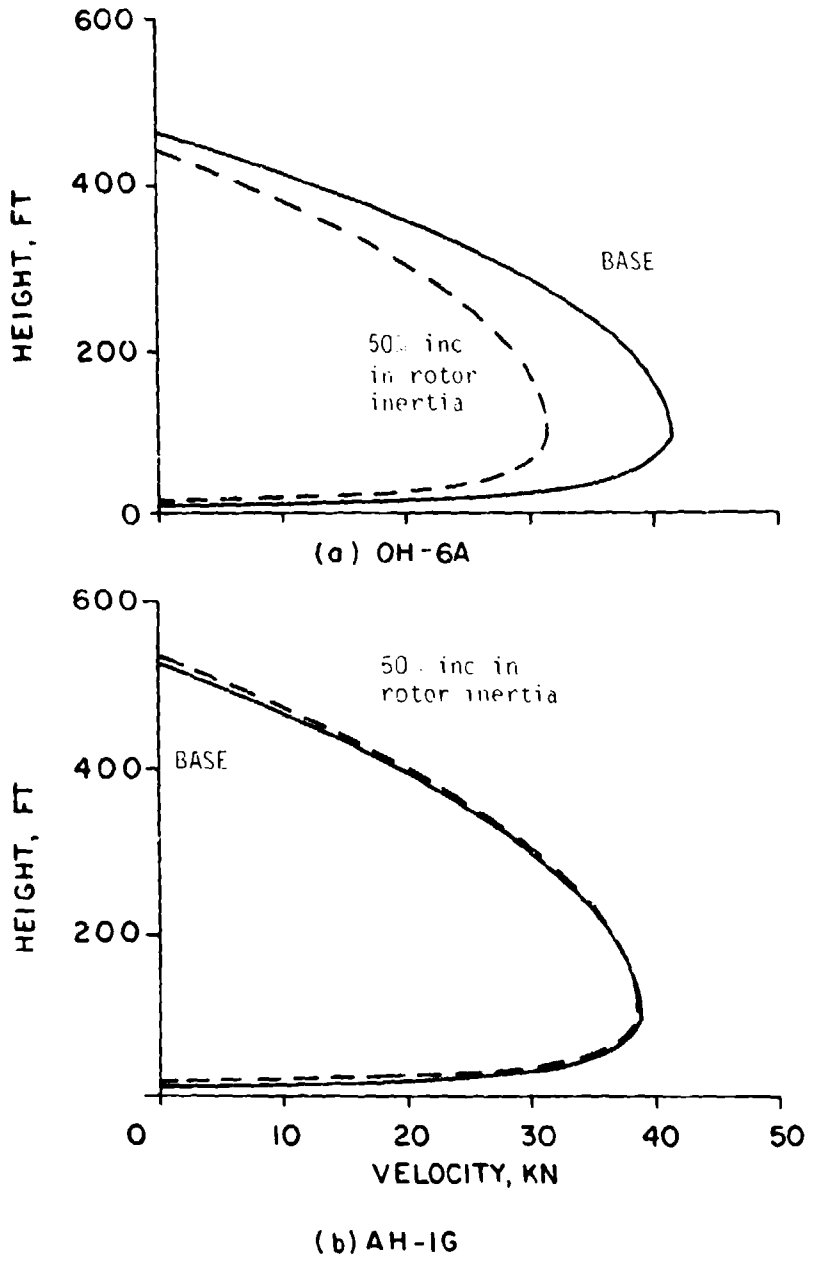

Figure A-4. Effect of Rotor Inertia on H-V Envelope.

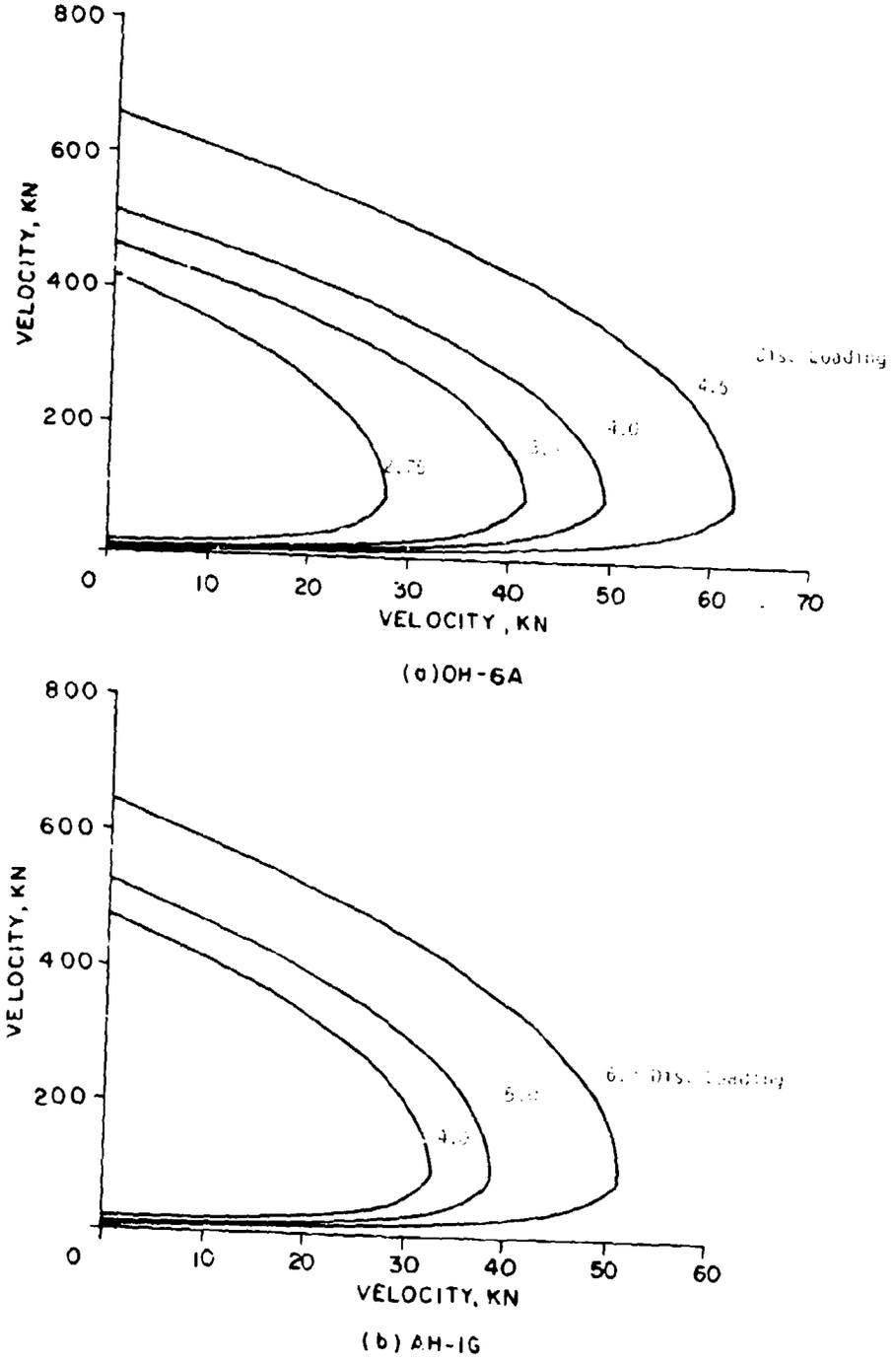

Figure A-5. Effect of Disc Loading on H-V Envelope.

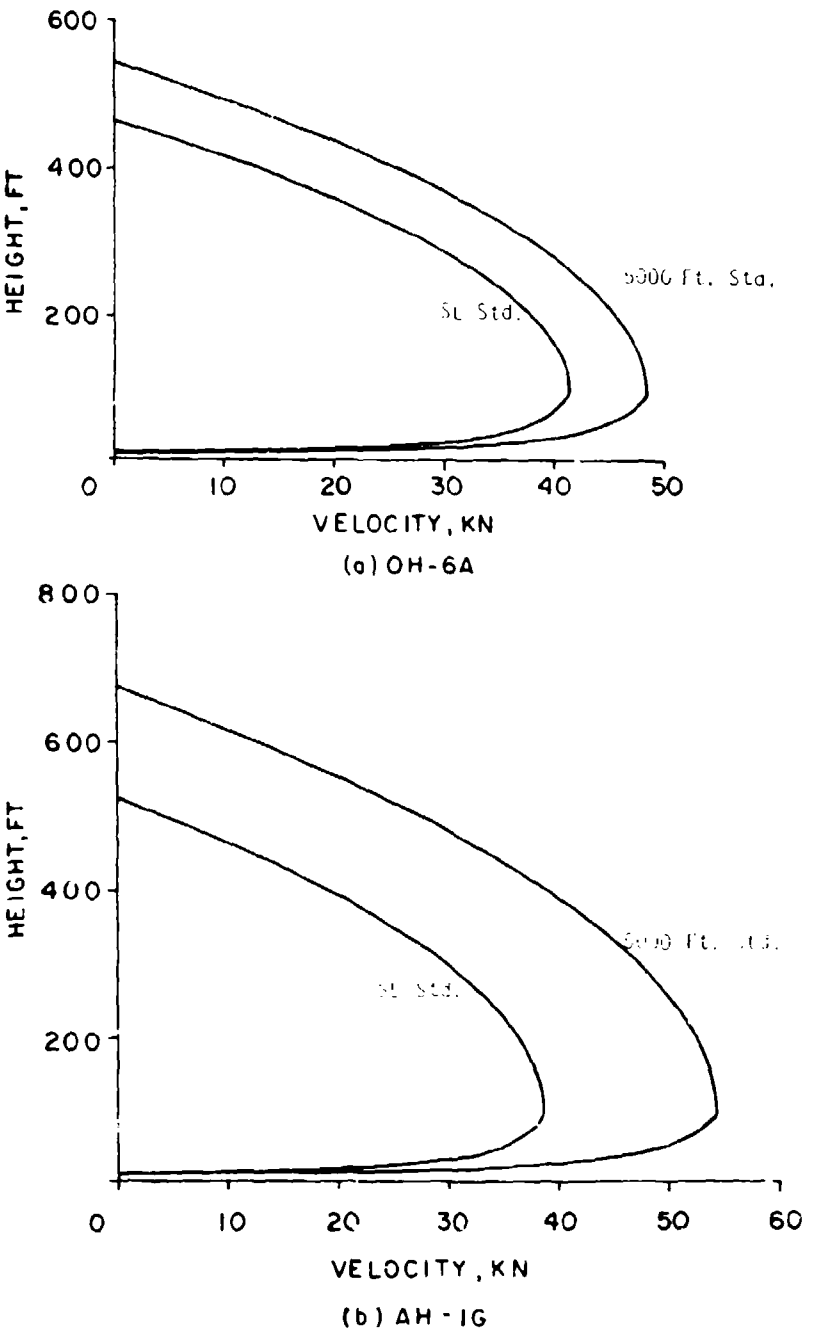

Figure A-6. Effect of Altitude on H-V Envelope.

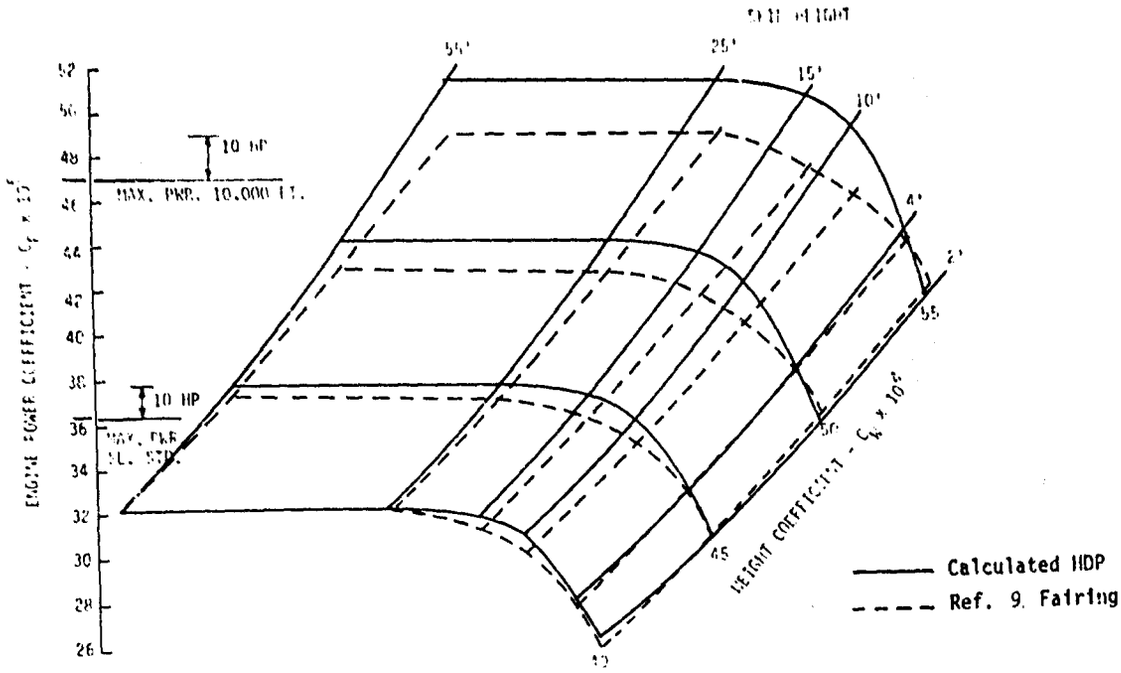

(a) OH-6A

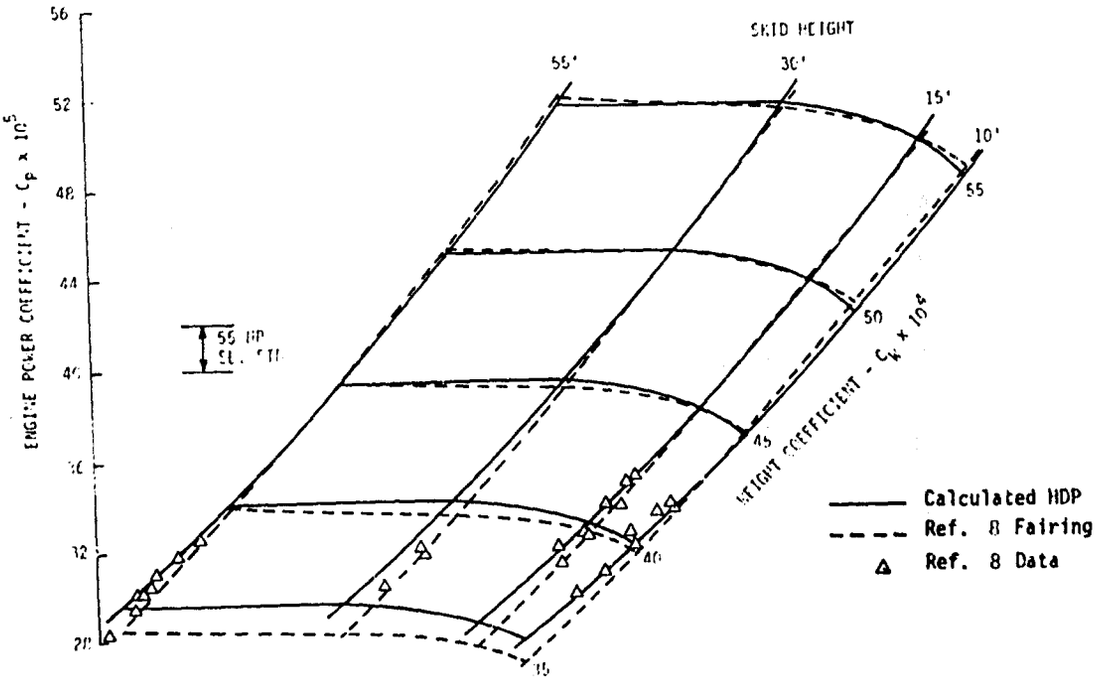

(b) AH-1G

Figure A-7. Hover Performance.

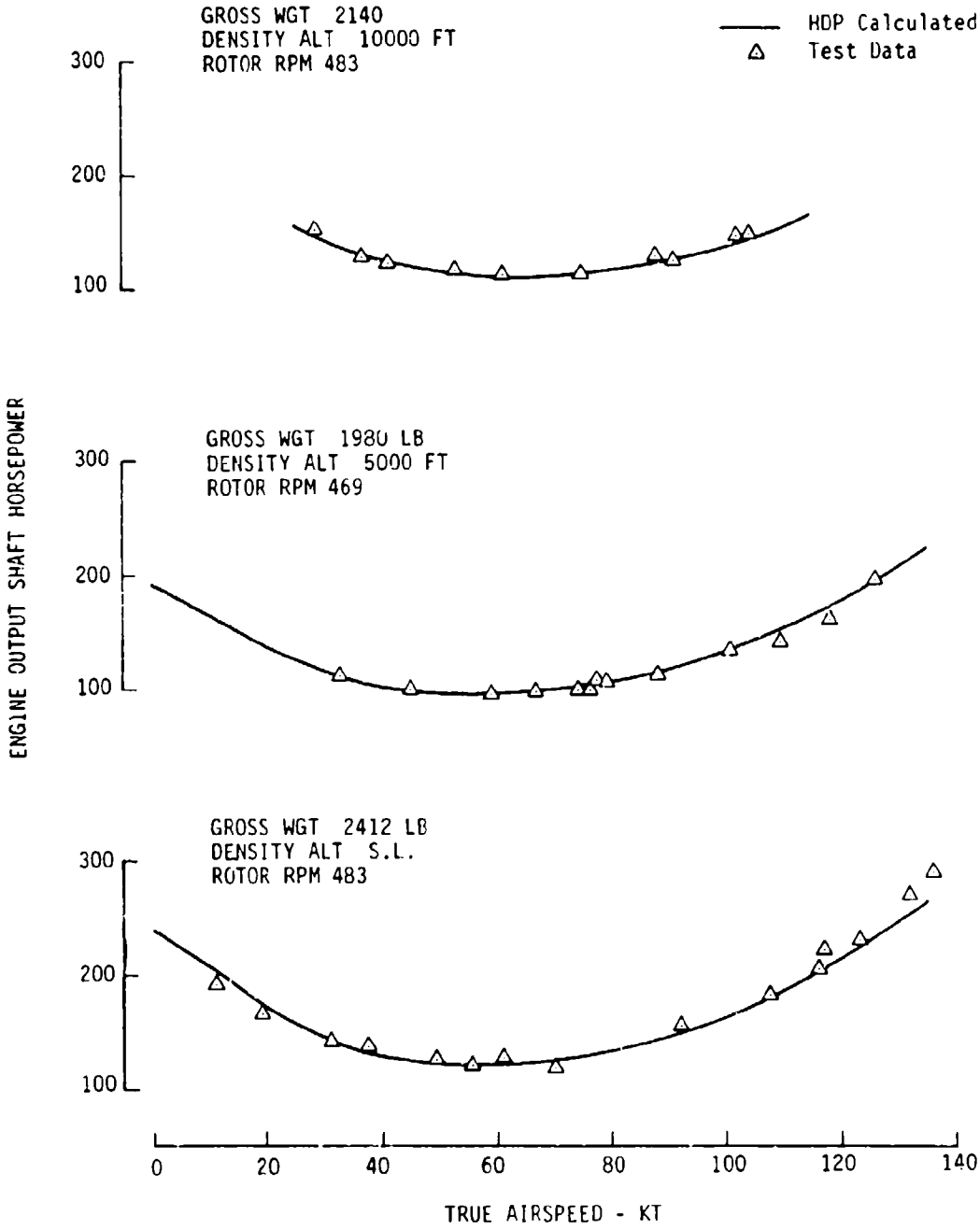

Figure A-8. OH-6A Level Flight Performance (Clean Configuration).

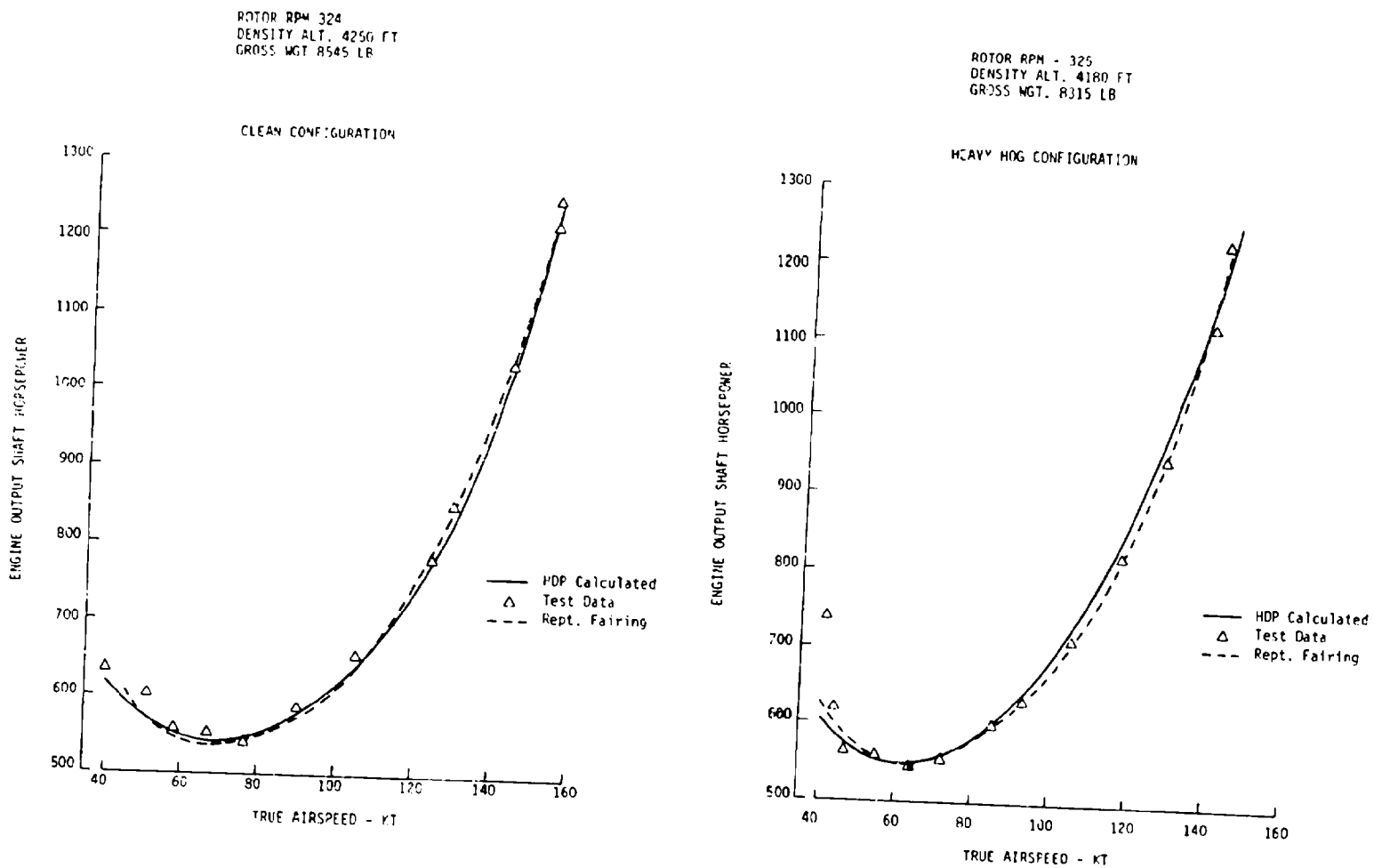

Figure A-9. AH-1G Level Flight Performance.

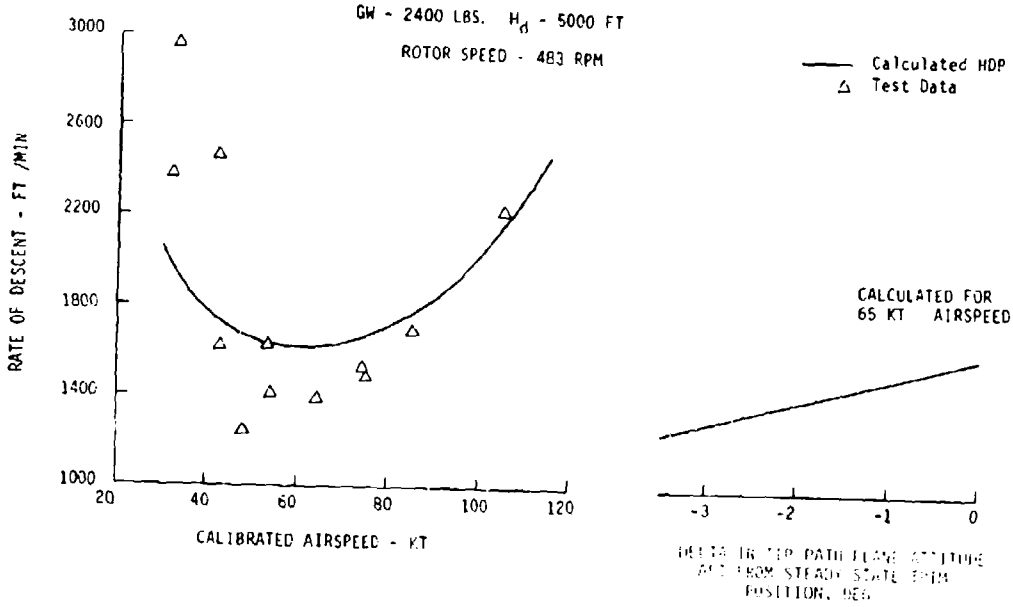

(a) OH-6A

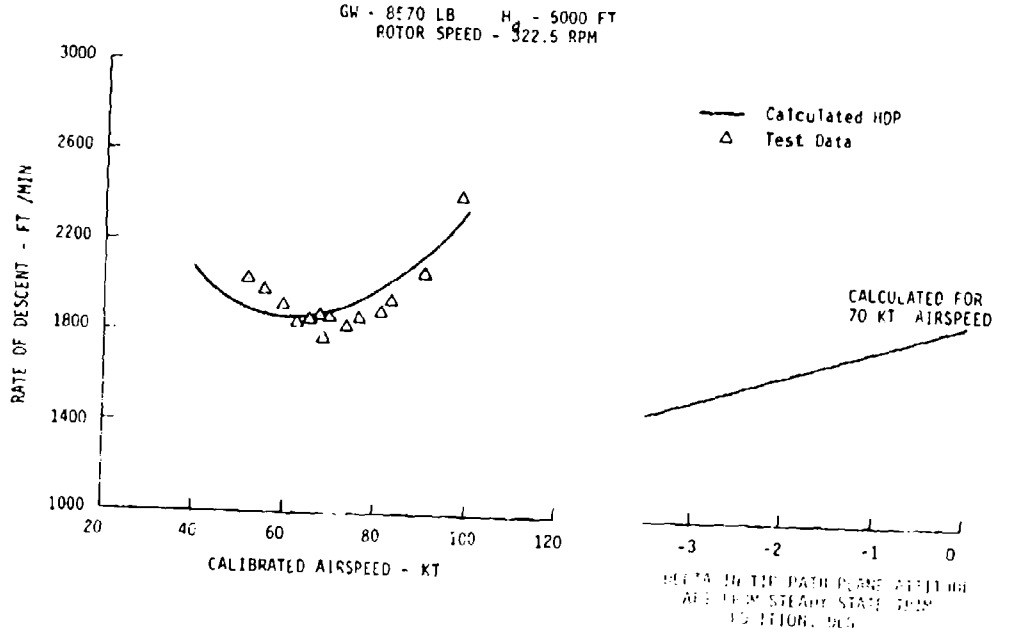

(b) AH-1G

Figure A-10. Autorotation Performance.

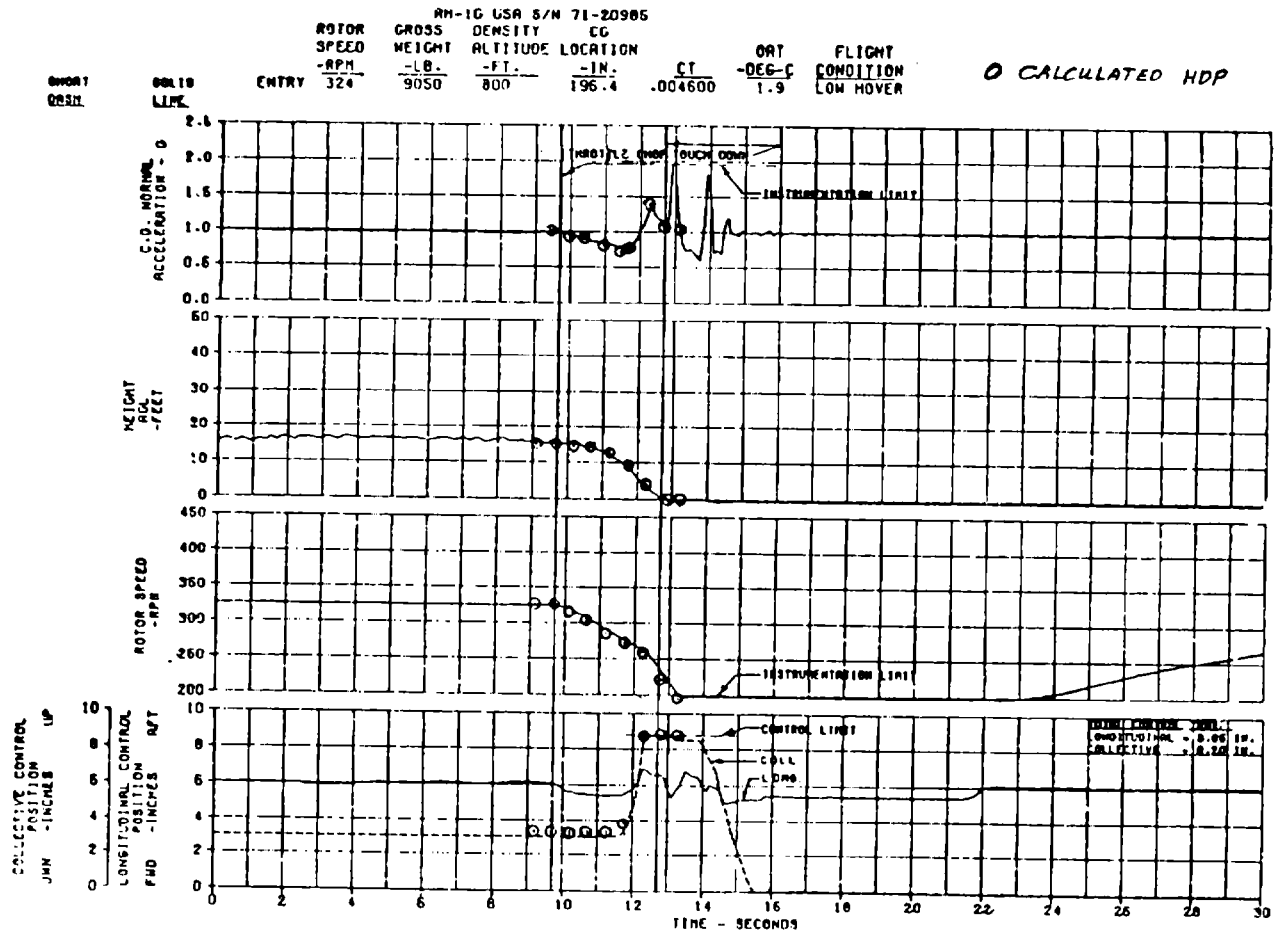

(a) Flight Test Data (Low Hover Height)

Figure A-11. Time History of Autorotational Landing.

AH-1G

OPERATING WGT.	=	9050.0	LBS.	NO. OF BLADES	=	2.	
PRESSURE ALT.	=	2000.0	FT.	BLADE CHORD	=	2.25	FT.
AMBIENT TEMP.	=	1.9	C.	BLADE RADIUS	=	22.0	FT.
WIND VELOCITY	=	0.0	KTS.	BLADE TWIST	=	-10.0	DEG.
WIND DIR. HORIZ	=	0.0	DEG.	DISC SOLIDITY	=	0.0650	
WIND DIR. VERT.	=	0.0	DEG.	AIRFRAME F	=	24.0	FT**2
				DISC AREA PROJ	=	1520.5	FT**2
CASE NUMBER	=	1.		AREA RATIO	=	1.000	

FLIGHT SUMMARY

TIME (SEC)	HGT (FT)	DIST (HORIZ)	DIST (LAT)	VEL (KTS) LONG	VEL FPM VERT	ANR PERCENT	TPP ATT LONG DEG	TPP ATT LAT DEG	SHP	M.R.THRUST (LBS)
				START OF EVENT 1						
0.0	15.0	0.0	0.0	0.0	0.0	100.0	0.0	0.0	1000.1	9274.4
				START OF EVENT 2						
0.500	15.0	0.0	0.0	0.0	-0.0	100.0	0.0	0.0	1000.1	9274.4
				START OF EVENT 3						
2.500	9.8	0.0	0.0	0.0	-515.5	84.6	0.0	0.0	0.0	6735.8
				START OF EVENT 4						
2.969	4.8	0.0	0.0	0.0	-748.6	81.1	0.0	0.0	0.0	6778.5
				START OF EVENT 5						
3.485	0.0	0.0	0.0	0.0	-379.0	67.9	0.0	0.0	0.0	9456.6
				CONDITIONS AT END OF FLIGHT						
4.485	0.0	0.0	0.0	0.0	-0.0	52.0	0.0	0.0	0.0	7415.0

DISTANCES ARE REFERENCED TO CYCLIC FLARE POINT

VERTICAL TOUCHDOWN VELOCITY WAS -6.3 FT/SEC

CT/SIGMA LIMIT EXCEEDED DURING FLIGHT ** CHECK ROTOR BLADES **

MAXIMUM CT/SIGMA ENCOUNTERED ON FLIGHT WAS 0.186

(b) Calculated Data (Low Hover Height)

Figure A-11. Concluded.

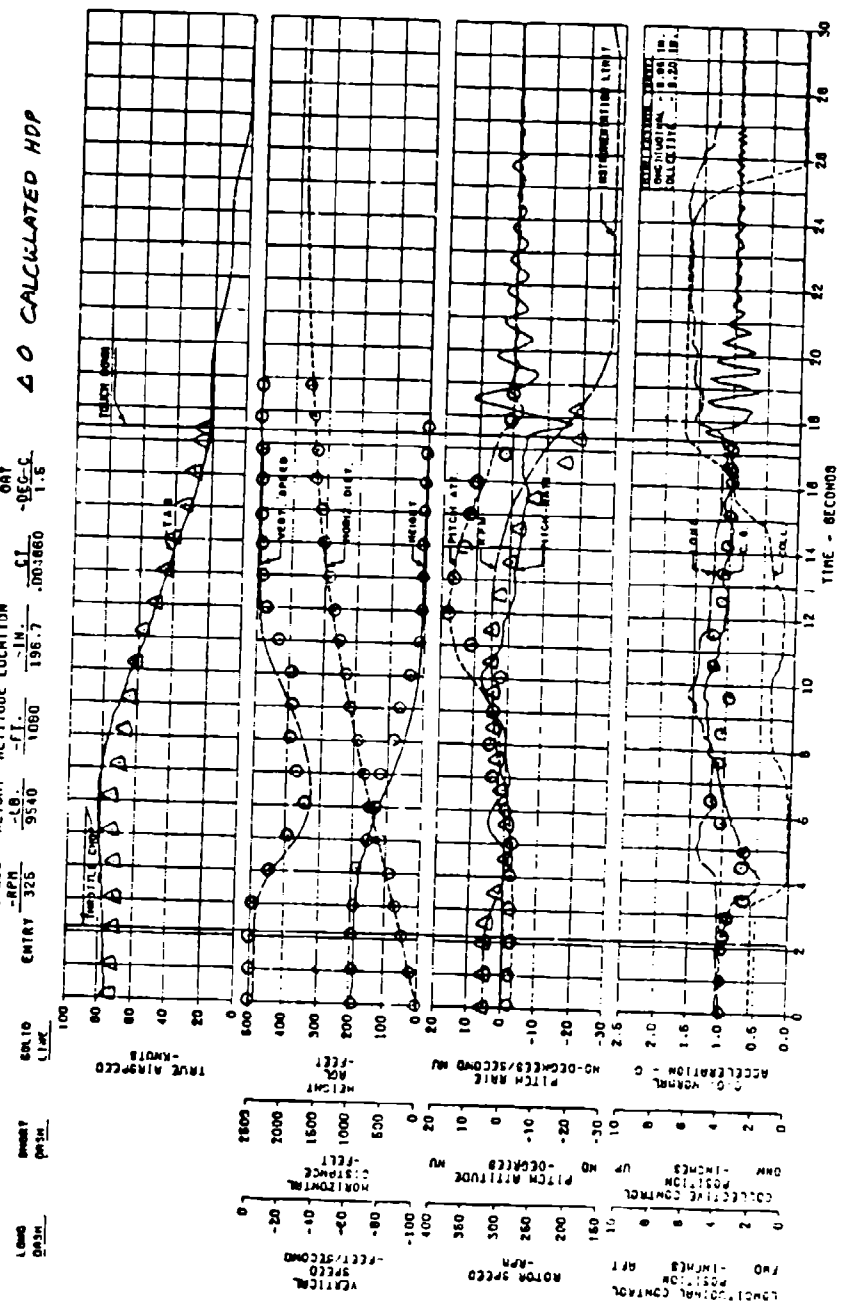

(a) Flight Test Data (Forward Speed Approach)

Figure A-12. Time History of Autorotational Landing.

AH-1G

OPERATING WGT.	=	9540.0	LBS.	NO. OF BLADES	=	2.	
PRESSURE ALT.	=	2000.0	FT.	BLADE CHORD	=	2.25	FT.
AMBIENT TEMP.	=	1.6	C.	BLADE RADIUS	=	22.0	FT.
WIND VELOCITY	=	0.0	KTS.	BLADE TWIST	=	-10.0	DEG.
WIND DIR. HORIZ	=	0.0	DEG.	DISC SOLIDITY	=	0.0650	
WIND DIR. VERT.	=	0.0	DEG.	AIRFRAME F	=	24.0	FT**2
				DISC AREA PROJ	=	1520.5	FT**2
CASE NUMBER	=	1.		AREA RATIO	=	1.000	

FLIGHT SUMMARY

TIME (SEC)	HGT (FT)	DIST (HORIZ)	DIST (LAT)	VEL (KTS) LONG	VEL FPM VERT	ANR PERCENT	TPP ATT LONG DEG	TPP ATT LAT DEG	SHP	M.R.THRUST (LBS)
				START OF EVENT 1						
0.0	195.0	-386.9	0.0	72.0	0.0	100.3	2.4	0.0	639.7	9570.6
				START OF EVENT 2						
2.000	195.1	-143.6	0.0	72.0	2.5	100.3	2.4	0.0	639.7	9571.7
				START OF EVENT 3						
3.000	194.7	-21.9	0.0	72.0	-63.8	96.3	2.4	0.0	85.7	9026.5
				START OF EVENT 4						
5.000	171.4	220.5	0.0	71.5	-1295.1	89.5	2.4	0.0	0.0	6503.6
				START OF EVENT 5						
9.571	55.0	741.4	0.0	62.7	-1410.5	98.9	-2.7	0.0	0.0	9543.4
				START OF EVENT 6						
11.457	20.0	931.0	0.0	54.3	-617.8	99.8	-16.3	0.0	0.0	12846.9
				START OF EVENT 7						
16.793	0.0	1293.1	0.0	28.3	-128.4	5.2	-12.0	0.0	0.0	9095.2
				CONDITIONS AT END OF FLIGHT						
20.793	0.0	1428.7	0.0	11.8	-0.0	73.3	-10.0	0.0	0.0	6031.8

DISTANCES ARE REFERENCED TO CYCLIC FLARE P

VERTICAL TOUCHDOWN VELOCITY WAS -2.1 FT/SE

CT/SIGMA LIMIT EXCEEDED DURING FLIGHT ** CHE . . . JT . BLADES **

MAXIMUM CT/SIGMA ENCOUNTERED ON FLIGHT WAS 0.179

(b) Calculated Data (Forward Speed Approach)

Figure A-12. Concluded.

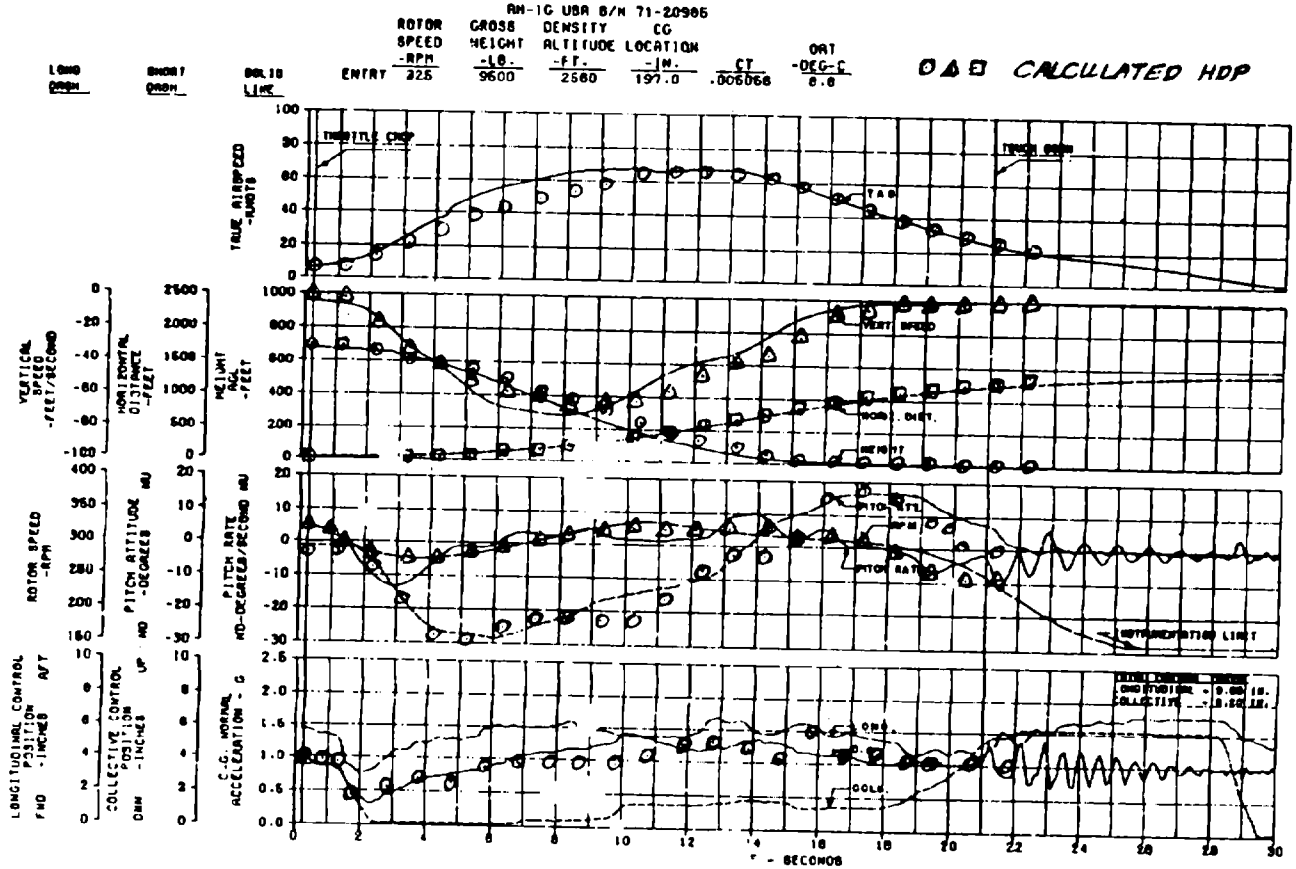

(a) Flight Test Data (High Hover Height)

Figure A-13. Time History of Autorotational Landing.

AH-1G

OPERATING WGT.	=	9500.0	LBS.	NO. OF BLADES	=	2.	
PRESSURE ALT.	=	2000.0	FT.	BLADE CHORD	=	2.25	FT.
AMBIENT TEMP.	=	8.8	C.	BLADE RADIUS	=	22.0	FT.
WIND VELOCITY	=	0.0	KTS.	BLADE TWIST	=	-10.0	DEG.
WIND DIR. HORIZ	=	0.0	DEG.	DISC SOLIDITY	=	0.0650	
WIND DIR. VERT.	=	0.0	DEG.	AIRFRAME F	=	24.0	FT**2
				DISC AREA PROJ	=	1520.5	FT**2
CASE NUMBER	=	2.		AREA RATIO	=	1.000	

FLIGHT SUMMARY

TIME (SEC)	HGT (FT)	DIST (HORIZ)	DIST (LAT)	VEL (KTS) LONG	VEL FPM VERT	ANR PERCENT	TPP ATT LONG DEG	TPP ATT LAT DEG	SHP	M.R. THRUST (LBS)
				START OF EVENT 1						
0.0	670.0	-16.0	-0.0	6.0	0.0	100.3	0.0	0.0	1093.6	9738.6
				START OF EVENT 2						
0.500	670.0	-10.9	-0.0	6.0	0.0	100.3	0.0	0.0	1093.6	9738.8
				START OF EVENT 3						
1.500	669.4	-0.8	-0.0	6.1	-97.2	93.8	0.7	0.0	146.5	8928.5
				START OF EVENT 4						
4.500	597.8	48.3	0.0	16.7	-2472.6	84.8	24.0	0.0	0.0	7361.8
				START OF EVENT 5						
14.507	60.0	292.6	0.0	60.1	-2028.2	100.0	1.4	0.0	0.0	10292.8
				START OF EVENT 6						
17.553	10.0	1066.1	0.0	44.0	-417.4	95.8	-17.0	0.0	0.0	9552.6
				START OF EVENT 7						
20.065	0.0	1221.6	0.0	30.4	-267.5	78.4	-12.1	0.0	0.0	9930.1
				CONDITIONS AT END OF FLIGHT						
26.065	0.0	1404.6	0.0	5.3	-0.0	86.8	-8.2	0.0	0.0	4725.9

DISTANCES ARE REFERENCED TO CYCLIC FLARE POINT

VERTICAL TOUCHDOWN VELOCITY WAS -2.8 FT/SEC

MAXIMUM CT/SIGMA ENCOUNTERED ON FLIGHT WAS 0.142

(b) Calculated Data (High Hover Height)

Figure A-13. Concluded.

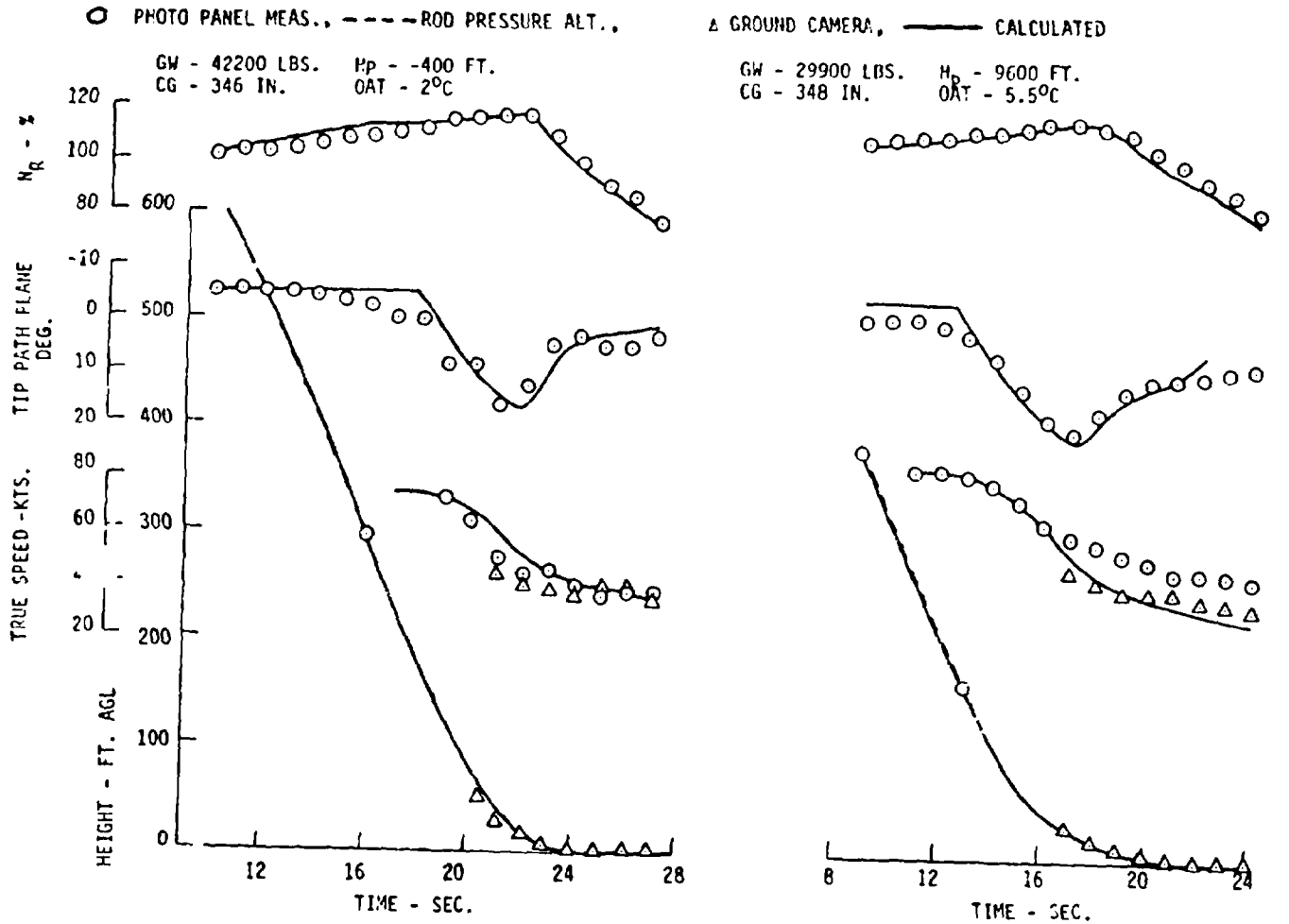

Figure A-14. CH-54B Autorotative Landings.

TABLE A-1. PARAMETRIC VARIATIONS AND EFFECTS

AIRCRAFT - OH-6A

RUN ↓	GW	DL	ALT	CG	JM	FLARE ANGLE	AIR-FOIL	TIME DELAY	NR %	DRAG	STATIC STAB.	VVTD	TD BODY ATT.	CT/ SIGMA	GW	GW	GW
LOC →	27	-	25 26	16	5	124 HI 261 NOSE	221- 224	45	38 & 101	13	298	232	235	35	27	27	27
1		2.75															
2	1905	3.5	0/15	0.333	255	20	0015	1.0	103	7.0	0.1	5.0	12.0	.15	1500		
3		4.5														2448	
4			5000														
5				-40.33													
6					383												
7						15											
8							009.5										
9								2.0									
10									105								
11										10.5							
12											.05						
13												8.0					
14													8.0				
15														.12			
16		4.0															2117

RUN	2	4	5	6	7	8	9	10	11	12	13	14	15	1	3	16
HLO		7.3	9.9	16.0	9.9	10.4	2.6	10.2	9.9	9.9	15.0	9.9	8.1	17.8	5.1	7.8
VCR		48.5	43.5	31.5	41.5	35.5	45.5	41.5	39.5	41.5	35.5	43.5	--	27.5	62.4	49.3
HHI	463.8	543.6	463.8	442.4	548.1	398.8	526.5	434.5	516.9	463.8	463.8	463.8	--	418.5	657.0	512.9
VHTD																
NOSE	28.1	33.5	35.4	17.6	28.2	22.2	29.8	27.4	25.3	28.1	23.1	33.6	--	14.0	44.0	33.7
VHTD																
HIGH	27.4	32.3	31.8	21.5	24.0	19.4	28.6	23.0	26.9	27.4	28.9	31.2	--	16.5	42.7	32.0
ΔHLO		-2.6	0.0	+6.1	0.0	+0.5	-7.3	+0.3	0.0	0.0	+5.1	0.0	-1.8	+7.9	-4.6	-2.9
ΔVCR		+7.0	+2.0	-10.0	0.0	-6.0	+4.0	0.0	-2.0	0.0	-6.0	+2.0	--	-14.9	+20.9	+7.8
ΔHHI	BASE	+79.8	0.0	-21.4	+84.3	-65.0	+62.7	-29.3	+53.1	0.0	0.0	0.0	--	-45.5	+193.2	+49.1
ΔVHTD																
NOSE	LINE	+5.4	+7.3	-10.5	+0.1	-5.9	+1.7	-0.7	-2.8	0.0	-5.0	+5.5	--	-14.1	+15.9	+5.6
ΔVHTD																
HIGH		+4.9	+4.4	-5.9	-3.4	-8.0	+1.2	-4.4	-0.5	0.0	+1.5	+3.8	--	-10.9	+15.3	+4.6

NOTE: Run No. 2 is baseline case.

TABLE A-2. PARAMETRIC VARIATIONS AND EFFECTS

AIRCRAFT - AH-1G

RUN ↓	GW	DL	ALT	CG	JM	FLARE ANGLE	AIR-FOIL	TIME DELAY	NR %	DRAG	STATIC STAB.	VVTD	TD BODY ATT.	CT/ SIGMA	GW	GW
LOC →	27	-	25 26	16	5	124 HI 261 NOSE	221- 224	45	38 & 101	13	298	232	235	35	27	27
1		4.0													6082	
2	7603	5.0	0/15	0.816	2670	20	009.5	1.0	100	16.5	0.1	5.0	8.0	.15		
3		6.0														9123
4			5000													
5				-40.816												
6					4005											
7						15										
8							0012									
9								2.0								
10									105							
11										23.5						
12											0.2					
13												8.0				
14													12.0			
15														.12		

RUN	2	4	5	6	7	8	9	10	11	12	13	14	15	1	3
HLO	11.7	9.6	11.7	18.9	11.7	9.8	2.7	13.7	11.7	11.7	18.7	11.7	9.6	18.4	7.7
VCR	38.8	54.3	38.8	38.8	38.8	42.8	46.8	42.7	38.9	38.8	42.8	44.8	62.8	32.6	51.4
MHI	526.4	674.3	526.4	536.0	600.0	564.4	537.4	495.6	526.6	526.4	554.9	526.4	526.4	475.2	644.2
VHTD NOSE	24.8	37.5	27.9	21.4	24.9	27.2	31.2	26.9	24.5	24.8	26.5	26.2	46.4	16.5	36.3
VHTD HIGH	26.1	29.9	27.6	27.6	24.6	31.7	29.8	30.5	26.6	26.1	33.6	20.6	28.7	24.4	38.9

Δ HLO		-2.1	0.0	+7.2	0.0	-1.9	-9.0	+2.0	0.0	0.0	+7.0	0.0	-2.1	+6.7	-4.0
Δ VCR		+15.5	0.0	0.0	0.0	+4.0	+8.0	+4.1	+0.1	0.0	+4.0	+6.0	+24.0	-6.2	+12.6
Δ MHI	BASE	+148.4	0.0	+9.6	+73.6	+38.2	+11.0	-30.8	+0.3	0.0	+28.5	0.0	0.0	-51.2	+117.8
Δ VHTD NOSE	LINE	+12.7	0.0	-3.4	+0.1	+2.4	+6.4	+2.1	-0.3	0.0	+1.7	+1.4	+11.6	-8.3	+11.5
Δ VHTD HIGH		+10.5	+3.8	+1.5	-1.5	+5.6	+3.7	+4.4	+0.5	0.0	+7.5	-5.5	+2.6	-1.7	+12.8

TABLE A-3. GENERALIZED PARAMETER SENSITIVITY

Parameter	Effect on H-V	
	OH-6A	AH-1G
Disc Loading (increased)	degrades	degrades
Altitude (increase)	degrades	degrades
CG (moving aft)	degrades	degrades
Rotor Inertia (increase)	improves	improves
Allowable Flare Angle (decrease)	degrades	degrades
Airfoil (decrease drag)	improves	improves
Time Delay (increase)	degrades	degrades
Initial N_R (increase)	improves	improves
Airframe Drag (increase)	degrades	degrades
Airframe Static Stability (decrease)	no change noted	no change noted
Vertical Impact Speed (increase)	improves	improves
Body Altitude at Touchdown (decrease)	degrades	degrades
Max. Allowable C_T/σ (decrease)	degrades	degrades

TABLE A-4. PARAMETRIC VARIATIONS FROM BASELINE

Parameter	OH-6A % H-V CHG/RF			AH-1G % H-V CHG/RF		
	Low Hvr	"Nose"	Hi Hvr	Low Hvr	"Nose"	Hi Hvr.
Baseline	0./1.1	0/1.17	0/1.23	0/1.03	0/1.15	0/1.06
CG (moving aft)	0/1.1	5/1.06	0/1.14	0/1.03	0/1.15	0/1.03
Rotor Inertia (increase)	62/1.03	-24/1.11	-5/1.23	62/1.03	0/1.24	2/1.43
Allowable Flare Angle (decrease)	0/1.1	0/1.17	18/1.07	0/1.03	0/1.15	14/2.01
Airfoil (decrease drag)*	5/1.2	-14/1.10	-14/1.07	-16/1.23	10/1.06	7/1.32
Time Delay (increase)	-74/-	10/1.11	14/1.05	77/-	21/1.19	2/1.30
Initial RPM (increase)	3/1.17	0/1.10	- 6/1.11	17/1.02	10/1.25	- 6/1.33
Airframe Drag (increase)	0/1.1	- 5/1.12	11/1.07	0/1.03	0/1.14	0/1.19
Static Stability (decrease)	0/1.1	0/1.17	0/1.23	0/1.03	0/1.15	0/1.06
Vertical Impact Speed (increase)	52/1.22	-14/1.22	0/1.32	60/1.11	10/1.32	5/1.34
Touchdown Attitude (decrease)**	0/1.1	5/1.14	0/1.16	-18/1.03	62/1.28	0/1.06
Disc Loading (decrease)	79/1.03	-35/1.33	-10/1.43	-18/1.06	-16/1.17	-10/1.70
Disc Loading (increase)	-48/1.02	50/1.04	42/1.03	57/1.10	32/1.05	22/1.06
Disc Loading (increase)	-29/1.10	19/1.02	11/1.01	—	—	—
Altitude +5000 Ft.	-26/1.13	17/1.05	17/1.11	-18/1.05	40/1.06	28/1.13

* AH-1G AIRFOIL DRAG WAS INCREASED
** AH-1G TOUCHDOWN ATTITUDE WAS INCREASED
RF-RATING FACTOR
LOW HOVER IN % HGT
"NOSE" IN % SPEED
HI HOVER IN % HGT

LIST OF SYMBOLS

a	Rotor lift curve slope, acceleration	ft/sec^2
a'	Axial interference factor	-
a''	Radial interference factor	-
a_H	Horizontal Acceleration	ft/sec^2
A	Rotor disc area	ft^2
A_F	Area of front rotor (tandems)	ft^2
A_o	Total disc area	ft^2
A_{TOT}	Total projected disc area	ft^2
ANG	Tip path plane angle	deg
b	Number of rotor blades on rotor hub	-
$\overline{B}$	Rotor efficiency	-
C	Blade chord	ft
C_D	Drag coefficient	-
C_{D_V}	Vertical drag coefficient	-
C_{D_w}	Wetted area drag coefficient	-
C_e	Effective blade chord	ft
CF	Centrifical force	lb
$C_{L_{(M)}}$	Mean lift coefficient	-
C_{P_a}	Available power coefficient	-
C_{P_c}	Climb power coefficient	-
C_{P_i}	Induced power coefficient	-
C_{P_o}	Profile power coefficient	-
C_{P_p}	Parasite power coefficient	-
C_{P_s}	Stall power coefficient	-
C_Q	Torque coefficient	-

C_{Q_D}	Drag torque coefficient	-
C_T	Thrust coefficient	-
C_w	Weight coefficient	-
d	Longitudinal distance between tandem rotors	ft
df	Rotor interference factor	-
df_H	Rotor interference factor (hover)	-
df_{FR}	Rotor interference factor (forward rotor on rear rotor)	-
df_l	Rotor interference factor (low rotor co-axial system)	-
df_{LF}	Rotor interference factor (level flight)	-
df_{RF}	Rotor interference factor (rear rotor on front rotor)	-
df_u	Rotor interference factor (upper rotor co-axial system)	-
D	Drag	lb
D_c	Rotor drag component in climb	lb
D_o	Profile drag	lb
D_p	Parasite drag	lb
D_R	Resultant distance main rotor centroid to airframe center of gravity	ft
D_{TR}	Distance from airframe center of gravity to tail rotor centroid (Horizontal for pitch; vertical for roll)	ft
D_V	Vertical drag	lb
e	Blade hinge offset	ft
f( )	Function of	-
F	Equivalent flat plate area for drag; force	ft^2; lb
F_x	Unbalanced force in longitudinal direction	lb
F_y	Unbalanced force in lateral direction	lb
F_z	Unbalanced force in vertical direction	lb
g	Acceleration of gravity -32.2 ft/sec^2	ft/sec^2

GW	Gross weight	lb
h_1	Initial height	ft
h_{CR}	H-V nose point height	ft
h_{hi}	High hover height	ft
h_{lo}	Lower hover height	ft
hp_a	Horsepower available	-
hp_c	Horsepower to climb	-
hp_i	Induced horsepower	-
hp_o	Profile horsepower	-
hp_p	Parasite horsepower	-
hp_s	Stall horsepower	-
h_x	Wheel height at arbitrary point	ft
H_M	Hub moment = $\Omega^2 be \frac{M_b}{2}$	ft-lb
HP	Horsepower	-
HP_{a_R}	Horsepower available - tip rockets	-
HP_{AV}	Horsepower available	-
HP_{acc_h}	Horsepower to accelerate horizontally	-
HP_{acc_v}	Horsepower to accelerate vertically	-
HP_Ω	Horsepower derived from rotor RPM change	-
HP_{REQ}	Horsepower required	-
HP_{UNS}	Unsupported power loading	-
HP_∞	Power required to hover OGE	-
I_{XX}	Airframe inertia about longitudinal axis	ft-lb-sec^2
I_{YY}	Airframe inertia about lateral axis	ft-lb-sec^2
I_{ZZ}	Airframe inertia about vertical axis	ft-lb-sec^2

J_M	Rotor inertia about rotation axis	ft-lb-sec^2
K	Time step counter	-
KE	Kinetic energy	ft-lb
M	Mass	slugs
MB	First flapping moment of rotor blade	slug-ft
$M_{1,90}$	Advancing tip Mach number	-
n	Profile drag correction factor	-
N	Arbitrary percentage of weight	%
N_o	Aerodynamic efficiency in climb	-
N_R	Rotor speed	%
P	Power	ft-lb/sec
P_A	Airframe pitch acceleration	deg/sec^2
P_i	Induced power	-
P_M	Airframe pitching moment	ft-lb
QF	Torque factor	-
R	Rotor blade radius (measured from center of rotation)	ft
R_M	Airframe rolling moment	ft-lb
S	Displacement	ft
S_π	Wetted area	ft^2
SHP	Shaft horsepower	-
t	Time	sec
T	Thrust	lb
T_f	Thrust front rotor (tandems)	lb
T_{MR}	Thrust main rotor	lb
T_R	Thrust rear rotor or rocket thrust	lb
T_{TR}	Tail rotor thrust	lb

u	Induced velocity	ft/sec
u_o	Induced velocity in hover	ft/sec
$\bar{u}$	Induced velocity ratio u/u_o	-
V	Velocity	ft/sec
V_{CR}	Critical velocity	ft/sec
V_H	Horizontal velocity	ft/sec
V_R	Flight path velocity	ft/sec
vs	Vertical distance between tandem rotors	ft
V_v	Vertical velocity	ft/sec
V_{V_D}	Vertical velocity design	ft/sec
V_W	Wind velocity	ft/sec
V_X	Velocity at arbitrary point	ft/sec
$\bar{V}$	Flight path velocity ratio V_H/Uo	-
W	Aircraft weight	lb
W_X	Wind component, longitudinal axis	ft/sec
W_Y	Wind component, lateral axis	ft/sec
W_Z	Wind component, vertical axis	ft/sec
X	Longitudinal axis (earth axis system)	-
Y	Lateral axis (earth axis system)	-
Y_1	Initial wheel (skid) height	ft
Z	Vertical axis (earth axis system)	-
α	Blade element angle of attack	deg
α_{TPP}	Rotor tip path plane angle (earth axis)	deg
α_s	Rotor shaft angle	deg
α_w	Rotor tip path plane angle (wind axis)	deg

β	Airframe pitch attitude	deg
$\dot{\beta}$	Airframe pitch rate	deg/sec
$\ddot{\beta}$	Airframe pitch acceleration	deg/sec^2
β_o	Airframe pitch attitude (previous time step)	deg
γ	Rotor overlap angle (tandems); climb angle	deg; deg
δ	Mean profile drag coefficient	-
Δ	Increment of	-
ξ	Wake skew angle (tandems)	deg
θ	Impressed blade pitch angle	-
θ_e	Equivalent linear blade twist	rad
θ_{75}	Impressed blade pitch at 0.75 R	deg
λ	Rotor inflow ratio	-
Λ	Ground effect parameter	-
μ	Rotor tip speed ratio	-
μ_H	Horizontal component of tip speed ratio	-
μ_{MIN}	Tip speed ratio at minimum power point	-
μ_V	Vertical component of tip speed ratio	-
π	Constant 3.14159. . .	-
ρ	Air density	$lb\text{-}sec^2/ft^4$
ρ_o	Air density at sea level standard	$lb\text{-}sec^2/ft^4$
σ_e	Rotor disc solidity	-
Σ	Summation of	-
ϕ	Rotor induced velocity angle	-
Ω	Angular velocity of main rotor	rad/sec
Ω_d	Design angular velocity of main rotor	rad/sec

LIST OF EQUATIONS

This section lists the major equations used in the Helicopter Dynamic Performance Program. All equations are numbered as referred to in the text.

1. $$hp_a = hp_i + hp_o + hp_p + hp_c + hp_s$$

2. $$T = \rho\pi R^2 (V_R + u)\, 2u$$

3. $$u_o = \left[\frac{T}{2\rho\pi R^2}\right]^{1/2}$$

4. $$\bar{V} = -\bar{u} \sin\alpha_w + (\bar{u}^2 \sin^2\alpha_w - \bar{u}^2 + 1/\bar{u}^2)^{1/2}$$ (Reference 1)

5. $$u_{o_{\text{actual rotor}}} = \left[\frac{T}{2\pi\rho(\bar{B}R)^2}\right]^{1/2}$$

6. $$C_{P_i} = \frac{550\, hp_i}{\rho\pi R^2(\Omega R)^3} = \frac{C_T^{3/2}}{\sqrt{2}\,\bar{B}}\,\bar{u}\,\Lambda$$

7. $$P_i/P_{i_o} = [A_o/A]^{1/2}$$

8. $$A/A_o = 1 - \frac{\gamma - \sin\gamma\cos\gamma}{\pi}$$

9. $$P_{i_2} = 2P_{i_1}\left[\frac{A_2}{A_{TOT}}\right]^{1/2}$$

10. $$df_H = 2\left[\frac{1}{1 - \frac{\gamma - \sin\gamma\cos\gamma}{\pi}}\right]^{1/2}$$

11. $$df_{LF} = df_{FR} + df_{RF} = 2/(1 + \rho^2\cos^2\varsigma)$$

12. $$df = df_H + \frac{df_{LF} - df_H}{\zeta_{TAN}} \zeta$$

13. $$df = df_H \cos^2 \zeta$$

14. $$P_{i_{total}} = 2.5T^2/2\rho Au \left[1 + \frac{df_U + df_l}{2}\right]$$

15. $$C_{L_{(M)}} = .2\, C_{T/\sigma_e} \left[\frac{1}{\frac{\bar{B}^3}{3} + \frac{\bar{B}\mu^2}{2} - \frac{4\mu^3}{9\pi}}\right]$$

16. $$C_{P_0} = \frac{\sigma_e \delta}{8} (1 + n\mu^2)$$

17. $$hp_o = \frac{\sigma_e \delta}{8} (1 + n\mu^2) \frac{\rho \pi R^2 (\Omega R)^3}{550}$$

18. $$u = -\frac{V}{2} \pm \left[\frac{V^2}{4} + \frac{T}{2\rho\pi R^2}\right]^{1/2}$$

19. $$u/u_o = -\frac{V}{2u_o} \pm \left[1/4 \left(\frac{V}{u_o}\right)^2 + 1\right]^{1/2} = \bar{u}$$

20. $$u(1 + \alpha')\bar{B} = u_o = \left[\frac{T}{2\rho\pi R^2}\right]^{1/2}$$

21. $$u(1 + \alpha') = \left[\frac{T}{2\rho\pi(\bar{B}R)^2}\right]^{1/2}$$

22. $$u(1 + \alpha') = 550\, hp_i / T$$

23. $$\bar{B} = 1 - \frac{[1.34C_T]^{1/b}}{b}$$

24. $$\bar{B} = 1 - \frac{[1.34C_T]^{1/b}}{b} - [0.14325\theta_e + 0.035]$$

25. $$V/u_o = V/\left[\frac{T}{2\pi\rho(\bar{B}R)^2}\right]^{1/2}$$

26. $$\Delta\bar{B}_\mu = x_\mu(2/C_T)^{1/2} + \left[\frac{y_\mu^2}{C_T} + 1\right]^{1/2} - \left[\frac{z_\mu^2}{C_T} + 1\right]^{1/2}$$

26(a). $$\Delta\bar{B}_\mu = 0.0905\mu\left[\frac{2}{C_T}\right]^{1/2} + \left[\frac{\mu^2}{2C_T} + 1\right]^{1/2} - \left[\frac{0.6974\mu^2}{C_T} + 1\right]^{1/2}$$

27. $$\bar{B} = 1 - \frac{[1.34C_T]^{1/b}}{b} + 0.0905\mu\left[\frac{2}{C_T}\right]^{1/2} + \left[\frac{\mu^2}{2C_T} + 1\right]^{1/2} - \left[\frac{0.6974\mu^2}{C_T} + 1\right]^{1/2} - [0.14325\,\theta_e + 0.035]$$

28. $$\mu_{\bar{B}} = [V_H^2 + V_v^2]^{1/2}/\Omega R$$

29. $$\int_0^1 \left|\hat{\theta}_e(x-0.8)\right| x^3 dx = \int_0^1 \left|\hat{\theta}\, x\right| x^3 dx$$

30. $$D = \frac{F\rho V^2}{2}$$

31. $$C_{P_p} = \frac{F}{2\pi R^2}\mu^3$$

32. $$hp_p = C_{P_p}\frac{\rho\pi R^2(\Omega R)^3}{550}$$

33. $$C_T \cos \alpha_{TPP} = C_W + C_{D_V}\left[u/u_o + \frac{\sqrt{2\bar{B}}\mu_V}{C_T^{1/2}}\right]^2 \frac{C_T}{2\bar{B}^2}$$

33(a). $$C_{D_V} = 2\bar{B}^2 \left(1 - \frac{1}{1+N}\right)$$

34. $$hp_c = (T \cos \alpha_{TPP})V_V \, (\rho_o/\rho)/550$$

35. $$C_{P_{CLIMB}} = (C_T \cos \alpha_{TPP})\mu_V(\rho_o/\rho)$$

36. $$C_e = \int_o^1 Cx^3dx / \int_o^1 x^3dx$$

37. $$\sigma_e = \frac{b}{\pi R} \int_o^1 Cx^3dx / \int_o^1 x^3dx = 4b/\pi \int_o^1 C/R \, x^3dx$$

38. $$f(C_D/\sigma, M_{1,90}, \theta_e) = [1750.(C_D/\sigma)^2 - 208.5 \, C_D/\sigma(3.6M^2-3.71(M+1))$$
$$+(((C_D/\sigma + .01)^2/.00G133)-.752)(M-.7)+38.7M-21M^2-9.9]$$
$$(1.17+1.2175\theta_e)$$

39. $\mu<.25$
$$f(C_L/\sigma-(C_L/\sigma)_{crit})=(1.-(.33+3.\mu)C_L/\sigma+.133\mu+.036)-(C_L/\sigma)_{crit.}$$

40. $\mu>.25$
$$f(C_L/\sigma-(C_L/\sigma)_{crit})=C_L/\sigma-(C_L/\sigma)_{crit}-(1.08C_L/\sigma-.071)$$

41. $$C_L/\sigma - (C_L/\sigma)_{LSL} < 0.018$$
$$f(C_L/\sigma-(C_L/\sigma)_{LSL}) = 3.0(C_L/\sigma-(C_L/\sigma)_{LSL})$$

42. $C_L/\sigma-(C_L/\sigma)_{LSL} > 0.018$

$$f(C_L/\sigma-(C_L/\sigma)_{LSL}) = 833.33(C_L/\sigma-(C_L/\sigma)_{LSL})^2 + 30.65(C_L/\sigma-(C_L/\sigma)_{LSL}) + .336$$

43. $$C_{P_S} = [f(C_L/\sigma-(C_L/\sigma)_{crit})^2/.01]\sigma C_T + [f(C_L/\sigma-(C_L/\sigma)_{LSL})]\sigma(C_L/\sigma)_{LSL})$$

44. $$hp_s = C_{P_S}\,\rho\pi R^2(\Omega R)^3/550$$

45. $$\alpha_{TPP}(K+1) = ANG_0 + (ANG_{MAX}-ANG_0)\,\sin\left[\pi/2\left(\frac{t(K+1)-t_0}{t_{RATE}}\right)\right]$$

46. $$\alpha_{TPP}(K+1) = \alpha_{TPP_{V_z}}\sin\left[\pi/2\left(\frac{V_x - V(K)}{V_x}\right)\right] + \tan^{-1}(D/T)$$

47. $$SHP(K+1) = SHP(K) + HP_{MAX}/(t_{RATE})$$

48. $$HP_\Omega = [J_M/1100](\Omega_1^2 - \Omega_2^2)/\Delta t$$

49. $$N_R = N_{R_0} + \Delta N_R\,\sin\left[\pi/2\,\left(\frac{t(K+1)-t_0}{t_{RATE}}\right)\right]$$

50. $$\alpha = \frac{(1+1.5\mu^2)\frac{6C_T}{\sigma a} + 1.5\lambda\,(1-0.5\mu^2)}{(1-\mu^2+2.25\mu^4)}$$

51. $$\alpha = \theta_{75} - \phi$$

52. $$\lambda = -\mu_H \sin\alpha_s - \frac{\bar{u}\sqrt{.5C_T}}{\bar{B}}$$

53. $\phi = \tan^{-1}_{(\gamma)}$

54. $C_T = \frac{(1-\mu^2+2.25\mu^4)\alpha-1.5\lambda(1-0.5\mu^2)}{(1+1.5\mu^2)} \quad (\frac{\sigma a}{6})$

55. $\Omega_2 = [\Omega_1^2 - \frac{1100\ HP_\Omega \Delta t}{J_M}]^{1/2}$

56. $F_x = T\cos\alpha_{TPP_{LONG}} \sin\alpha_{TPP_{LAT}} - D_x$

57. $F_y = T\sin\alpha_{TPP_{LONG}} \cos\alpha_{TPP_{LAT}} - D_y$

58. $F_z = T\cos\alpha_{TPP_{LONG}} \cos\alpha_{TPP_{LAT}} - (GW+D_V)$

59. $a = F/M$

60. $V_{NEW} = V_{OLD} + adt$

61. $\Delta S = V_{OLD}dt + 1/2\ adt^2$

62. $S_{TOTAL} = \Sigma_o^t \Delta S$

63. $W_{(X)} = V_W\cos(DIR_X-HDG)\cos(DIR_Z)$

64. $W_{(Y)} = V_W\sin(DIR_X-HDG)\cos(DIR_Z)$

65. $W_{(Z)} = V_W\sin(DIR_X)$

66. $HP_{ACC} = \Delta KE/550\ \Delta t$

67. $$h_1 = \left[\frac{.11}{1.1 - V/V_x}\right] - .11$$

68. $$V_v = \left[\frac{.11V\ (h_x - y_1)}{(1.1V_x - V)^2}\right] a_H$$

69. $$\alpha_{TPP} = \cos^{-1}\left(\frac{GW+D_v}{T}\right)$$

70. $$P_M = T_{TR}D_{TR} - (2\ D_R\ T_{MR} + H_M)\ \sin(.5\beta)$$

71. $$\beta = \alpha_{TPP_t} + \beta_{t-1} - \beta_o$$

72. $$I_{yy_{MR}} = I_{yy_{CG}} + w/gD_R^2$$

73. $$P_A = P_M/I_{yy_{MR}} = \ddot{\beta}$$

74. $$\dot{\beta}_t = \dot{\beta}_{t-1} + \ddot{\beta}_t \Delta t$$

75. $$\beta_t = \dot{\beta}_t \Delta t + .5\ddot{\beta}_t \Delta t^2 + \beta_{t-1}$$

74.(m) $$\dot{\beta}_t = (\dot{\beta}_{t-1} + \ddot{\beta}_t \Delta t)PDAMP$$

76. $$HP_{UNS} = HP_{\infty\Lambda}(1 - HP_{AV}/HP_{\infty\Lambda})$$

77. $$h_{1o} = -\frac{J_M \Omega_d^2 V_v}{1100\ HP_{UNS}}\ (1 - 2.24\sqrt{C_T/\sigma})$$

78. $$C_L/\sigma = 2/\mu_{MIN}\ C_T/\sigma$$

79. $$\mu_{MIN} = 0.95\left[(C_T/\bar{B})^2 \frac{2\pi R^2}{6F}\right]^{1/4}$$

80. $$V_{CR} = (2.809V_{MIN} + 5.618\ C_L/\sigma - 169.776)\left(1 - \frac{HP_{AV}}{\left(HP_{\infty A} + \frac{GW\ V_{V_D}}{550}\right)}\right)$$

81. $$h_{ht} = 0.18V_{CR}^2 + 199.0$$

82. $$h_{hi} = \frac{GW}{\pi R^2}\left(1 - \frac{HP_{AV}}{\left(HP_{\infty A} + \frac{GW\ V_{V_D}}{550}\right)}\right) + 111.0$$

83. $$h_x = h_{lo} + (0.11/(1.1 - V_x/V_{CR}) - .11)(h_{CR} - h_{lo})$$

84. $$h_x = h_{hi} - (1-(1-V_x/V_{CR})^{1/2})\ (h_{hi} - h_{CR})$$

4659-80